3/17/65
b

SUBLIMATION DEHYDRATION IN THE CONTINUUM,
TRANSITION, AND FREE-MOLECULE FLOW REGIMES

A THESIS

Presented to

The Faculty of the Graduate Division

by

James Edward Hill

In Partial Fulfillment

of the Requirements for the Degree

Doctor of Philosophy

in the School of Mechanical Engineering

Georgia Institute of Technology

September, 1967

SUBLIMATION DEHYDRATION IN THE CONTINUUM,

TRANSITION, AND FREE-MOLECULE FLOW REGIMES

Approved:

Chairman

Date approved by Chairman: August 30, 1967

ACKNOWLEDGMENTS

The author is deeply indebted to many people who made this work possible. First of all, he would like to thank Dr. J. E. Sunderland, his advisor, who gave many hours of willing advice and encouragement, not only during all phases of this investigation, but throughout the entire duration of his graduate work at this institution. He would like to thank Dr. A. B. Huang and Dr. G. T. Colwell for their service on the reading committee. Also, the author is appreciative of the assistance given by Mrs. Jo Pell Holbrook in typing the rough draft of this thesis, and the assistance given by Mr. Ben Chinn in drafting many of the figures that appear here.

The author would like to express his gratitude for the Public Health Service Research Grants EF 00102-03 and EF 00102-04 from the Division of Environmental Engineering and Food Protection, and UI 00093-04 from the National Center for Urban and Industrial Health, which provided full support for this investigation.

Finally, the author would like to acknowledge his debt to his wife, Carol, and to his parents, Mr. and Mrs. Roy Hill. The attainment of his educational goals would not have been possible without their encouragement and support.

TABLE OF CONTENTS

LIST OF TABLES

LIST OF ILLUSTRATIONS

SUMMARY

Previous theoretical analyses have pointed out the role of the different heat and mass transfer mechanisms in the freeze-drying process. However, very few have made successful attempts to analytically describe the process by including all of the mechanisms. These include heat conduction in both the frozen and dried regions of the food, and hydrodynamic and diffusional vapor flow in the dried region. Therefore, the objective of this investigation is to make a detailed analysis is which all of mechanisms are included. The results will provide more accurate methods for estimating drying times under a variety of boundary conditions. In addition, relationships will be established between the many variables affecting the drying rate so as to indicate the best ways to improve the rate of freeze-drying. A primary aim will be to present closed form relations for the interface temperature and drying time which have been lacking in all previous analyses.

In the theoretical analysis, the energy equations governing heat conduction in the dried and frozen regions are solved. A temperature distribution is presented for the dried region, which contains a term showing the effect of mass transfer on the distribution. Vapor flow equations are presented for hydrodynamic and diffusional flow in the free-molecule, transition, and continuum flow regimes. The energy and vapor flow equations are coupled to give closed form equations for the interface temperature as a function of the drying regime, interface position, transport property data, and externally controlled boundary

conditions. The equations are valid for simultaneous hydrodynamic and diffusional flow in the continuum and transition flow regimes, and are valid for molecular diffusion in the free-molecule regime. Finally, closed form equations are presented for the interface position as a function of time for the cases where the interface temperature is either constant or a linear function of the interface position. Therefore, the theoretical analysis includes all of the heat and mass transfer mechanisms, and governs drying at all possible pressures.

The results of the theoretical analysis indicate that the interface temperature remains constant during drying if heat is transferred through the dried layer only. If heat is transferred through both the dried and frozen layers, the interface temperature will change as the interface position changes. Numerical calculations are carried out for freeze-drying beef, and it is found that drying time can be reduced by increasing the surface temperatures and reducing the water vapor partial pressure in the vacuum chamber. It is also found that the optimum pressure at which to dry beef is between 0.5 and 1.0 torr. An increase or decrease in pressure from this range results in a slower drying rate. In addition, for all beef samples 1-1/2 inches thick or less, drying is faster when it takes place from both faces than when it takes place from only one face and heat is conducted through the back face. The analysis also applies to the special case of atmospheric freeze-drying, and numerical calculations are carried out to show the feasibility of this process to thin samples.

The experimental investigation involved measuring the equilibrium vapor pressure of chopped sirloin, lamb, veal, pork, chicken, and beef

fat for a temperature range of -26°C to -4°C. Measurements are presented for a leg of veal, leg of lamb, center cut loin of pork, fat from sirloin steak, chopped sirloin steak, and the white and dark meat of chicken. The results show that the equilibrium vapor pressure of all of the meats tested is between 13 per cent and 20 per cent lower than the vapor pressure of pure ice at the same temperature. The vapor pressure measurements are used with the Clausius-Clapeyron equation to obtain the latent heats of sublimation for all of the meats. The latent heat of sublimation of frozen meats is about 9 to 22 per cent higher than the latent heat of sublimation of ice under similar conditions.

NOMENCLATURE

English Symbols		Units
a	molar flux ratio, $1 + \frac{\tilde{N}_a}{\bar{N}_w}$	dimensionless
a'	constant defined on page 17	°R
A	constant defined on page 34	$lbf^2 sec/lbm\ ft^3$
b'	constant defined on page 17	°R/ft
B	parameter defined on page 34	lbf^2/ft^4
B_3	constant defined on page 114	$lbm\ ft^3/lbf\ sec$
B_4	constant defined on page 113	ft^4
B_5	constant defined on page 113	lbf/ft^2
B_6	constant defined on page 115	ft^2
B_7	constant defined on page 116	lbm ft/lbf sec
c'	constant defined on page 17	$°R/ft^2$
C	parameter defined on page 34	$lbm\ lbf^2/sec\ ft^5$
C_1	constant defined on page 23	mole/ft sec
C_2	constant defined on page 34	$1/ft^2$
C_3	constant defined on page 38	Btu/sec
C_4	constant defined on page 39	Btu/ft sec
C_5	constant defined on page 39	$Btu/ft^2 sec$
C_6	constant defined on page 39	Btu/ft^3

English Symbols		Units
C_7	constant defined on page 39	Btu/ft^2
C_8	constant defined on page 39	Btu/ft^4
C_9	constant defined on page 108	dimensionless
C_{10}	integration constant	
$\bar{C}_\nu$	constant defined on page 43	dimensionless
C_F	force coefficient defined on page 111	$lbf\ sec/ft^3$
C_p	specific heat	Btu/lbm°R
d	distance separating parallel plates	ft
D	mutual diffusion coefficient	ft^2/sec
D_k	Knudsen's diffusion coefficient defined by (2/3) $r_c\bar{v}$	ft^2/sec
F_2	parameter defined on page 17	1/ft
F_{wall}	force at wall of capillary	lbf
$F(r_c/\lambda)$	fraction of molecules not undergoing intermolecular collisions	dimensionless
g_c	constant equal to 32.2	$ft\ lbm/lbf\ sec^2$
H_i	weighting coefficient defined on page 43	dimensionless
ΔH	heat of sublimation	Btu/lbm
k	thermal conductivity	Btu/sec ft°R
K	Boltzmann's constant	ft lbf/molecule°R
Kn	Knudsen number	dimensionless

English Symbols		Units
$\tilde{K}$	pressure parameter defined on page 42	1/ft
l	length of capillary tube	ft
L	thickness of freeze-drying sample	ft
m	mass of gas molecule	lbm
M	molecular weight	
n	molecular density	molecules/ft^3
N	mass flow rate	lbm/ft^2sec
$\bar{N}$	molar flow rate	moles/ft^2sec
N'	mass flow rate	lbm/sec
P	total pressure	lbf/ft^2
$\bar{P}$	partial pressure	lbf/ft^2
ΔP	pressure difference	lbf/ft^2
P_ν	eigenvalue defined on page 43	dimensionless
Q	parameter defined on page 33	lbm/ft sec
$\bar{Q}$	flow rate defined on page 41	dimensionless
Q'	volume flow rate defined on page 42	dimensionless
r	radial dimension in capillary tube	ft
r_o	constant defined on page 38	°R
r_1	constant defined on page 38	°R/ft
r_c	capillary radius	ft
R	gas constant	ft lbf/lbm°R
$\bar{R}$	universal gas constant	ft lbf/mole°R
R_2	parameter defined on page 34	lbm^2/ft^4sec^2

English Symbols		Units
R_3	parameter defined on page 34	lbm/ft^3sec
S	reflection coefficient	dimensionless
t	time	sec
T	temperature	°R
$\bar{T}$	constant defined on page 43	dimensionless
u	macroscopic gas velocity	ft/sec
$\bar{v}$	average molecular velocity	ft/sec
x	freeze-dried model co-ordinate	ft
X	position of interface between dried and frozen regions	ft
y	molar concentration	$\frac{\text{moles of component}}{\text{moles of mixture}}$

Greek Symbols		
α_i	discrete point defined on page 42	dimensionless
β	parameter defined on page 15	1/ft
Γ	first order correction for non-roundness and other irregularities of the capillary	dimensionless
ε_D	permeability in the continuum regime	ft^2
ε	permeability in the transition regime	ft^2
ξ	coefficient of slip	ft
η	viscosity	$lbf\ sec/ft^2$
η_ν	eigenvalue defined on page 43	dimensionless

Greek Symbols		Units
λ	mean free path	ft
μ	viscosity	lbm/ft sec
ρ	density	lbm/ft^3
σ	porosity	dimensionless
τ	tortuosity factor	dimensionless

Subscripts

a	air
c	at capillary surface
e	effective
i	ice
L	position at frozen back face
m	mean or average
t	transition regime
w	water vapor
X	position of interface
0	position at dried surface
1	at capillary entrance
2	at capillary exit
I	dried region
II	frozen region

CHAPTER I

INTRODUCTION

General

Sublimation dehydration is a process whereby food or biological substances are preserved for future use by the methods of freezing and drying. The basic process involves the following steps: The substance to be dried is frozen and then placed in a vacuum chamber where the pressure is lower than the triple point of water. Heat is supplied to the product whereupon the frozen water component in the product sublimates and the vapor passes out into the chamber. The vapor is then collected or carried away. The process is depicted as a one-dimensional situation where the ice front recedes into the product as heat is continually supplied. The vapor flow is out through the resulting dried layer and occurs under the influence of a total pressure gradient and a partial pressure gradient of the water vapor.

Commercial and laboratory freeze-driers can use varied equipment to accomplish the drying. The most common ways of supplying the vacuum are by use of a mechanical vacuum pump or by use of steam ejectors. However, the steam ejector is much more costly and also it is difficult to obtain a pressure lower than approximately 0.65 mm Hg. The heat energy necessary for sublimation can be supplied by conduction where a heated platen is in direct contact with the product, by radiation where the heated platen is not in direct contact with the product, or by some elaborate means such as dielectric heating where the material is placed in a high-frequency electric field. The latter method is extremely expensive and in addition, there have been problems with ionization of the residual gas in the chamber. The water vapor is usually removed by a refrigerated condenser or a chemical absorption unit. Extended surfaces of activated alumina or silica in the chamber could also be used and would serve the same purpose as the chemical desiccants.

The freeze-drying process originated in the early 1940's because there was a need to preserve certain biological substances. The main application today is for food preservation. Some of the foods that are freeze-dried in big volumes are: chicken, beef, mushrooms, shrimp, crab, strawberries, blueberries, peaches, soluble coffee, chives, cottage cheese, tea, ham, tuna, sausage, asparagus, snap beans, celery, bell peppers, and eggs.

After drying the food, it has to be packaged so that it will not rehydrate until ready for use. In addition, many foods need protection from light and oxygen to keep oxidation at a minimum. Common containers are tin cans and aluminum foil-polyethylene laminated bags. Some foods are also packaged with nitrogen to prevent oxidation. Most dried products can be rehydrated in two to ten minutes by the addition of water or other liquids.

There are many advantages of freeze-drying over other types of food preservation. Chemical and flavor losses are avoided, and nutrients remain dispersed in their original position within the food. This is in contrast to evaporation drying and other types of atmospheric drying where the nutrients migrate to the surface with the water and remain there after the water evaporates. Bacteria, molds, and yeasts have little chance of multiplying, and the foods have a shelf life of up to two years. In evaporation drying, the food cells collapse when the water migrates to the surface. Consequently, there is shrinkage and the food is hard to rehydrate. In freeze-drying the cells do not collapse and rehydration occurs quickly. The resulting food product is light in weight (beef is approximately 75 per cent water) and needs no refrigeration.

Literature

General

A majority of literature concerning freeze-drying deals with a general discussion of the process and/or the biological aspects. One of the first books written was by Flosdorf (1).* A great deal of his material deals with applications, not only to the food industry but also to the medical field. A survey of the biological aspects is contained in a book edited by Harris (2). In addition, books by Van Arsdel (3), Desrosier (4), and Charm (5) all devote a portion of their works to freeze-drying.

Two of the most comprehensive studies concerning the field are given by Harper and Tappel (6) and Burke and Decareau (7). Their work is aimed primarily at the food industry and they discuss, among other things, the methods and equipment used for laboratory and commercial application. They also review the important analytical work that has

---

*Numbers in parentheses refer to references given in the Bibliography.

been done, report the important property data that has been measured, discuss applications to specific types of food, and list additional research needs. Hardin (8) and Dyer (9), besides presenting important analytical and experimental work of their own, also give excellent detailed discussions and criticisms of the previous literature concerning experimental and analytical work in freeze-drying.

Heat and Mass Transfer Analyses

Harper and Tappel (6) present an analytical investigation in which they consider hydrodynamic and diffusional flow of the vapor in the dried region. They do not combine the two modes of vapor transport, and their results are for the case of heat transfer only through the dried region. The main conclusion of their work is that drying time is proportional to the square of the thickness of the food sample.

Bannister (10) and Koumoutsos and Sunderland (11) present similar analyses on the basis of hydrodynamic and diffusional flow through a bundle of capillaries. Their diffusion equation is only applicable to the case of constant total pressure which does not correspond to the usual situation. They solve the heat transfer and mass transfer equations simultaneously with several simplifying assumptions (such as no heat transfer through the frozen region) for the various flow regimes, but indicate that additional work is needed to clarify when the various effects must be accounted for. Also, they make no provision for specifying the interface temperature and pressure that appear in the equations. Their chief results coincide with those of Harper and Tappel.

Hardin (8) presents an analysis for the general mathematical model considered in this thesis in which heat transfer is assumed to take place through the dried and frozen regions and thus, the interface temperature is allowed to vary throughout the process. However, he considers only hydrodynamic flow in the transition regime. He does present important experimental data for temperature and pressure distributions and drying rates for beef over a range of chamber pressures and concentrations.

Dyer and Sunderland (12) present a mathematical solution to the transient heat conduction equation governing the freeze-drying model used in this thesis. They also present a drying rate equation as a result of their analysis. A major simplifying assumption which limits the generality of the solution is that no heat transfer takes place through the frozen region, and thus as will be shown in Chapter 2, the interface temperature remains constant as the drying proceeds.

Dyer and Sunderland (13) derive and solve the differential equation of motion for the vapor species in an air-sublimating vapor diffusion process. The analysis is for flow in the transition regime and is valid for the case where a total pressure gradient is superimposed on the diffusion process. Their results are in the form of effective diffusion coefficients and are compared with experimental measurements. A major drawback is the fact that the solution to the differential equation is a series solution.

Dyer and Sunderland (14) present an analytical solution for freeze-drying in the transition regime by coupling the energy, diffusion, and hydrodynamic equations. They consider the general case where heat is transferred through both the dried and frozen regions and the interface temperature varies throughout the process. Aside from only considering drying in the transition regime, they assume that the temperature distribution in the dried region is linear. This seems to be quite valid for drying of beef, but might limit the application of the solution to other processes. In addition, the calculation procedure involves trial and error solutions that must be carried out on a computer.

Lambert (15) presents an extensive and detailed study of heat and mass transfer effects in freeze-drying. He considers the mass transfer rate as a particular driving force/resistance system and presents his results in terms of an overall coefficient which he calls "cake permeability." This analysis does not show clearly how the different heat and mass transfer mechanisms are related.

Kan and de Winter (16) present an analysis of the freeze-drying process where drying occurs from both sides of the sample. They assume the interface temperature to be constant (which will be shown to be correct for the model they chose), the temperature profile in the dried layer to be linear, and the total pressure in the dried layer to be constant. They therefore assume that the vapor flux is entirely by diffusion. This seems to be valid when a purged atmosphere of non-condensable gas surrounds the sample, which was the case in their experimental work, but is certainly not valid for the standard freeze-drying process.

Transport Properties

Important experimental measurements are presented by Hill, et al. (17), for the thermal conductivity of frozen beef, pork, lamb, and veal. They also present a summary of previously available thermal conductivity data for various meats. Thermal conductivity of dried meats is presented by Harper and El Sahrigi (18), Lusk, et al. (19), and Massey and Sunderland (20). Dyer, et al. (21), present experimental data for the equilibrium vapor pressure of beef. Also, Sevcik and Sunderland (22) give the results of measurements of the thermal emissivity of beef fat, and fresh and freeze-dried beef.

Harper (23), Harper, et al. (24), and Harper and Chichester (25) all present transport properties for the freeze-drying process. These include thermal conductivity of the dried product, permeability, diffusivity, and porosity. The results were used by Harper (23) to present tortuosity factors and mean capillary diameters for beef, apple, and peach samples. Dyer and Sunderland (13) present data for the diffusion coefficient in dried beef, and Dyer (9) presents experimental measurements of the permeability of dried beef to water vapor.

Other Related References

Several other publications that are not concerned directly with heat and mass transfer analyses or transport properties are also important to a thorough investigation into the problem. Hatcher (26) used a gamma radiation beam to study the interface movement while freeze-drying beef. Massey (27) also presents drying times for beef that were determined in conjunction with his thermal conductivity measurements. Kennard (28), Loeb (29), and Present (30) all present discussions of transition and free-molecule flow, and Carman (31) discusses the application of their equations to flow in porous media. Schneider (32) analyzes conduction and convection heat transfer in porous media, and Bird, et al. (33), present a general discussion of diffusive mass transfer. Scott and Dullien (34) and (35) conduct an analysis of diffusive and bulk flow in the transition regime with special emphasis on flow in porous media. Dyer (36) presents an analysis for bulk and diffusional transport in the continuum regime of a binary gas mixture flowing through a tube.

Purpose and Scope

One of the primary aims in a study of the freeze-drying process is to determine the rates and times for drying. In order to carry out a significant analysis, all of the mechanisms involved must be considered; in addition, a vast amount of experimental data are needed. Values of permeability, diffusivity, thermal conductivity of the frozen and dried material, equilibrium vapor pressure of the frozen material, latent heat of sublimation, and porosity are just some of the quantities that must be known for any one product under study. It would be short of impossible in a single project to experimentally determine all these quantities for a given material and then to conduct an analysis on the drying of this material. The purpose of this thesis will be to make additional experimental measurements of property data, significant to the drying of several different meats. In addition, an analytical study of the general drying process will be conducted. Numerical calculations will be carried out on the drying of beef, about which a great deal is known.

One of the boundary conditions used when coupling the mass transfer and heat transfer equations is that the temperature of the interface is assumed to equal the equilibrium temperature of the frozen substance at the pressure that exists at that position. The scope of the experimental work will include the measurement of this vapor pressure-temperature relationship for meats that are commonly freeze-dried. These include veal, lamb, pork, beef fat, lean beef, and the white and dark meat of chicken. By taking several measurements on each meat or fat, an equilibrium vapor pressure-temperature curve will be established. These results will be plotted on semi-logarithmic paper and by using the Clausius-Clapeyron equation, the latent heats of sublimation will be determined.

The scope of the analytical work will include a comprehensive analysis coupling the heat transfer through the dried and frozen regions with the mass transfer of vapor through the dried region. Bulk and diffusional flow will be studied in the continuum, transition, and free-molecule flow regimes. The validity of the analysis will be checked by comparing the results with experimental data previously presented for drying of beef.

CHAPTER II

THEORETICAL ANALYSES

General

Freeze-drying is assumed to take place as shown in Figure 1. As drying proceeds, a dried layer forms and is distinctly separated from the frozen layer of the product. The interface thickness between the dried and frozen layers has been measured during drying of beef by Hatcher (26) and found to be less than 5 mm thick. Hatcher also found that after the phase front passed a specific point in the meat, there was no more than a 3 per cent variation in the moisture content there for the remainder of the process. In addition, there was less than a 3 per cent change in the moisture content of the frozen section until the passage of the phase front. Now some foods like meats have a construction similar to wood in that they have a grain growth in a certain direction. This grain or fiber direction is usually oriented parallel to the heat and vapor transport, as this allows the fastest drying time. The reason for this is that the thermal conductivity of the product is a maximum parallel to the grain, and also this path offers the least resistance to vapor flow. The pore structure of the dried region is therefore such that there is a complex path in one general direction which can be idealized as a tortuous bundle of capillary tubes of non-uniform cross section. The heat required for sublimation may be transferred by conduction through the porous dried layer, or it may be

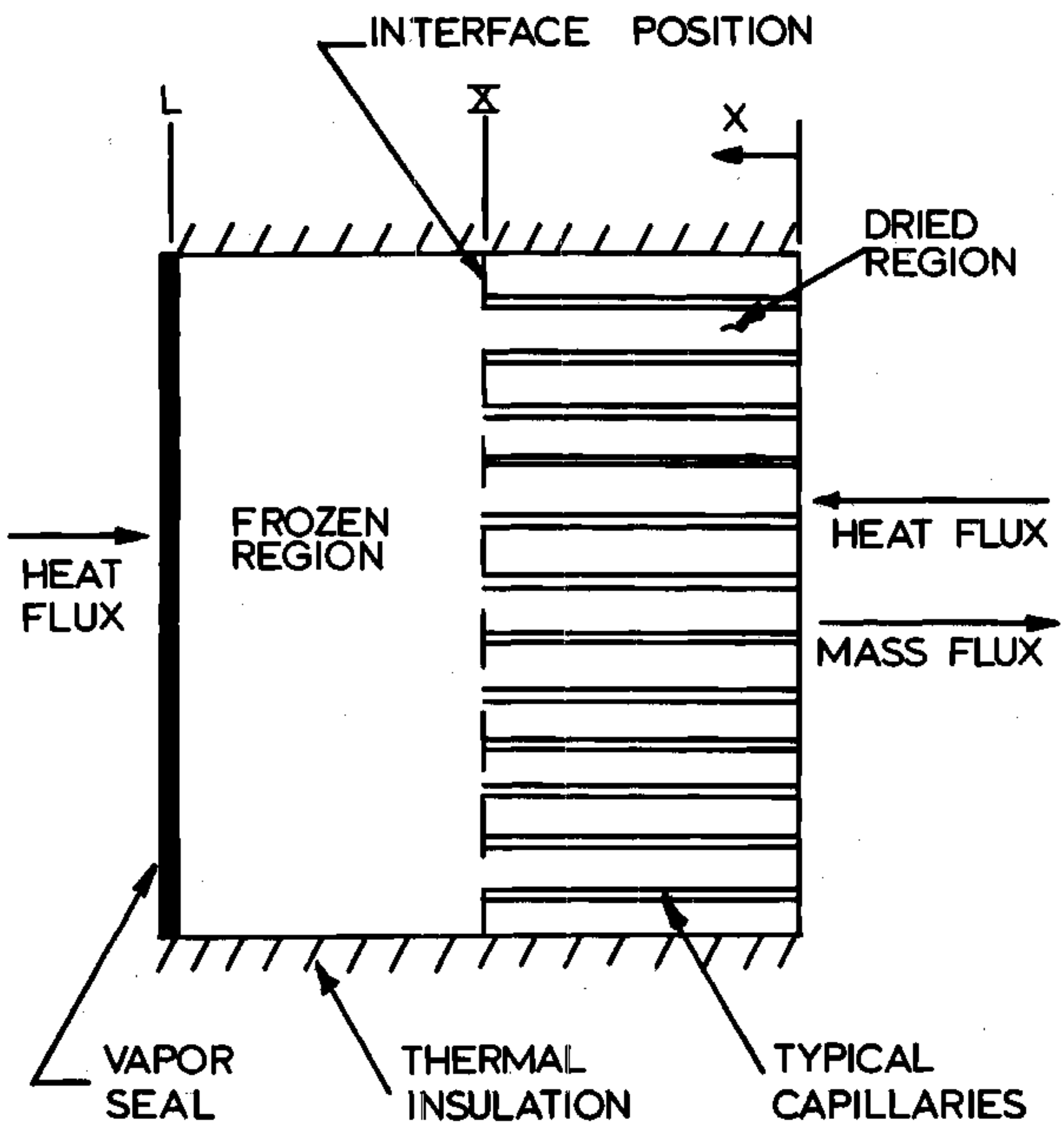

Figure 1. Model of Freeze-Drying Process.

conducted through the frozen layer, or it may be conducted through both. The sublimated vapor flows through the dried layer under the influence of both a total pressure gradient and a partial pressure gradient. If the total chamber pressure is low compared to the equilibrium vapor pressure of the frozen product, the primary driving force for the vapor flow will be a total pressure gradient. However, if the chamber pressure is approximately equal to the interface pressure, the primary driving force will be a partial pressure gradient or concentration gradient of the water vapor. The model described above can easily be adapted to the special case where there is equal drying from both sides by simply letting $x = L$ be the center line of the product and setting the heat transfer through the frozen layer equal to zero.

The theoretical analyses involve solving the energy equation for both the dried and frozen regions, solving the continuity and momentum equations for the vapor flux in the continuum, transition, and the free-molecule flow regimes, and combining the equations to determine how the interface temperature varies throughout the drying process. With the interface temperature established, equations will be derived for both the drying rate and the drying time as a function of the sample thickness and drying regime.

All transport properties which are pressure and/or temperature dependent will be evaluated at the vacuum chamber pressure and mean temperature, respectively. Thus, for a given vacuum chamber pressure and fixed boundary temperatures, all transport properties will be treated as constants. In addition, at any point in the dried layer, the vapor temperature and the dried food product temperature are assumed equal.

This has been confirmed experimentally (32).

All of the energy, continuity, and momentum equations used will be one-dimensional and "quasi-steady." This implies that both the heat and mass fluxes are zero except in the x-direction, and that the time rates of change of properties are assumed negligible in comparison to the space rate of change. This assumption appears to be valid since it takes approximately 30 hours to dry a slab of beef 1-1/2 inches thick. In addition, Dyer (9) solved the "exact" and "quasi-steady" energy equations assuming that the interface temperature remained constant. He used the results to get drying times and found that the two separate methods differed by only 2 per cent.

The type of flow in the capillary channels depends upon the degree to which the vapor is rarefied. The flow is free-molecule for highly rarefied gases. In this type of flow, viscosity does not play a role, and the regime is characterized by the fact that collisions of the air and water vapor molecules with the wall are large in number in comparison to intermolecular collisions. For more dense gases the flow is Poiseuille flow for laminar conditions, with the well-known parabolic velocity distribution and zero wall velocity. In this regime, wall collisions are insignificant with respect to intermolecular collisions. For gases which are only moderately rarefied, the flow is known as transition flow, in which there is a finite velocity at the wall due to the "slip flow" of molecules along the wall. In this type of flow viscosity also plays a role, and both types of collisions are significant.

The particular type of flow depends upon the ratio of the mean-free path of the vapor molecules to the capillary diameter which is known as the Knudsen number.

$$Kn = \lambda/2r_c \tag{1}$$

The type of flow for different ranges of the Knudsen number is given by the following

$2 < Kn$	Free-molecule flow
$.01 \leq Kn \leq 2$	Transition flow
$Kn < .01$	Continuum flow

Energy Equations

The equation governing the heat transfer in the dried region is derived in Appendix A and is given by

$$\frac{d^2T_I}{dx^2} + \frac{C_p\rho_i\sigma}{k_I}\frac{dX}{dt}\frac{dT_I}{dx} = 0 \tag{2}$$

The first term represents the heat transfer by pure conduction and the second term represents the contribution of the mass transfer to the temperature distribution. If the second term were small in comparison to the first (i.e., the mass transfer rate was small), the governing equation would simply be the same as that for one-dimensional conduction in a slab, the solution being a linear temperature profile. Therefore, the mass transfer accounts for the nonlinearity of the temperature profile in the dried region.

The boundary conditions applied to Equation (2) are

$$T_I = T_0 \qquad \text{at } x = 0 \tag{3}$$

$$T_I = T_X \qquad \text{at } x = X \tag{4}$$

The solution to Equation (2) is given by Schneider (32) and takes the form

$$\frac{T_I - T_0}{T_X - T_0} = \frac{1 - e^{-\beta x}}{1 - e^{-\beta X}} \tag{5}$$

where

$$\beta = \frac{\rho_i \; \sigma \; C_p}{k_I} \; \frac{dX}{dt} \tag{6}$$

It will be seen later in the theoretical analyses that T_X actually varies during the drying process if heat is conducted through both the dried and frozen layers. Since the interface movement is extremely slow, it will be assumed that Equation (5) still adequately represents the temperature distribution in the dried region at any instant.

The equation governing the heat transfer in the frozen region is

$$\frac{d^2T_{II}}{dx^2} = 0 \tag{7}$$

The boundary conditions for Equation (7) are

$$T_{II} = T_X \qquad \text{at } x = X \tag{8}$$

$$T_{II} = T_L \qquad \text{at } x = L \tag{9}$$

The solution to Equation (7) is

$$\frac{T_{II} - T_L}{T_X - T_L} = \frac{x - L}{X - L} \tag{10}$$

Now it will become evident when relations are being developed for the interface temperature and the drying time, that the above temperature distribution in the dried region cannot be used if closed form equations are desired. The reason is that the interface position and its derivative both appear in the argument of the exponential term. Some approximation to the above profile must then be used. Dyer and Sunderland (14) expanded the exponential terms into series and neglected all terms of higher order than one. This amounts to the same thing as assuming a linear profile in the dried region. The approach used in this thesis will be similar to that used by Goodman (37) and (38) where he studies heat transfer problems using an integral technique.

A second order temperature profile is assumed in the dried region and the boundary conditions used to solve for the three constants are given by Equations (3) and (4) and also a heat balance at the interface.

$$\Delta H \; \rho_i \; \sigma \frac{dX}{dt} = k_{II} \left. \frac{dT_{II}}{dx} \right|_{x=X} - k_I \left. \frac{dT_I}{dx} \right|_{x=X} \qquad (11)$$

The two terms on the right side of the equation represent the energy conducted to the interface through both regions, and the left side of the equation represents the energy used for the sublimation of the frozen liquid. The result of applying Equations (3), (4), (10), and (11) to an equation of the form

$$T_I = a' + b'x + c'x^2 \qquad (12)$$

is

$$\frac{T_I - T_0}{T_X - T_0} = \frac{x}{X} + \left[1 - \frac{x}{X}\right] \left[\frac{x}{X} - F_2 x\right] \qquad (13)$$

where

$$F_2 = \frac{\Delta H \; \rho_i \; \sigma \frac{dX}{dt} - k_{II} \left[\frac{T_X - T_L}{X - L}\right]}{\left[T_0 - T_X\right] k_I} \qquad (14)$$

Continuity Equations

For either the sublimated vapor or air, from the conservation of mass for steady, one-dimensional flow, it follows that the flow rate is constant. Since for the air species the flow rate is zero at the interface, it is zero throughout the entire dried layer.

Momentum Equations

Free-Molecule Flow Regime

The momentum equation for a gaseous mixture in the free-molecule flow regime, in a capillary tube of uniform cross-section and length is given by Present (30)

$$N = \frac{2\ r_c}{3}\ \bar{v}\ \frac{\Delta P}{\ell RT} \tag{15}$$

Equation (15) was derived for isothermal flow. Therefore, in order to use this equation, it will be assumed that the temperature gradient in the dried region has no effect on the flow rate, and the vapor properties can be evaluated at an average temperature. Dyer (9) showed both experimentally and analytically that this thermal transpiration effect is negligible in the transition regime. It is shown in Appendix B that the effect is also negligible in the free-molecule and continuum regimes. According to Present, if a free-molecule flow of a binary gas mixture takes place, the component gases will diffuse along the tube independently of each other and Equation (15) can be applied to each gas separately, if ΔP is interpreted as the partial pressure drop.

Several corrections must be made to Equation (15) in order to make it applicable to flow in porous media. The flow rate as given in Equation (15) is per unit area of the capillary tube. In order to convert the flow to per unit surface area of the food sample, the equation must be multiplied by the porosity, which is defined as the ratio of the pore volume to the total food volume. The vapor actually travels a longer, tortuous path through the food sample, so the equation is corrected by multiplying the dried region thickness by a tortuosity factor τ. In addition, a first order correction for the nonroundness and other irregularities of the capillaries can be made by multiplying the equation by a constant Γ. The temperature of the vapor in Equation (15) will be taken as the average temperature between the interface and the surface. Therefore, the momentum equation representing the flow rate of water vapor in the free-molecule flow regime is given by

$$N_w = \frac{4\ r_c\ \Gamma\ \bar{v}_w\ \sigma\ [\bar{P}_{w0} - \bar{P}_{wX}]}{3\ \tau\ X\ R\ [T_0 + T_X]} \tag{16}$$

<u>Continuum Flow Regime</u>

The momentum equation for the gaseous mixture is derived from Darcy's law (31) for flow through a porous material

$$N = -\frac{\rho}{\eta}\epsilon_D\frac{\partial P}{\partial x} \tag{17}$$

The law states that the flow rate is proportional to the density and pressure gradient and inversely proportional to the viscosity.

The proportionality constant ϵ_D is called permeability and is usually experimentally determined for the material under study. If the equation is integrated, again assuming isothermal flow, and the symbols are changed to represent the parameters of the dried region of the freeze-drying model, the equation takes the form

$$N_w = \frac{\rho \ \epsilon_D \left[P_0 - P_X\right] g_c}{\mu \ X} \tag{18}$$

In the analytical model, the pressure quantities that are assumed known are the total chamber pressure, P_0, partial pressure of the water vapor in the chamber, $\bar{P}_{w0}$, and the partial pressure of the water vapor at the interface, $\bar{P}_{wX}$. The latter quantity is assumed to be the equilibrium vapor pressure of the frozen solid at the temperature that exists at the interface. This relationship will be determined for several frozen meats in the experimental phase of this thesis. Note that in Equation (18), the total pressure at the interface appears and is therefore an unknown quantity. It must be eliminated by use of an additional momentum equation for this regime.

Johnson (39) suggests that the steady diffusion equation for continuous transport can be interpreted as an equation of motion of one of the constituent gases. Dyer and Sunderland (13) adapted the suggestion to give the following differential equation of motion for the sublimated vapor

$$\bar{P}_w \frac{dP}{P} - d\bar{P}_w = \frac{KT}{n\,D_{aw}} n_a\, n_w\, [u_w - u_a]\, dx \qquad (19)$$

The first term in Equation (19) is the total external force per unit area on the vapor component due to the total pressure gradient, the second term is the force per unit area on the vapor component due to a partial pressure gradient, and the third term is the momentum transfer to the vapor component due to collisions with the air. Equation (19) is valid for the case of combined bulk and diffusional flow in the continuum regime, under the condition of a non-uniform total pressure gradient. The main assumption implied in the derivation of the above equation is that since a small total pressure gradient exists, the Maxwell-Boltzmann distribution function evaluated at the average pressure is very nearly the same as for the uniform pressure case. Therefore, the third term in Equation (19), which was originally for the uniform pressure case, still adequately describes the momentum exchange between the two constituents.

Now, by using the definition of concentration, the left side of Equation (19) has the form

$$\bar{P}_w \frac{dP}{P} - d\bar{P}_w = -P\, d\left[\frac{\bar{P}_w}{P}\right] = -P\, dy_w \qquad (20)$$

By combining Equations (19) and (20)

$$-\frac{P}{\bar{R}T}\,dy_w = \frac{\bar{N}_w\left[n_a - n_w\,\dfrac{\bar{N}_a}{\bar{N}_w}\right]}{n\;D_{aw}}\,dx \tag{21}$$

From Dalton's law of partial pressures,

$$y_w + y_a = 1.0 \tag{22}$$

by defining a,

$$a = 1 + \frac{\bar{N}_a}{\bar{N}_w} \tag{23}$$

by making use of the definition of y_w and y_a, and by combining Equations (21), (22), and (23), the result is

$$-\frac{P}{\bar{R}T}\,dy_w = \frac{\bar{N}_w}{D_{aw}}\,[1 - ay_w]\,dx \tag{24}$$

For the small pressure gradients considered, it is assumed that P can be expanded in a Taylor series neglecting the second-order terms to give

$$P = P_O + \frac{dP}{dx}\,x \tag{25}$$

Also, $\frac{dP}{dx}$ is approximated by $\frac{\Delta P}{X}$ so that

$$P = P_0 + \frac{\Delta P}{X} x \tag{26}$$

From kinetic theory and again assuming isothermal flow

$$\frac{P\ D_{aw}}{\bar{R}\ T} = C_1 \tag{27}$$

where C_1 is a constant. Combining Equations (24), (26), and (27) gives

$$\frac{dy_w}{dx} - \frac{\bar{N}_w\ a}{C_1} y_w = - \frac{\bar{N}_w}{C_1} \tag{28}$$

By solving the differential equation and applying the boundary conditions,

$$y_w = y_{w0} \qquad \text{at } x = 0 \tag{29}$$

and

$$y_w = y_{wX} \qquad \text{at } x = X \tag{30}$$

it can be shown that

$$\bar{N}_w = \frac{P\ D_{aw}}{\bar{R}TaX} \ln \left[\frac{\frac{1}{a} - y_{wX}}{\frac{1}{a} - y_{w0}}\right] \tag{31}$$

Now by applying the conservation of mass of the air species, $\bar{N}_a = 0$

$$a = 1 \tag{32}$$

the result is

$$N_w = \frac{P\ D_{aw}}{RTX} \ln \left[\frac{1 - y_{wX}}{1 - y_{w0}}\right] \tag{33}$$

Equation (33) correctly represents the flow if the diffusion coefficient is the effective diffusion coefficient for flow in a porous medium. In applying the theory, a value for $[D_{aw}]_e$ of 1/3 the value for free diffusion in air at atmospheric pressure, as suggested by Harper and Chichester (25), will be used.

Now Equations (18) and (33) can be combined to eliminate the total pressure at the interface.

$$N_w = \frac{\rho\ [D_{aw}]_e}{X} \ln \left[\frac{1 - \dfrac{\bar{P}_{wX}}{P_0 - [\mu\ X\ N_w/\rho\ \varepsilon_D\ g_c]}}{1 - \dfrac{\bar{P}_{w0}}{P_0}}\right] \tag{34}$$

Transition Flow Regime

The momentum equation for the gaseous mixture is derived in Appendix C and was previously derived by Dyer (9).

$$N_w = \frac{\rho\ \varepsilon\ [P_O - P_X]\ g_c}{\mu\ X} \tag{35}$$

Note, the equation takes the same form as that of the continuum regime with the exception that ε is now the permeability of the porous solid filled with gases at a pressure in the transition regime. From molecular theory it can be shown that the flow rate in the transition regime will not be directly proportional to the pressure difference as seems to be indicated by Equation (35). However, this is consistent with the present analysis since the permeability itself contains pressure difference terms.

As in the continuum regime, the total pressure must be eliminated from Equation (35) by the use of an additional momentum equation. Dyer and Sunderland (13) further extended the use of the steady diffusion equation by presenting the following differential equation of motion for the sublimated vapor in the transition regime

$$\frac{\bar{P}_w}{P}\,dP - d\bar{P}_w = \frac{KT}{n\ D_{aw}}\,n_a\ n_w\ [u_w - u_a]\ dx$$

$$+ S\ m_w\ u_w\ n_w\ \bar{v}_w\ \frac{dx}{2\ r_c} \tag{36}$$

The first three terms are the same as before and the fourth term has been added to account for the momentum exchange occurring when vapor molecules collide with the wall.

Now, introducing the definition of Knudsen's diffusion coefficient,

$$D_{kw} = \frac{2}{3} r_c \bar{v}_w \tag{37}$$

and combining Equations (20), (36), and (37), the result is

$$-\frac{P\, dy_w}{\bar{R}T} = \bar{N}_w\, dx \left[\frac{n_a - n_w \dfrac{\bar{N}_a}{\bar{N}_w}}{n\, D_{aw}} + \frac{8\, S}{3\pi\, D_{kw}}\right] \tag{38}$$

Using Dalton's law of partial pressures along with the definitions of a, y_w, and y_a

$$\bar{N}_w\, dx = \frac{-\dfrac{P\, dy_w}{\bar{R}T}\, D_{aw}}{1 - ay_w + \dfrac{8\, S\, D_{aw}}{3\, \pi\, D_{kw}}} \tag{39}$$

The Taylor series approximation of the pressure (Equation (26)) and Equation (27) are introduced to give the following differential equation for the water vapor concentration

$$\frac{dy_w}{dx} - \frac{\bar{N}_w\, a}{C_1} y_w = -\frac{\bar{N}_w}{C_1}\left[1 + \frac{8S}{3\, \pi\, D_{kw}}\ \frac{C_1 \bar{R}T}{P_0 + \dfrac{\Delta P}{X} x}\right] \tag{40}$$

A solution to this differential equation is presented by Dyer and Sunderland (13). However, the solution is a series solution and cannot be used in combination with the other equations to give closed form relations for the interface temperature and the drying time. The approach to solve Equation (40) in this thesis will be to use an integral technique. A linear concentration profile of the water vapor is assumed

$$y_w = y_{w0} + \frac{y_{wX} - y_{w0}}{X}\, x \qquad (41)$$

and Equation (40) is integrated term by term to obtain an algebraic equation for the flux of water vapor.

$$\int_0^X \frac{dy_w}{dx}\, dx - \int_0^X \frac{\bar{N}_w\, a\, y_w}{C_1}\, dx \qquad (42)$$

$$= - \int_0^X \frac{\bar{N}_w}{C_1} \left[1 + \frac{8\ S}{3\ \pi\ D_{kw}} \ \frac{C_1 \bar{R} T}{P_0 + \frac{\Delta P}{X} x} \right] dx$$

The result is

$$\left[y_{wX} - y_{w0} \right] - \frac{\bar{N}_w\, a}{C_1} \left[y_{w0}\, X + \frac{y_{wX} - y_{w0}}{X}\ \frac{X^2}{2} \right] \qquad (43)$$

$$= - \frac{\bar{N}_w}{C_1} X - \frac{\bar{N}_w\ 8\ S\ \bar{R} T}{3\ \pi\ D_{kw}}\ \frac{X}{\Delta P} \ln \left[\frac{P_0 + \Delta P}{P_0} \right]$$

After rearranging

$$\bar{N}_w = \frac{y_{wX} - y_{w0}}{\frac{a\ X}{C_1}\left[\frac{y_{wo} + y_{wX}}{2}\right] - \frac{X}{C_1} - \frac{8\ S\ \bar{R}T}{3\ \pi\ D_{kw}}\frac{X}{\Delta P}\ln\left[\frac{P_0 + \Delta P}{P_0}\right]} \tag{44}$$

For the particular model under consideration, it has already been pointed out that a = 1. In addition, completely diffuse momentum transfer will be assumed giving S = 1. Although S has not been measured for the present case, data presented by Carman (31) for similar cases indicate that this assumption is relatively accurate. If the definition of C_1 is also inserted into Equation (44), it takes the form

$$N_w = \frac{\rho}{X}\,\frac{y_{wX} - y_{w0}}{\frac{1}{D_{aw}}\left[\frac{y_{w0} + y_{wX}}{2} - 1\right] - \frac{8}{3\ \pi\ D_{kw}}\frac{P_m}{\Delta P}\ln\left[1 + \frac{\Delta P}{P_0}\right]} \tag{45}$$

If the following approximation is made,

$$\frac{P_m}{\Delta P}\ln\left[1 + \frac{\Delta P}{P_0}\right] = \frac{P_m}{\Delta P}\left[\frac{\Delta P}{P_0} - \frac{1}{2}\left[\frac{\Delta P}{P_0}\right]^2 + \frac{1}{3}\left[\frac{\Delta P}{P_0}\right]^3 - \cdots\right] \tag{46}$$

and all of the terms of higher order are neglected due to the small pressure drop considered,

$$\frac{P_m}{\Delta P} \ln \left[1 + \frac{\Delta P}{P_0}\right] = \frac{P_m}{\Delta P} \frac{\Delta P}{P_0} \approx 1 \tag{47}$$

Equation (45) takes the following form

$$N_w = \frac{\rho}{X} \frac{y_{wX} - y_{w0}}{\frac{1}{D_{aw}}\left[\frac{y_{wo} + y_{wX}}{2} - 1\right] - \frac{8}{3\ \pi\ D_{kw}}} \tag{48}$$

Just as was the case in the continuum regime, Equation (48) can be correctly applied if D_{aw} and D_{kw} are effective coefficients. Again, a value for $[D_{aw}]_e$ of 1/3 the value for free diffusion in air at atmospheric pressure will be used. The effective value of the Knudsen diffusion coefficient will be obtained by a formula suggested by Scott and Dullien (35)

$$\frac{[D_{aw}]_e}{[D_{kw}]_e} \approx \frac{D_{aw}}{D_{kw}} \tag{49}$$

It is convenient to define an effective diffusion coefficient for the transition regime by means of the following equation

$$N_w = \frac{\rho[D_t]_e}{X} \ln \left[\frac{1 - y_{wX}}{1 - y_{wO}}\right] \tag{50}$$

By combining Equations (50) and (48), the value of the effective average diffusion coefficient is given by

$$[D_t]_e = \frac{y_{wX} - y_{w0}}{\ln\left[\frac{1 - y_{wX}}{1 - y_{w0}}\right]} \quad \frac{1}{\frac{1}{[D_{aw}]_e}\left[\frac{y_{w0} + y_{wX}}{2} - 1\right] - \frac{8}{3\,\pi\,[D_{kw}]_e}} \tag{51}$$

Pollard and Present (40) give the following simple equation for calculating the transition regime diffusion coefficient. They state that it gives almost the same values as their more complex expression, both being derived for the special case of counter diffusing gases having equal molecular weights.

$$[D_t]_e = \frac{1}{\frac{1}{[D_{aw}]_e} + \frac{1}{[D_{kw}]_e}} \tag{52}$$

The similarity between Equations (51) and (52) can be immediately seen.

Harper and Chichester (25) state that experimental thermal conductivity data for gases in the transition regime can be used to predict the product of pressure and diffusion coefficient, $P\ D_{aw}$. They point out that for the continuum flow regime, simple kinetic theory shows that both the thermal conductivity and $P\ D_{aw}$ are independent of pressure. Furthermore, in the transition regime, due to the analogy between heat and mass transfer, both quantities should decrease in a similar manner with decreasing pressure. In reference (13), it is pointed out that the two mechanisms of transfer are not exactly analogous in the continuum regime, and therefore would probably not be in the transition regime either.

Their reasoning seems to be correct in view of the numerical results obtained by the two separate methods. Table 1 contains Dyer and Sunderland's experimentally determined effective average diffusion coefficients for freeze-dried beef. In addition, values are also presented that were calculated by Dyer and Sunderland's series solution, Equation (51) of this thesis, and the theory of Harper and Chichester. As can be seen, the exact and integral solutions give favorable results and those of Harper and Chichester are somewhat off.

Now Equations (35) and (48) can be combined to eliminate the total pressure at the interface.

$$N_w = \frac{\rho}{X} \frac{\dfrac{\bar{P}_{wX}}{P_0 - \mu X N_w/\rho \varepsilon g_c} - \dfrac{\bar{P}_{w0}}{P_0}}{\dfrac{1}{[D_{aw}]_e}\left[\dfrac{\dfrac{\bar{P}_{w0}}{P_0} + \dfrac{\bar{P}_{wX}}{P_0 - \mu X N_w/\rho \varepsilon g_c}}{2} - 1\right] - \dfrac{8}{3\pi [D_{kw}]_e}} \tag{53}$$

Interface Temperature

An energy balance at the interface is used to couple the energy and momentum equations to get the interface temperature relations.

$$\left[k_{II} \frac{dT_{II}}{dx}\bigg|_{x=X}\right] - \left[k_I \frac{dT_I}{dx}\bigg|_{x=0} - C_p N_w [T_0 - T_X]\right] = [-N_w \Delta H] \tag{54}$$

The first term in brackets is the energy input to the interface from the

Table 1. Effective Average Diffusion Coefficients for Freeze-Dried Beef

Average Pressure $(P_O + P_X)/2$ (torr)	y_{wX}	y_{wO}	$[D_t]_e$ Obtained Experimentally (ft^2/s)	$[D_t]_e$ Obtained by Theory--Integral Solution (ft^2/s)	$[D_t]_e$ Obtained by Theory--Exact Solution (ft^2/s)	$[D_t]_e$ Calculated by Theory of Reference (25) (ft^2/s)
1.44	0.805	0.585	0.015	0.0152	0.017	0.031
1.58	0.77	0.565	0.019	0.0156	0.018	0.028
1.64	0.856	0.57	0.012	0.0133	0.015	0.028
2.25	0.813	0.52	0.010	0.0128	0.010	0.021
2.28	0.683	0.55	0.017	0.0145	0.015	0.020

frozen region, the second term the energy input to the interface from the dried region, and the last term is the energy required to sublimate the mass at the interface. If the temperature gradients are obtained from Equations (10) and (13), and Equation (54) is slightly rearranged, the result is

$$\frac{\dfrac{k_{II}[T_X - T_L]}{X - L} + \dfrac{k_I[T_O - T_X]}{X}}{\Delta H + \dfrac{C_p}{2}[T_O - T_X]} = -N_W \tag{55}$$

After substitution of the appropriate flow equation (Equation (16) for the free-molecule regime, Equation (34) for the continuum regime, and Equation (53) for the transition regime) into Equation (55), it was found that the interface relationship had the same form for all three regimes.

$$\frac{X}{X - L} = \frac{k_I[T_X - T_O] + \left[\Delta H + \dfrac{C_p}{2}[T_O - T_X]\right] Q}{k_{II}[T_X - T_L]} \tag{56}$$

where expressions for Q are given below for the three flow regimes. For the free-molecule flow regime,

$$Q = [\bar{P}_{wX} - \bar{P}_{wO}]\, \frac{2}{3}\, r_c\, \frac{\Gamma}{\dagger}\, \bar{v}_w\, \frac{\sigma}{R}\, \frac{2}{T_O + T_X} \tag{57}$$

In the transition flow regime,

$$Q = \frac{R_3 - [4\ C_2\ R_2 + R_3{}^2]^{1/2}}{2\ C_2} \tag{58}$$

where

$$C_2 = \frac{\bar{P}_{w0}\ \mu}{P_0\ \rho\ \varepsilon\ 2\ [D_{aw}]_e} - \frac{\mu}{\rho\ \varepsilon\ [D_{aw}]_e} - \frac{8\ \mu}{3\ \pi\ \rho\ \varepsilon\ [D_{kw}]_e} \tag{59}$$

$$R_2 = \rho\ [\bar{P}_{w0} - \bar{P}_{wX}]\ g_c \tag{60}$$

$$R_3 = g_c \left[\frac{P_0}{[D_{aw}]_e} + \frac{8\ P_0}{3\ \pi [D_{kw}]_e} + \frac{\bar{P}_{w0}\ \mu}{P_0\ \varepsilon\ g_c} - \frac{\bar{P}_{w0} + \bar{P}_{wX}}{2[D_{aw}]_e} \right] \tag{61}$$

For the continuum flow regime,

$$Q = \frac{-B + [B^2 - 4\ A\ C]^{1/2}}{2\ A} \tag{62}$$

where

$$A = \frac{2\ P_0\ \mu}{\rho\ \varepsilon_D\ g_c} - \frac{\bar{P}_{w0}\ \mu}{\rho\ \varepsilon_D\ g_c} \tag{63}$$

$$B = 2\ P_0{}^2 - \bar{P}_{w0}\ P_0 - \bar{P}_{wX}\ P_0 + \frac{\bar{P}_{w0}\ \mu}{\rho\ \varepsilon_D\ g_c}\ 2\rho [D_{aw}]_e \tag{64}$$

$$C = 2\rho [D_{aw}]_e\ [\bar{P}_{w0}\ P_0 - \bar{P}_{wX}\ P_0] \tag{65}$$

In order to obtain the closed form relationship (Equation 56) for the interface temperature, certain approximations had to be made to the flow equations in the transition and continuum regimes. The approximations in the transition regime have already been given in the form of Equations (46) and (47). The approximations in the continuum regime along with an estimation of the error for both regimes is given in Appendix D.

Special Case of No Back Face Heating

For the special case where the back face is perfectly insulated or there is equal drying from both sides, Equation (55) takes the form

$$\frac{k_I[T_O - T_X]}{\Delta H + \frac{C_p}{2}[T_O - T_X]} = -N_w X \tag{66}$$

If Equation (16) is inserted into Equation (66) the result for the free-molecule flow regime is

$$\frac{k_I[T_O - T_X]}{\Delta H + \frac{C_p}{2}[T_O - T_X]} = \frac{4\ r_c\ \Gamma\ \vec{v}_w\ \sigma[\bar{P}_{wX} - \bar{P}_{wO}]}{3\ \tau\ R[T_O + T_X]} \tag{67}$$

Note that the interface position X does not appear and T_X is therefore a constant throughout the process. Equation (67) could be solved directly for T_X except that it appears in the argument of an exponential term which is the form of the equation for $\bar{P}_{wX}$. The interface temperature can be solved for by graphically plotting the left and right side of Equation (67) and noting the value of T_X at the intersection point.

In the continuum flow regime, the interface temperature again is seen to be constant from the relation resulting from the combination of Equations (66) and (34).

$$\frac{k_I[T_0 - T_X]}{\Delta H + \frac{C_p}{2}[T_0 - T_X]} = \rho[D_{aw}]_e \ln\left[\frac{1 - \frac{\bar{P}_{w0}}{P_0}}{1 - \frac{\bar{P}_{wX}}{P_X}}\right] \tag{68}$$

where

$$P_X = P_0 + \frac{\mu}{\rho\ \epsilon_D\ g_c}\left[\frac{k_I[T_0 - T_X]}{\Delta H + \frac{C_p}{2}[T_0 - T_X]}\right] \tag{69}$$

The interface temperature can be solved for as before, graphically.

As with the other two regimes, the interface temperature in the transition flow regime is constant and is solved for from

$$\frac{k_I[T_0 - T_X]}{\Delta H + \frac{C_p}{2}[T_0 - T_X]} = \rho \frac{\frac{\bar{P}_{w0}}{P_0} - \frac{\bar{P}_{wX}}{P_X}}{\frac{1}{[D_{aw}]_e}\left[\frac{\frac{\bar{P}_{w0}}{P_0} + \frac{\bar{P}_{wX}}{P_X}}{2} - 1\right] - \frac{8}{3\ \pi[D_{kw}]_e}} \tag{70}$$

where

$$P_X = P_0 + \frac{\mu}{\rho\ \varepsilon\ g_c}\left[\frac{k_I[T_0 - T_X]}{\Delta H + \frac{C_p}{2}[T_0 - T_X]}\right] \tag{71}$$

Drying Time Equations

The differential equation describing the interface movement is obtained by using the energy balance at the interface (Equation (54)) and combining it with a mass balance at the interface.

$$-N_w = \rho_i\ \sigma\ \frac{dX}{dt} \tag{72}$$

The right-hand side of Equation (72) represents the mass rate of sublimation of the frozen liquid, and the left-hand side represents the mass flux of the resulting vapor which must flow through the capillary channels of the porous dried layer to the free surface. The resulting differential equation takes the form

$$\frac{dX}{dt} = \frac{\frac{k_{II}[T_X - T_L]}{X - L} + \frac{k_I[T_0 - T_X]}{X}}{\rho_i\ \sigma\left[\Delta H + \frac{C_p}{2}[T_0 - T_X]\right]} \tag{73}$$

with boundary condition

$$X = 0 \quad \text{at} \quad t = 0 \tag{74}$$

Before Equation (73) can be solved, a relationship of T_X as a function of X must be substituted into the equation. The interface temperature-position relation is given by Equation (56) and is the inverse of what is needed here. Equation (56) will have to be solved, a plot of T_X versus X will have to be made, and the least squares method used to express T_X as a polynomial function of X.

If it is possible to express T_X by

$$T_X = r_o + r_1 X \tag{75}$$

then the differential equation can be solved in closed form to give

$$t = \frac{C_8}{C_5}\frac{X^2}{2} + \frac{C_6}{C_5} X \tag{76}$$

$$+ \frac{C_7\ C_5 - C_6\ C_4}{2\ C_5^{\ 2}} \ln\left[\frac{C_5}{C_3} X^2 + \frac{C_4}{C_3} X + 1\right]$$

$$+ \frac{C_6\ C_4^{\ 2} - 2\ C_6\ C_3\ C_5 - C_7\ C_4\ C_5}{2\ C_5^{\ 2}[C_4^{\ 2} - 2\ C_3\ C_5]^{1/2}} \ln\left[\frac{\dfrac{2\ C_5\ X + C_4 - [C_4^{\ 2} - 4\ C_3\ C_5]^{1/2}}{2\ C_5\ X + C_4 + [C_4^{\ 2} - 4\ C_3\ C_5]^{1/2}}}{\dfrac{C_4 - [C_4^{\ 2} - 4\ C_3\ C_5]^{1/2}}{C_4 + [C_4^{\ 2} - 4\ C_3\ C_5]^{1/2}}}\right]$$

where

$$C_3 = L\ k_I[r_o - T_O] \tag{77}$$

$$C_4 = k_{II}[r_o - T_L] + k_I r_1 L - k_I[r_o - T_0] \tag{78}$$

$$C_5 = r_1[k_{II} - k_I] \tag{79}$$

$$C_6 = \frac{\rho_i \sigma}{2}\left[2\,\Delta H + C_p r_1 L - C_p[r_o - T_0] + \frac{C_p k_{II}[r_o - T_L]}{[k_{II} - k_I]}\right. \tag{80}$$

$$\left. + \frac{C_p k_I r_1 L}{[k_{II} - k_I]} - \frac{C_p k_I[r_o - T_0]}{[k_{II} - k_I]}\right]$$

$$C_7 = \frac{\rho_i \sigma}{2} L\left[C_p[r_o - T_0] - 2\,\Delta H + \frac{C_p k_I[r_o - T_0]}{[k_{II} - k_I]}\right] \tag{81}$$

$$C_8 = -\frac{\rho_i \sigma}{2} C_p r_1 \tag{82}$$

The total time required for drying can be determined by substitution of $X = L$ into Equation (76).

For the case where Equation (75) does not adequately describe the interface relation an equation of higher order must be used, and the differential equation must be integrated numerically. The numerical technique used in this thesis is the following:

(1) Values of T_X are calculated for small increments of X from the polynomial approximation to the interface relation.

(2) Equation (55) is used to calculate the value of $-N_w$ at each incremental step of X.

(3) Equation (72) is approximated by

$$-N_w \simeq \rho_i \, \sigma \, \frac{\Delta X}{\Delta t} \tag{83}$$

(4) Equation (83) is used to calculate the time required to make the incremental step in X.

$$\Delta t = \rho_i \, \sigma \, \frac{\Delta X}{-N_w} \tag{84}$$

(5) All of the increments of time are added to obtain the total drying time.

It should be noted that since the properties change slowly with time, relatively large incremental changes in interface position can be used with good approximation.

Special Case of No Back Face Heating

For the special case where the back face is perfectly insulated or there is equal drying from both sides, Equation (73) takes the form

$$\frac{dX}{dt} = \frac{\dfrac{k_I[T_O - T_X]}{X}}{\rho_i \, \sigma \left[\Delta H + \dfrac{C_p}{2}[T_O - T_X]\right]} \tag{85}$$

As was pointed out by Equations (67), (68), and (70), the interface temperature remains constant for this case. Therefore, Equation (85) is easily integrated to give

$$t = \frac{\rho_i \; \sigma \left[\Delta H + \frac{C_p}{2} [T_0 - T_X] \right]}{k_I [T_0 - T_X]} \; \frac{X^2}{2} \qquad (86)$$

The total drying time is obtained by setting X = L in Equation (86).

Alternate Approach

The momentum equations used in the analytical phase of this thesis have been dependent upon the flow regime in which the drying takes place. This in turn is dependent upon the pressure and the mean capillary diameter. Certainly in any porous media, the dimension of the void space is not uniform and only the average dimension can be determined. If the pressure is such that the flow seems to be near the boundary separating two regimes, flow of both regimes could very well be taking place. It would be very convenient if one flow equation valid for all the regimes could be used.

Huang, et al., (41) present a general solution of the linearized Boltzmann equation with the Bhatnagar-Gross-Krook model for the problem of a rarefied gas flowing between two parallel, infinite plates and based on the discrete ordinate method. They present an analytical expression for the nondimensional volume flow rate in the form of a double summation where any desired degree of accuracy can be obtained.

$$\bar{Q} = \frac{8}{\pi} \sum_{i=1}^{n} \sum_{\nu=1}^{n-1} H_i \, \bar{C}_\nu \, \frac{\sinh[1/2 \; P_\nu]}{P_\nu [1 - n_\nu \, \alpha_i^{\,2}]} + \frac{1}{12} \left[\frac{d}{\lambda} \right]^2 + \bar{T} \qquad (87)$$

The volume flow rate Q' is determined from

$$Q' = \bar{Q}\left[\frac{1}{2}\,\bar{K}\,d\right] \tag{88}$$

where

$$\bar{K} = \frac{1}{P_X}\frac{dP}{dx} \tag{89}$$

and d is the distance separating the parallel plates. It would seem to be a good approximation to equate d to the mean capillary diameter, which has already been determined for many porous media. From observing the calculations of Huang, et al., a value of at least n = 4 must be chosen to give the desired flow minimum that occurs in the transition regime, and simultaneously fairly accurate results in the free-molecule regime. Equation (87) would then contain 14 terms and 20 parameters that must be specified. If the modified quadrature is used (which gave the best results for Huang, et al.), the following equations are used to specify the 20 parameters

$$\alpha_1 = 0.133776447 \tag{90}$$

$$\alpha_2 = 0.624324689 \tag{91}$$

$$\alpha_3 = 1.342537825 \tag{92}$$

$$\alpha_4 = 2.262664477 \tag{93}$$

$$H_1 = 0.325302999 \tag{94}$$

$$H_2 = 0.421107102 \tag{95}$$

$$H_3 = 0.133442501 \tag{96}$$

$$H_4 = 0.637432347 \times 10^{-2} \tag{97}$$

$$\eta_\nu = \left[\frac{\lambda}{d} P_\nu\right]^2 \quad \nu = 1,2,3,4 \tag{98}$$

$$\sum_{i=1}^{4} \frac{H_i}{1 - \eta_\nu \alpha_i^2} = \frac{1}{2} \pi^{1/2} \quad \nu = 1,2,3,4 \tag{99}$$

$$\frac{1}{\pi^{1/2}} \sum_{\nu=1}^{3} \bar{C}_\nu \left[\frac{e^{-\frac{P_\nu}{2}}}{1 + \eta_\nu^{1/2} \alpha_k} + \frac{e^{\frac{P_\nu}{2}}}{1 - \eta_\nu^{1/2} \alpha_K}\right] + \bar{T} \tag{100}$$

$$= 1 - \frac{1}{4} \left[\frac{d}{\lambda}\right]^2 - \alpha_k \left[\frac{d}{\lambda}\right] - 2\alpha_k^2 \quad K = 1,2,3,4$$

As was done with the free-molecule equation for flow in a capillary tube (Equation (15)), corrections must be applied to the above flow equation to make it applicable to flow in porous media. These include converting the flow rate to per unit surface area of the food, correcting the length of vapor travel by multiplication of the dried food region thickness by the tortuosity factor, and correcting the flow due to irregularities of the channels in the material, by a linear correction factor Γ. It should be noted that the previous equations are also for isothermal flow.

The advantage of using the above flow equation in place of Equations (16), (18), and (35) is somewhat offset by the fact that the flow of a binary gas mixture is being studied in which mutual diffusion takes place. Equation (87) would have to be coupled with the diffusion equation of the continuum and transition flow regimes and used alone in the free-molecule flow regime, in which case ΔP would be the water vapor partial pressure drop. Therefore, the three flow regimes would still be studied separately. However, the above approach would have the advantage that there would be no need for experimental permeabilities. Calculations of water vapor flow rates during drying of beef were carried out using Equations (87) and (88), and the results are given in Appendix G.

CHAPTER III

EXPERIMENTAL INVESTIGATION

Vapor Pressure Measurement

Instrumentation and Equipment

The same apparatus used for the experimental measurements of equilibrium vapor pressure was used previously by Dyer et al.(21) and is shown in Figure 2. A 2000 milliliter vacuum flask was submerged in acetone; the temperature of the system was controlled with a freon refrigeration unit. The refrigeration unit was constructed using a Copeland* model CSAL-0100-CAB-001 compressor unit. A Welch** model number 1402 mechanical vacuum pump was used to evacuate the vacuum flask. The temperatures of the acetone bath and of two positions in the sample were measured with 30-gage copper-constantan thermocouples. The pressure in the flask was measured with a type-160 absolute-pressure gage manufactured by the Wallace and Tiernan*** Company. The thermocouple output was measured by use of a portable potentiometer used in conjunction with a thermocouple multiple switch. The thermocouples were calibrated against secondary standard mercury-in-glass

---

*Copeland, Sidney, Ohio.

**W. M. Welch Scientific Co., 7300 N. Linder Avenue, Skokie, Illinois.

***Wallace and Tiernan, Incorporated, 25 Main Street, Belleville 9, New Jersey.

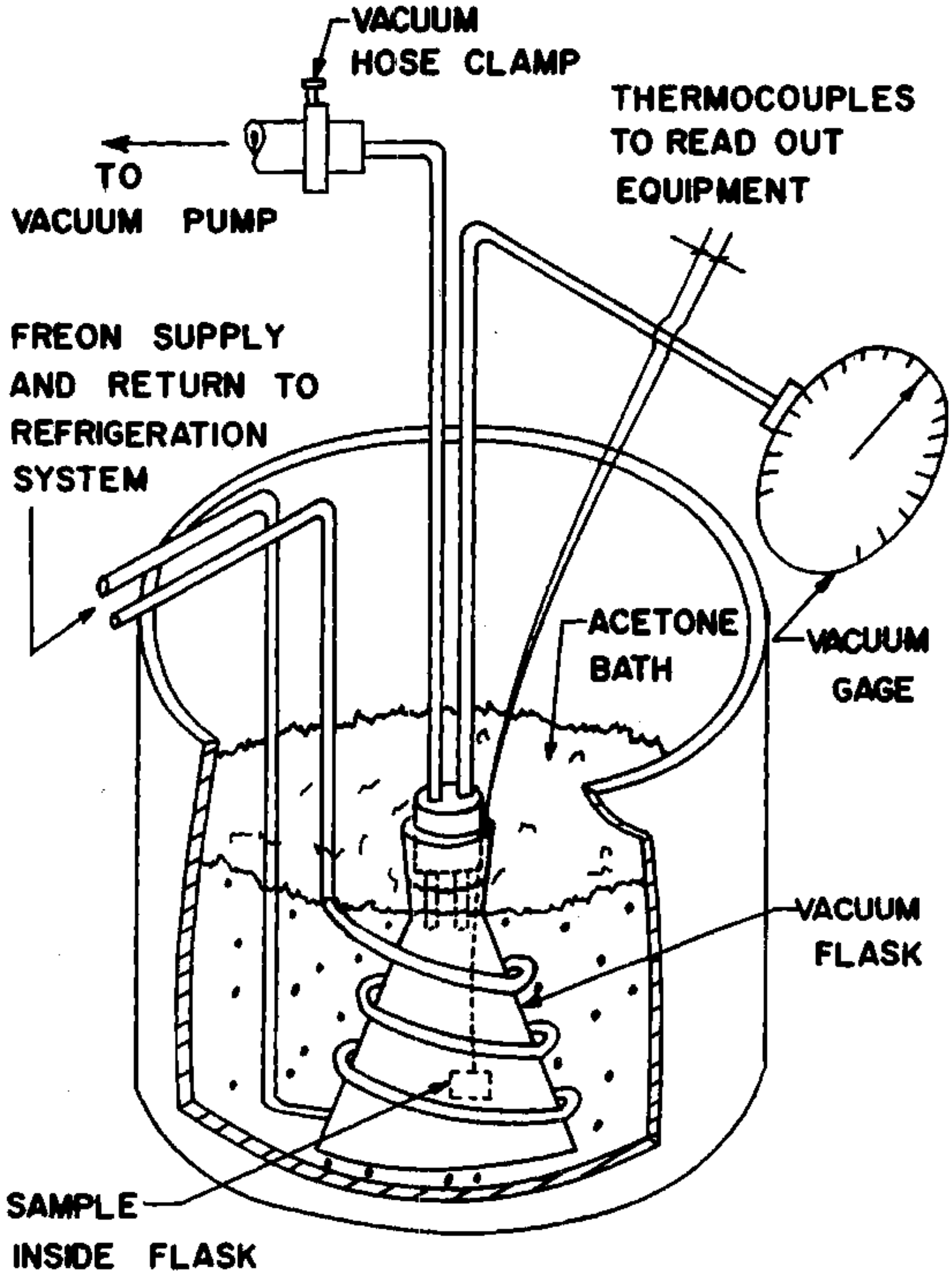

Figure 2. Experimental Apparatus for Vapor Pressure Determination.

thermometers, and the pressure gage was calibrated with the micromanometer arrangement described by Mayne (43).

Procedure

The following steps were taken to obtain vapor pressure data:

1. The vacuum system (see Figure 2) was assembled and pumped for approximately one day in order to remove contaminants without the sample being included and without refrigerating the acetone bath.

2. The refrigeration system was then started.

3. For tests on solid meat samples, two thermocouples were located in the meat and the meat was then frozen. The sample size used was approximately 1.0 by 2.0 by 3.0 cm. For measurements made on the chopped sirloin, chunks of sirloin steak were shreaded in a Waring blender and then packed into a spherical ball. For measurements on fat, strips of fat were cut from around the outside of the steak. Thermocouples were then placed in these two samples and then they were frozen.

4. The sample was then placed in the vacuum flask. Since the thermocouple wires were extremely small in diameter, it was possible to feed the wires out between the rubber stopper and the vacuum flask wall without introducing leaks. The stopper was then replaced in the flask.

5. The mechanical pump was started and the system pumped to a low pressure (approximately 0.5 torr). Note that this allowed a slight amount of residual air to remain in the flask.

6. The acetone bath was allowed to reach the temperature at which the vapor pressure measurement was desired and then to stabilize.

7. The hose clamp located between the pump and flask was closed.

8. The sample was allowed to come into temperature equilibrium with the external bath. This was determined by comparing the two thermocouple readings of the sample with the thermocouple reading of the bath. It was assumed that thermal equilibrium existed when the temperature of the sample was within $\pm 0.5^{\circ}C$ of the bath temperature.

9. The pressure in the flask was read. No changes of pressure were observed for periods up to 10 minutes following the establishment of thermal equilibrium.

10. In order to determine the residual air pressure, dry ice was introduced into the acetone bath. The low temperatures produced by the dry ice froze the water-vapor onto the inside walls of the flask. The temperature and pressure inside the flask were read. By using Dalton's law of partial pressures and the ideal gas law as described by reference (44), the new pressure obtained can be converted into the partial pressure of the residual air. Then, the actual vapor pressure is the total pressure initially read minus the computed air residual pressure.

After establishing that the leak rate for the apparatus was very small, step 10 was carried out to determine the initial residual air pressure. Several data points were taken as described in the first nine steps for different temperatures by slowly allowing the acetone bath temperature to change (thus, changing the sample temperature). The residual air pressure was again determined by step 10 and the leak rate calculated from the known initial and final air pressures. The data taken between the initial and final determination of the residual air pressure were corrected by means of the known leak rate.

Discussion of Experimental Accuracy

The overall accuracy of the experimental set-up was investigated by measuring the vapor pressure of pure ice. Measurements were made over the same range that was examined for the meats. The results of this check corresponded to published vapor pressure data for pure ice (45) with 2 per cent.

CHAPTER IV

DISCUSSION OF EXPERIMENTAL RESULTS

The equilibrium vapor pressure of frozen foods is a very important property that is used in the analytical studies of freeze-drying. One boundary condition which is essential for calculating drying rates involves the temperature at the interface where the dried and frozen layers meet. The temperature at this interface is usually assumed to equal the equilibrium temperature of pure ice at the pressure that exists at that position. Dyer, et al. (21), stated that for freeze-drying of beef, an error of $\pm 2^{\circ}$C in the assumed interface temperature could cause an error of 100 per cent in the calculated heat flux through the undried layer.

The equilibrium vapor pressure is also important in that it enables the calculation of the latent heat of sublimation of the food. This is accomplished by plotting the vapor pressure-temperature data on a semi-logarithmic plot and using the Clausius-Clapeyron equation to calculate the latent heat. As was seen in Chapter 2, these latent heats are required in order to predict freeze-drying rates.

The work by Dyer, et al. (21), showed that the vapor pressure for frozen beef was depressed somewhat below that of pure ice at the same temperature, and that the depression was larger for the frozen beef than for the frozen juices that had been extracted from the beef. These results prompted the present work, in which the equilibrium vapor pressure was measured for chopped sirloin, pork, veal, lamb, chicken, and fat (from sirloin steak).

Saravacos and Stinchfield (46) carried out a series of experiments on the adsorption of water vapor by freeze-dried beef. They report values of equilibrium vapor pressure for beef that had adsorbed 5, 10, and 20 per cent moisture. The values do not correlate with the data for beef containing approximately 75 per cent water that is reported by Dyer, et al. (21).

The experimental results are shown in Figures 3 through 9 in which the vapor pressure is plotted versus temperature for several meats and one fat sample. The points represent runs for both ascending and descending temperatures. Since there is no evidence of hysteresis, it is concluded that the pressures measured are equilibrium values.

In Figure 3 data are plotted for chopped sirloin and in Figure 4 fat from sirloin steak, both along with the curve for beef presented by Dyer, et al. (21). The former data were obtained to determine if small pockets of juices existed within the pieces of meat and prevented a true equilibrium situation. A piece of sirloin steak was chopped up in order to destroy these pockets if they existed. As can be seen, the data for chopped sirloin are identical with the frozen beef data presented by Dyer, et al. (21). This tends to show that if there were small pockets of frozen juices within the meats, they had no effect on the results. The results for fat show about an 18 per cent depression below the values for pure ice, while frozen beef data is about 20 per cent below published data for ice.

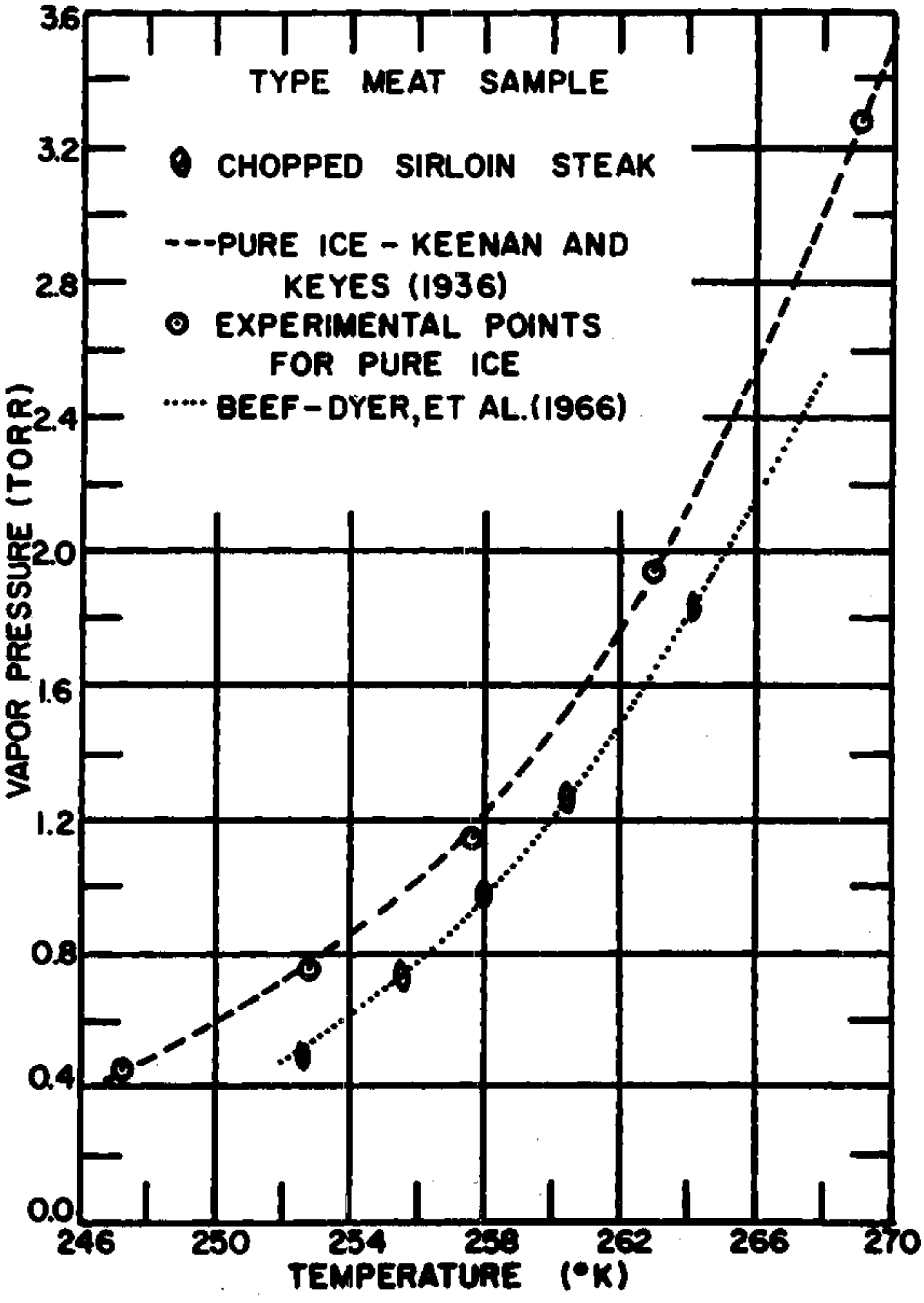

Figure 3. Equilibrium Vapor Pressure of Beef.

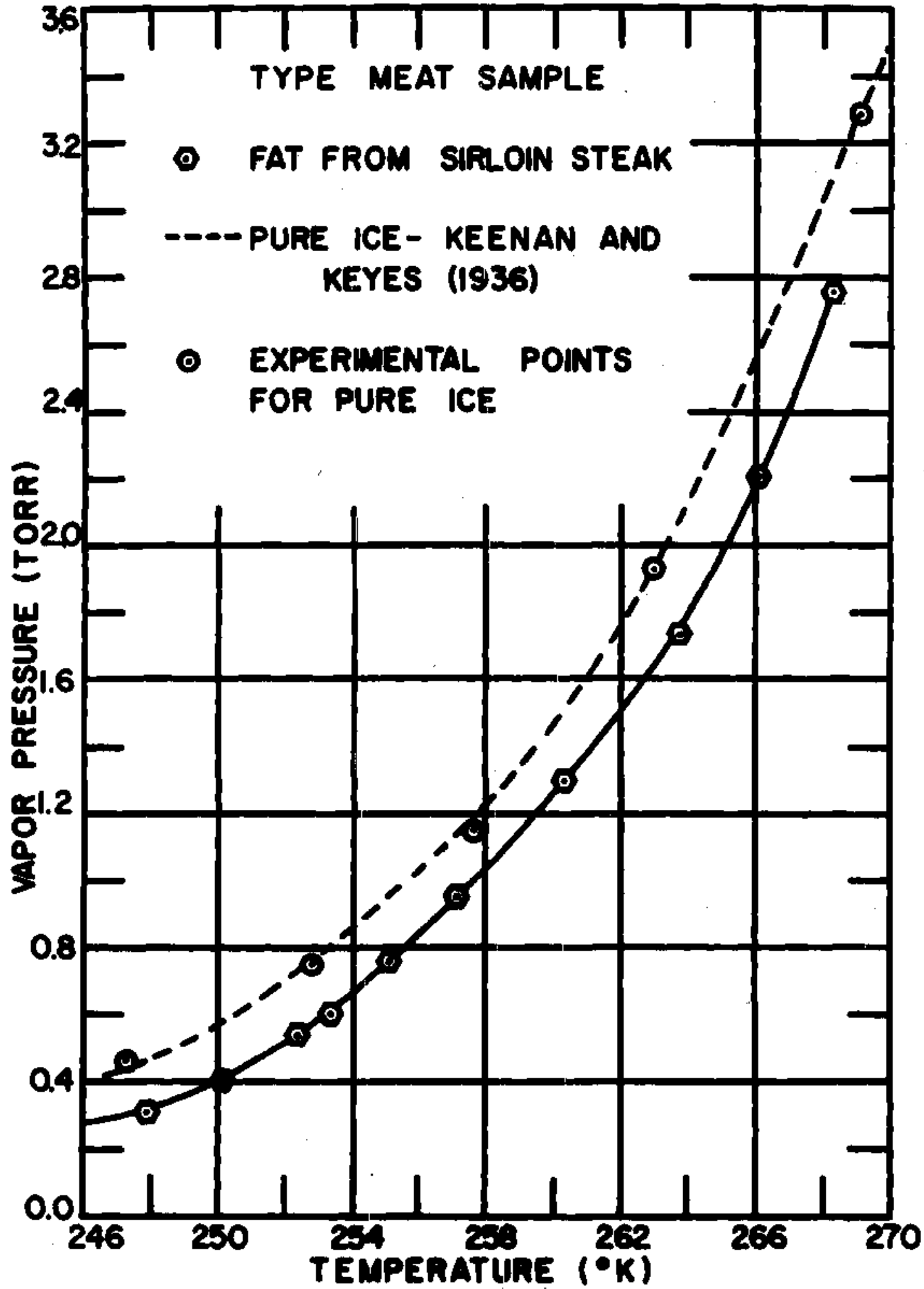

Figure 4. Equilibrium Vapor Pressure of Beef Fat.

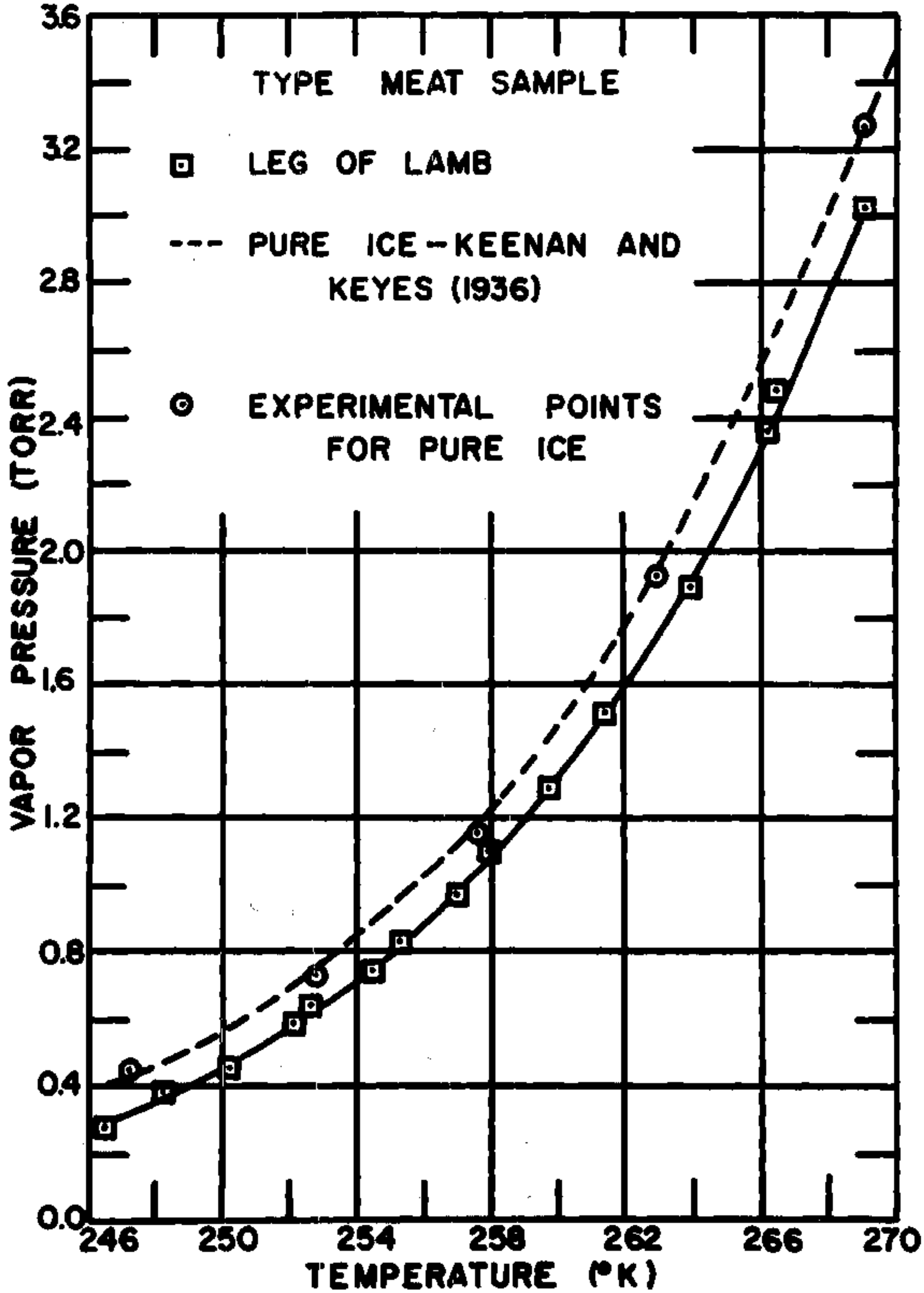

Figure 5. Equilibrium Vapor Pressure of Lamb.

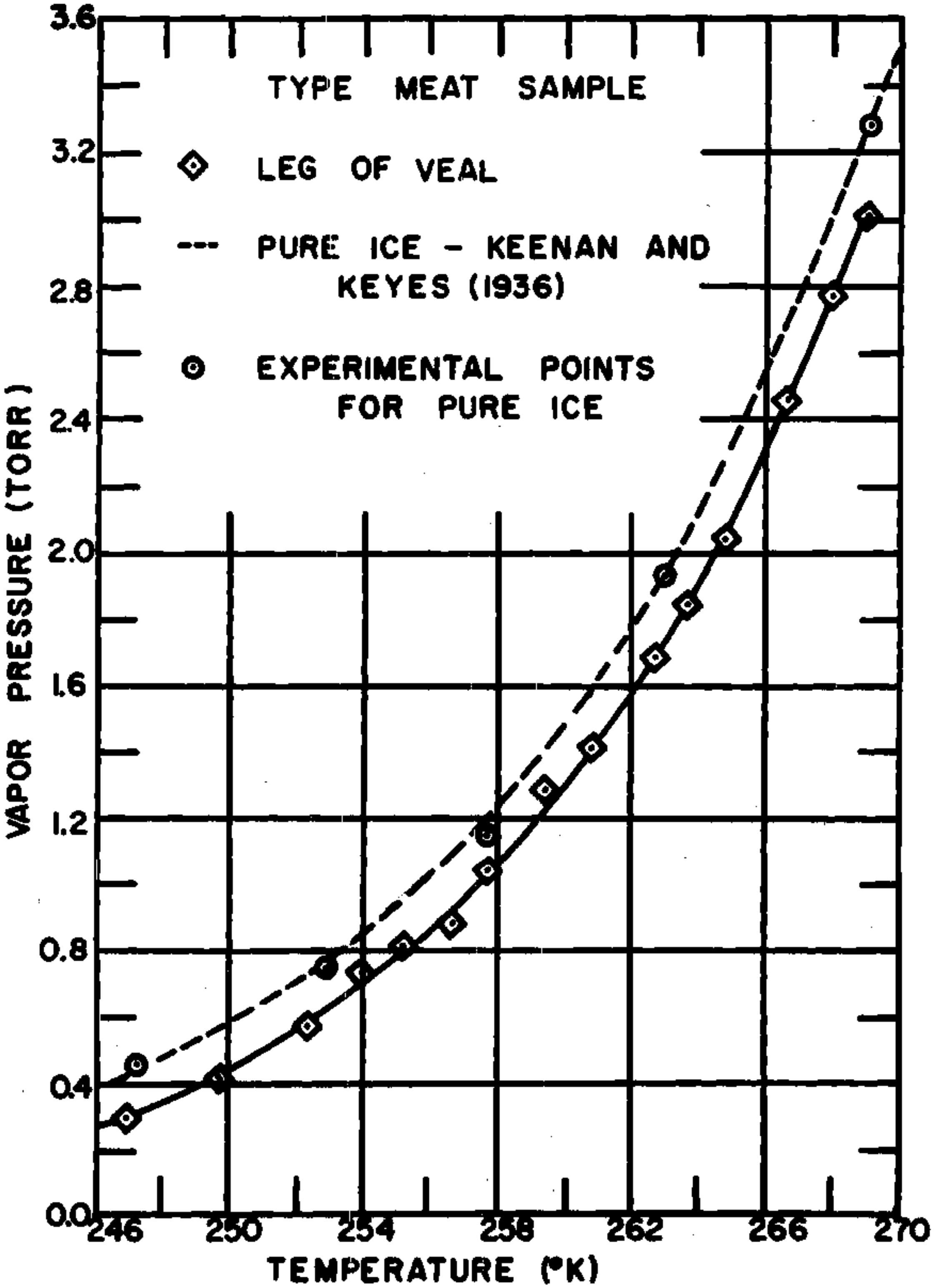

Figure 6. Equilibrium Vapor Pressure of Veal.

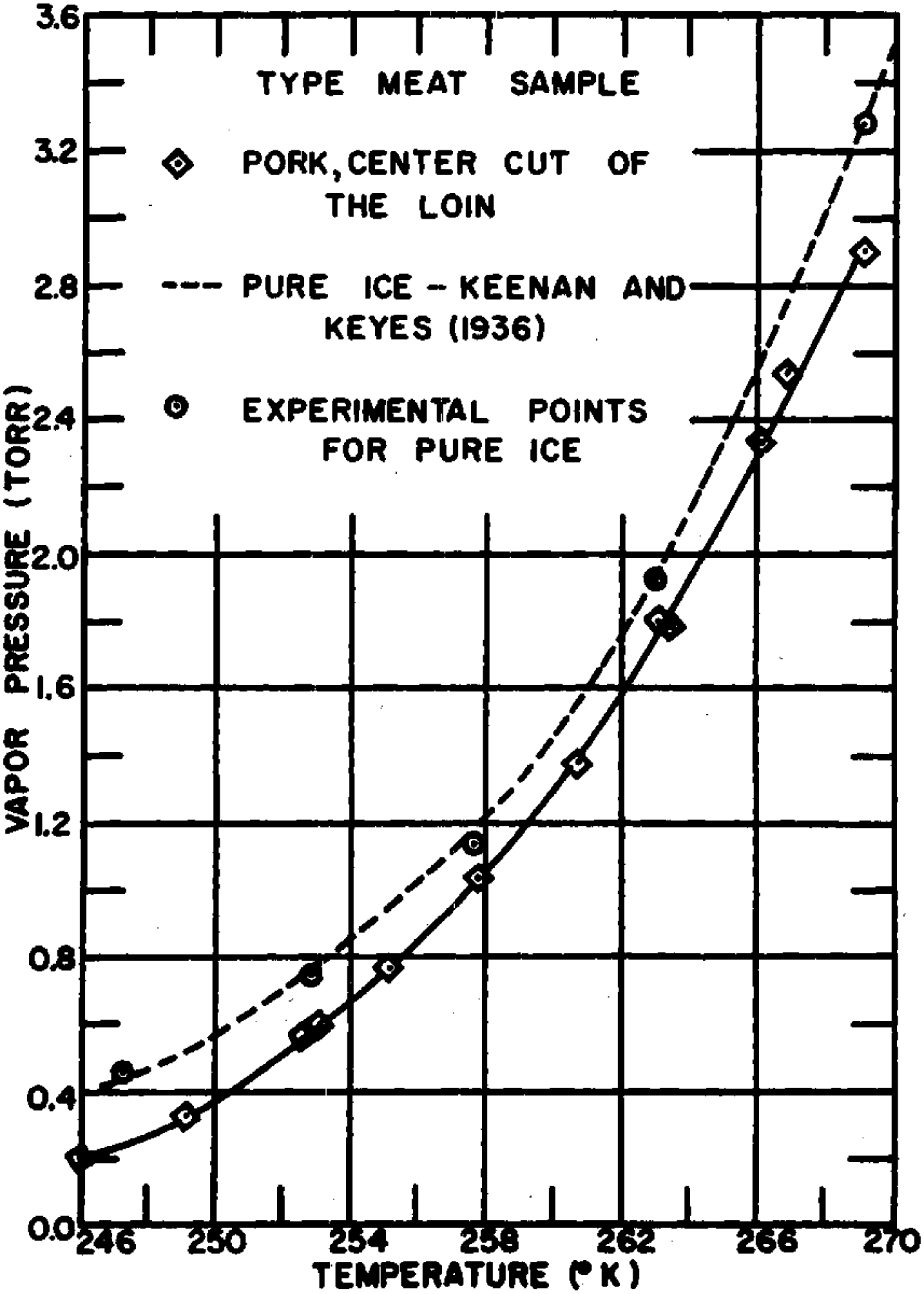

Figure 7. Equilibrium Vapor Pressure of Pork.

In Figures 5, 6, and 7, vapor pressure data are shown for lamb, veal, and pork, respectively. There is only a very slight difference between the lamb and veal over the whole temperature range, and the values for these two meats are approximately 13 per cent below those of pure ice. The pork differs significantly from lamb and veal only at the lower and upper ends of the temperature range shown. The vapor pressure depression for pork averages about 16 per cent.

In Figures 8 and 9, the vapor pressure-temperature relationship is shown for the white and dark meat of chicken. Even though the white meat has a slightly greater depression, the values of both are about 15 per cent below those of pure ice. To further insure that the data that was obtained represented equilibrium states, one test was made for a piece of white meat that remained in equilibrium for 24 hours before the final measurements were made. As can be seen, this measurement is in excellent agreement with the others.

In discussing the results for beef, Dyer, et al. (21), considered a piece of meat to consist of a frozen liquid phase which was dispersed throughout a solid matrix. This matrix could contain cavities and capillaries. The liquid phase, frozen meat juice, was considered to be a dilute aqueous solution containing dissolved proteins and salts. The equilibrium vapor pressure was then dependent on the nature of the frozen liquid phase, of the solid matrix, and of the interactions between these two. After careful analysis, they concluded that the difference between the vapor pressure of frozen meat and pure ice at the same temperature was due to the influence of the solute species in the frozen liquid. The greater the total concentration of these species

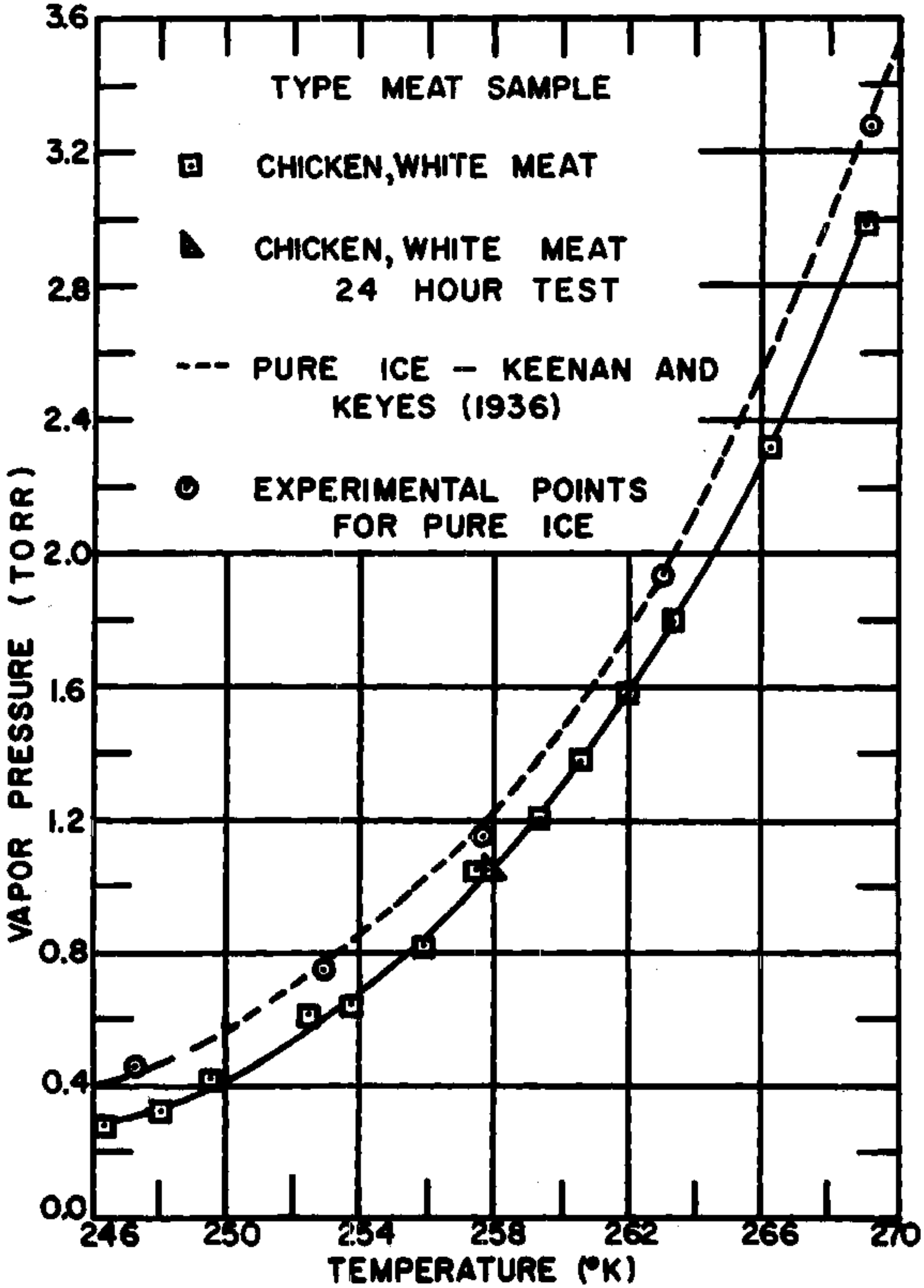

Figure 8. Equilibrium Vapor Pressure of the White Meat of Chicken.

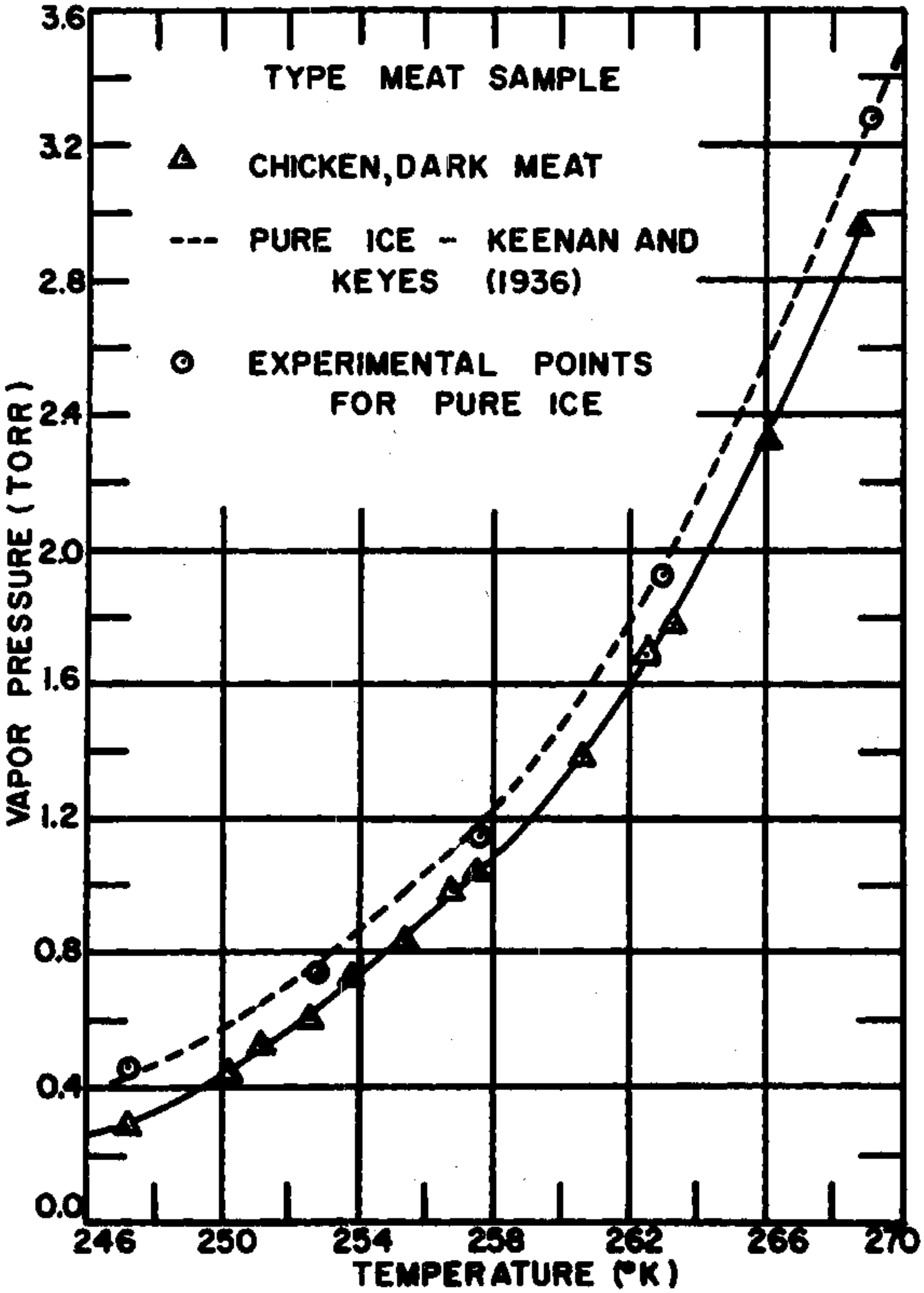

Figure 9. Equilibrium Vapor Pressure of the Dark Meat of Chicken.

present in the frozen liquid phase, the lower the vapor pressure of water over a frozen solution would be compared to that of pure ice at the same temperature. Now the fact that the meat juice values were not depressed as low as those for the frozen beef was explained by presenting an idealized model of the meat. The model shown in Figure 10 depicts the solid matrix as having ionic species attached permanently to it and they extend into the liquid phase. When the liquid solution was squeezed from the meat, these permanently attached species were not removed and thus the concentration of solute species in the meat juice which was removed was less than the concentration present in the meat itself.

The vapor pressure data enabled the calculation of the heats of sublimation of the meats tested from the Clausius-Clapeyron equation (47).

$$\frac{d \ln P}{d\left[\frac{1}{T}\right]} = -\frac{\Delta H}{\tilde{R}} \tag{101}$$

From this equation it can be seen that by plotting the natural logarithm of the vapor pressure against the reciprocal of the absolute temperature, a straight line with a negative slope is obtained. The value of this slope is the heat of sublimation divided by the universal gas constant. Figures 11 through 16 show plots of this sort for the meats tested in this thesis. The heat of sublimation results are listed in Table 2 along with the values obtained by Dyer, et al. (21).

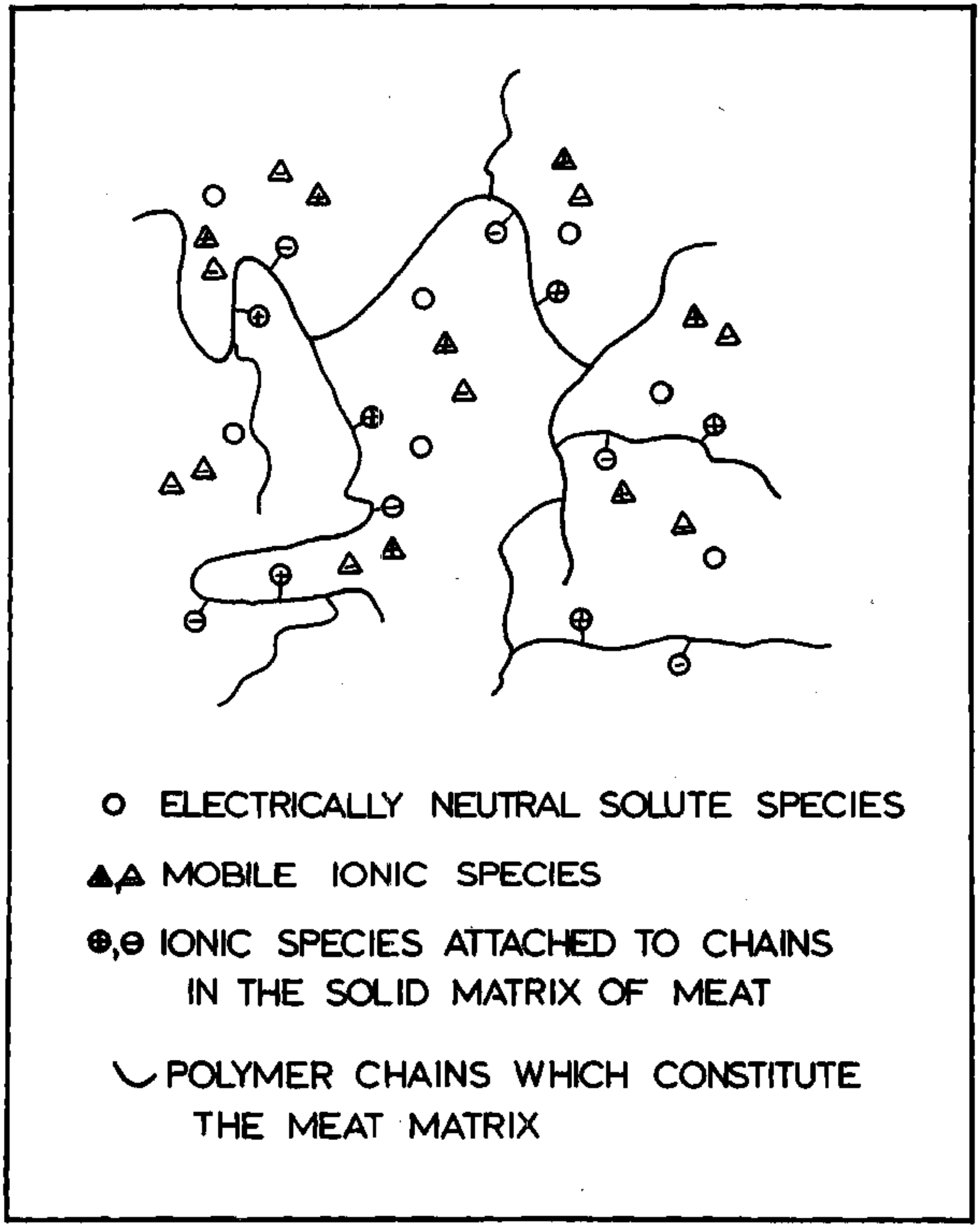

Figure 10. Idealised Model of Meat.

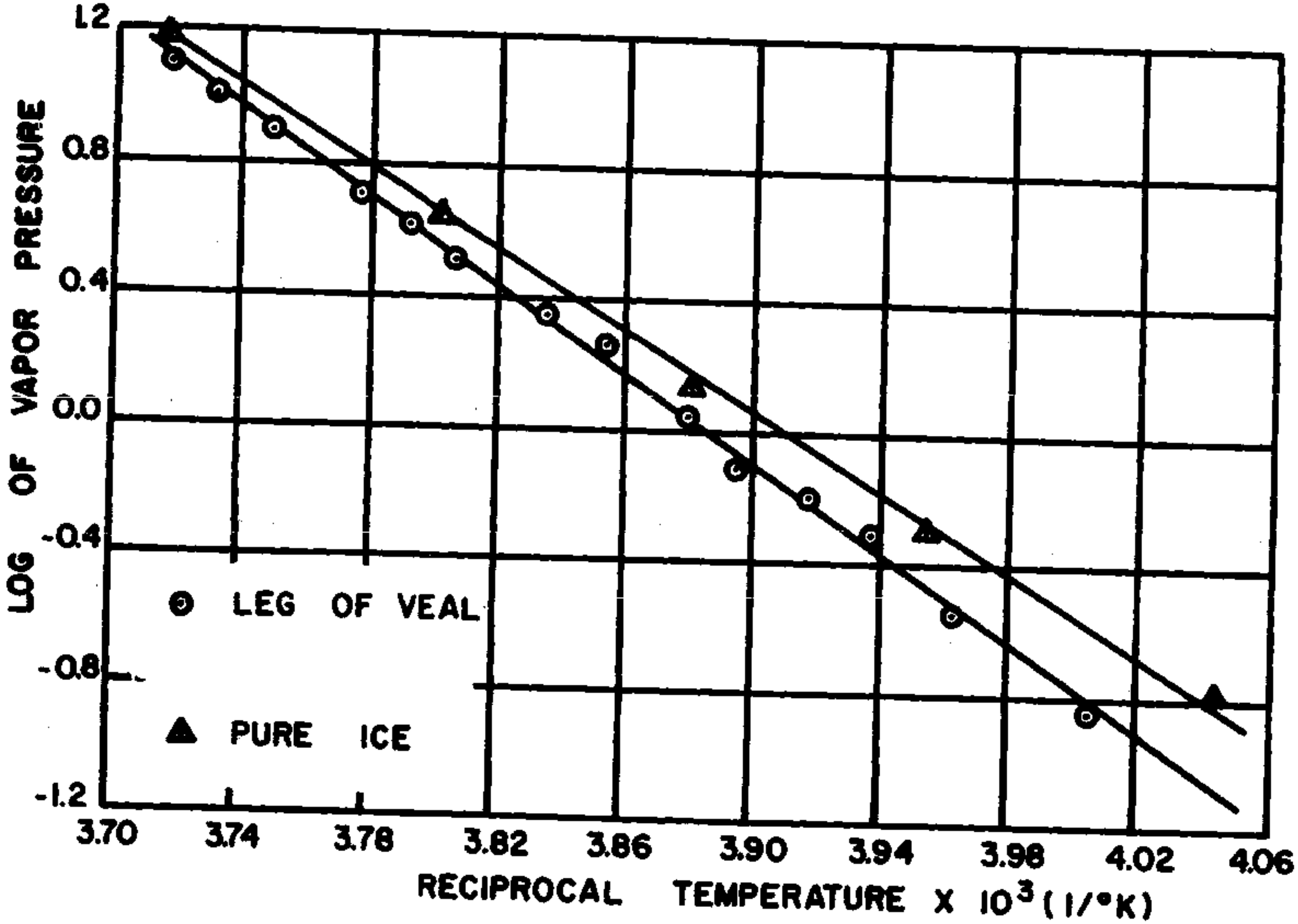

Figure 11. Logarithm of Vapor Pressure vs. Reciprocal of Temperature for Veal.

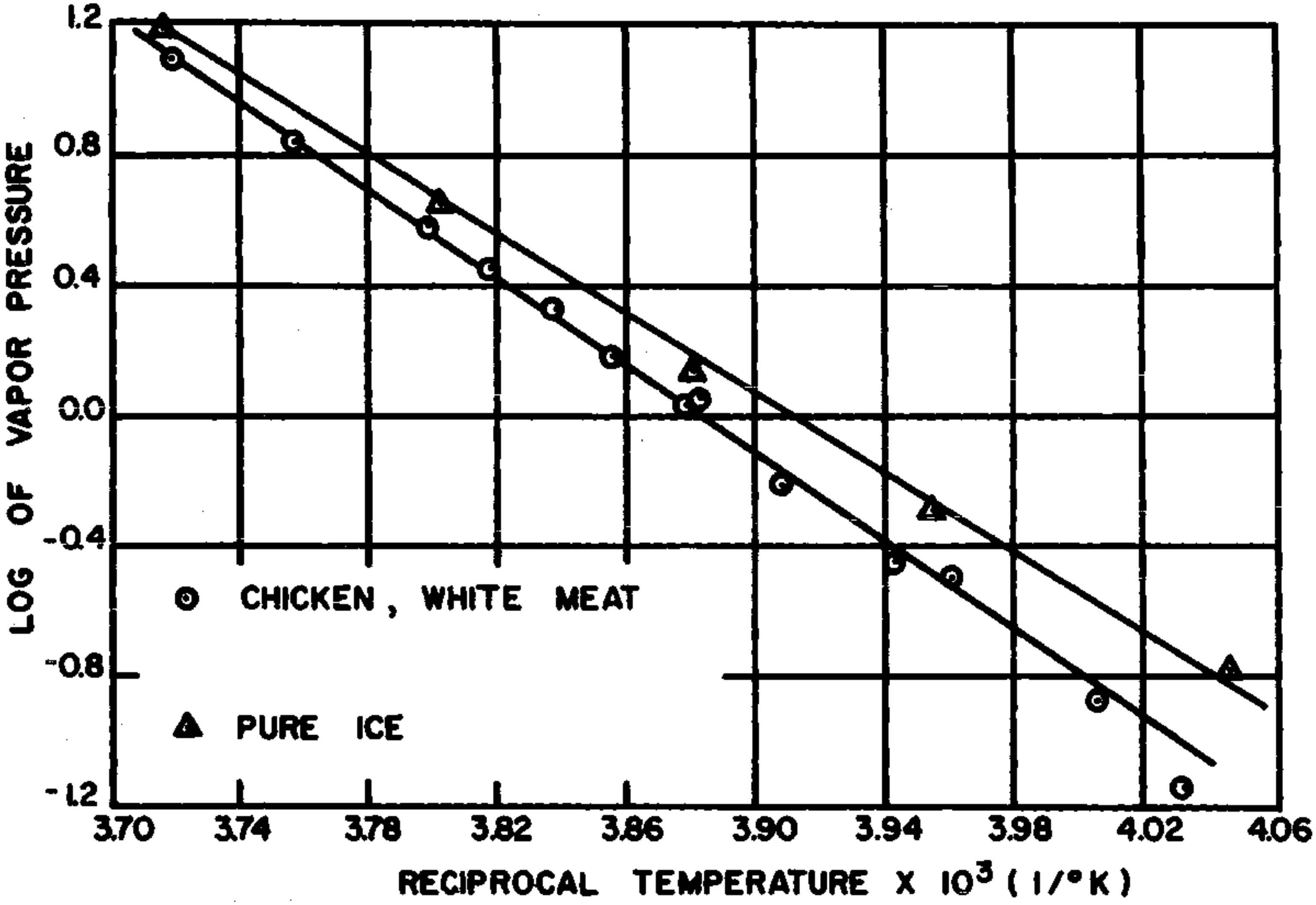

Figure 12. Logarithm of Vapor Pressure vs. Reciprocal of Temperature for the White Meat of Chicken.

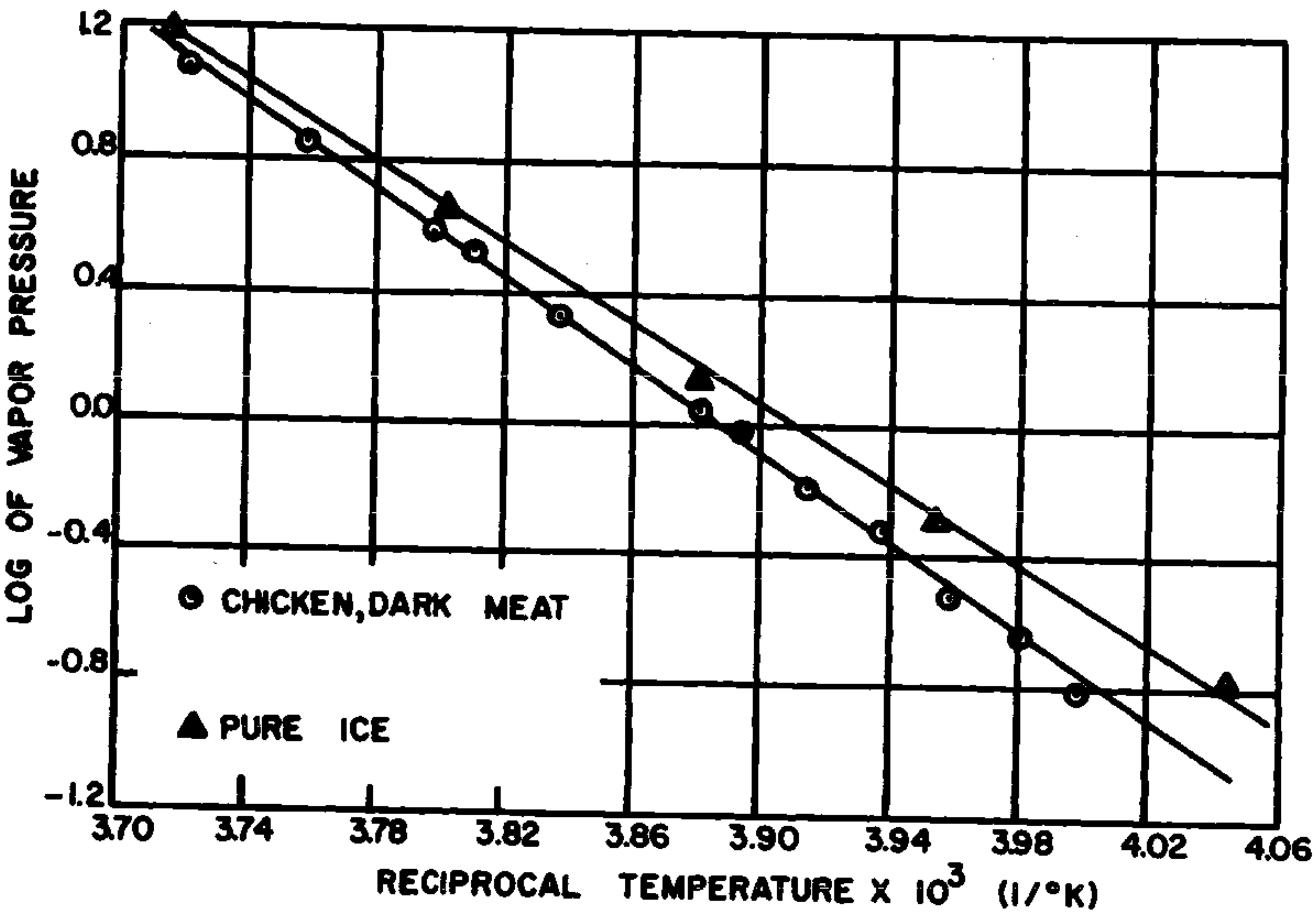

Figure 13. Logarithm of Vapor Pressure vs. Reciprocal of Temperature for the Dark Meat of Chicken.

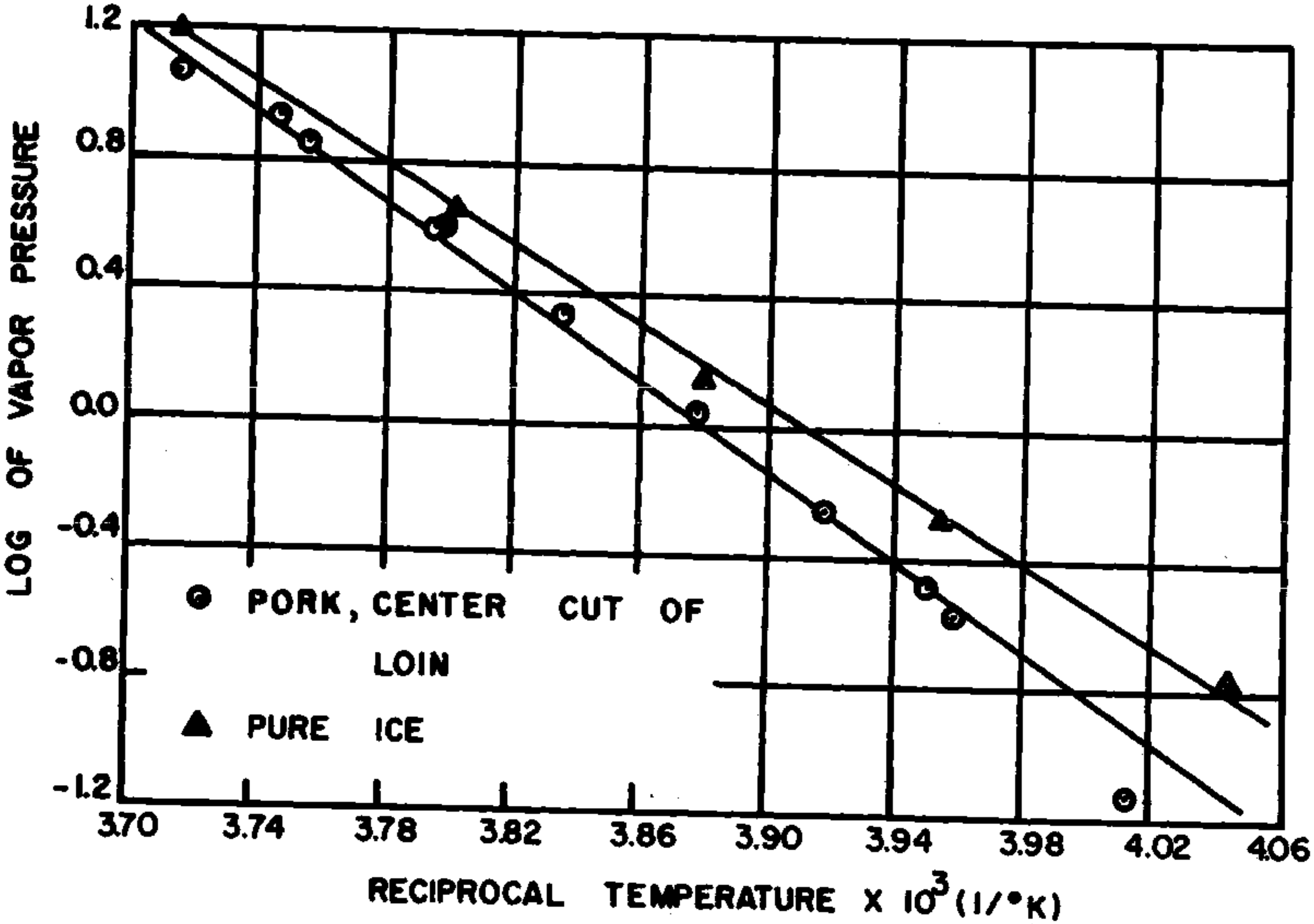

Figure 14. Logarithm of Vapor Pressure vs. Reciprocal of Temperature for Pork.

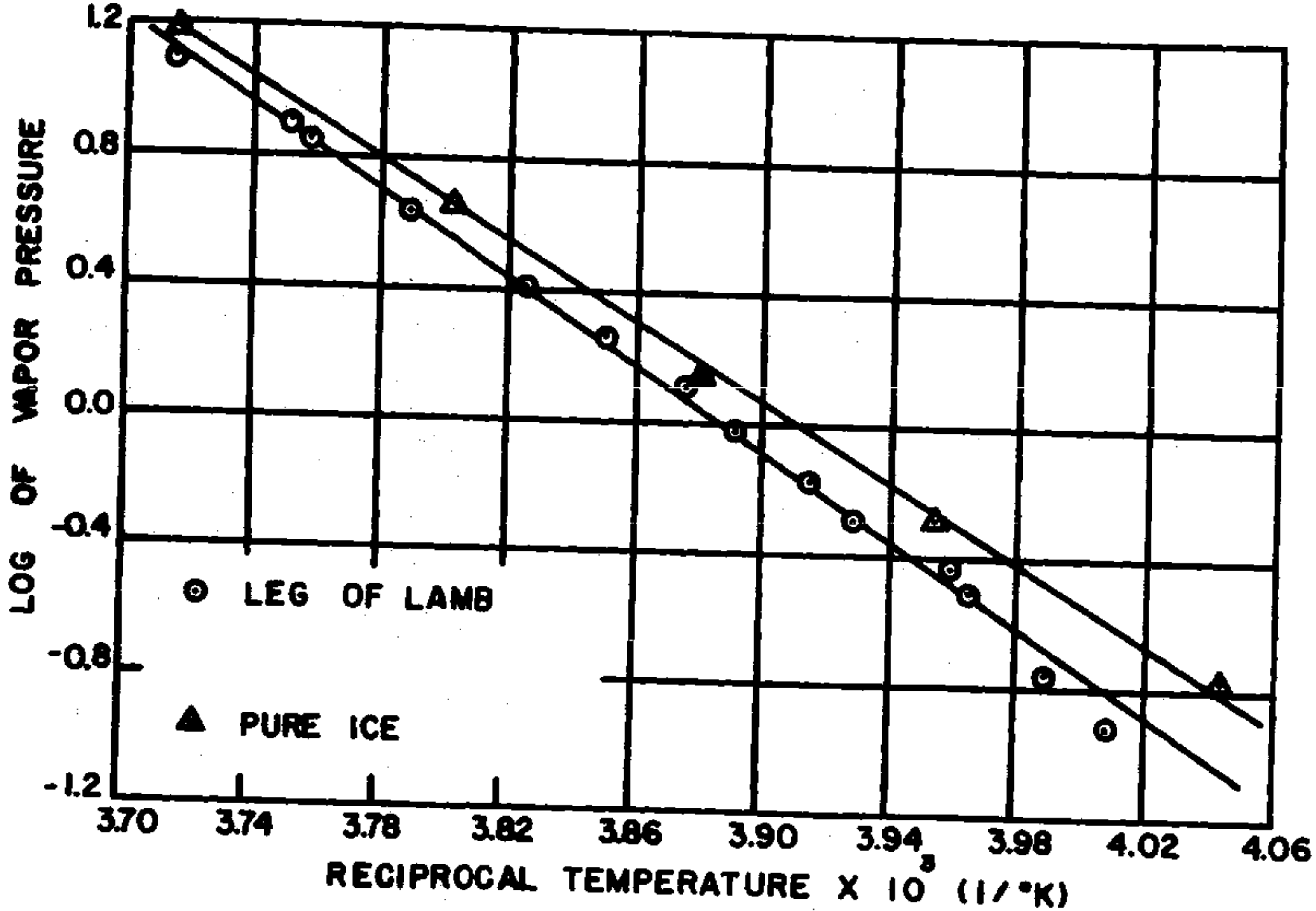

Figure 15. Logarithm of Vapor Pressure vs. Reciprocal of Temperature for Lamb.

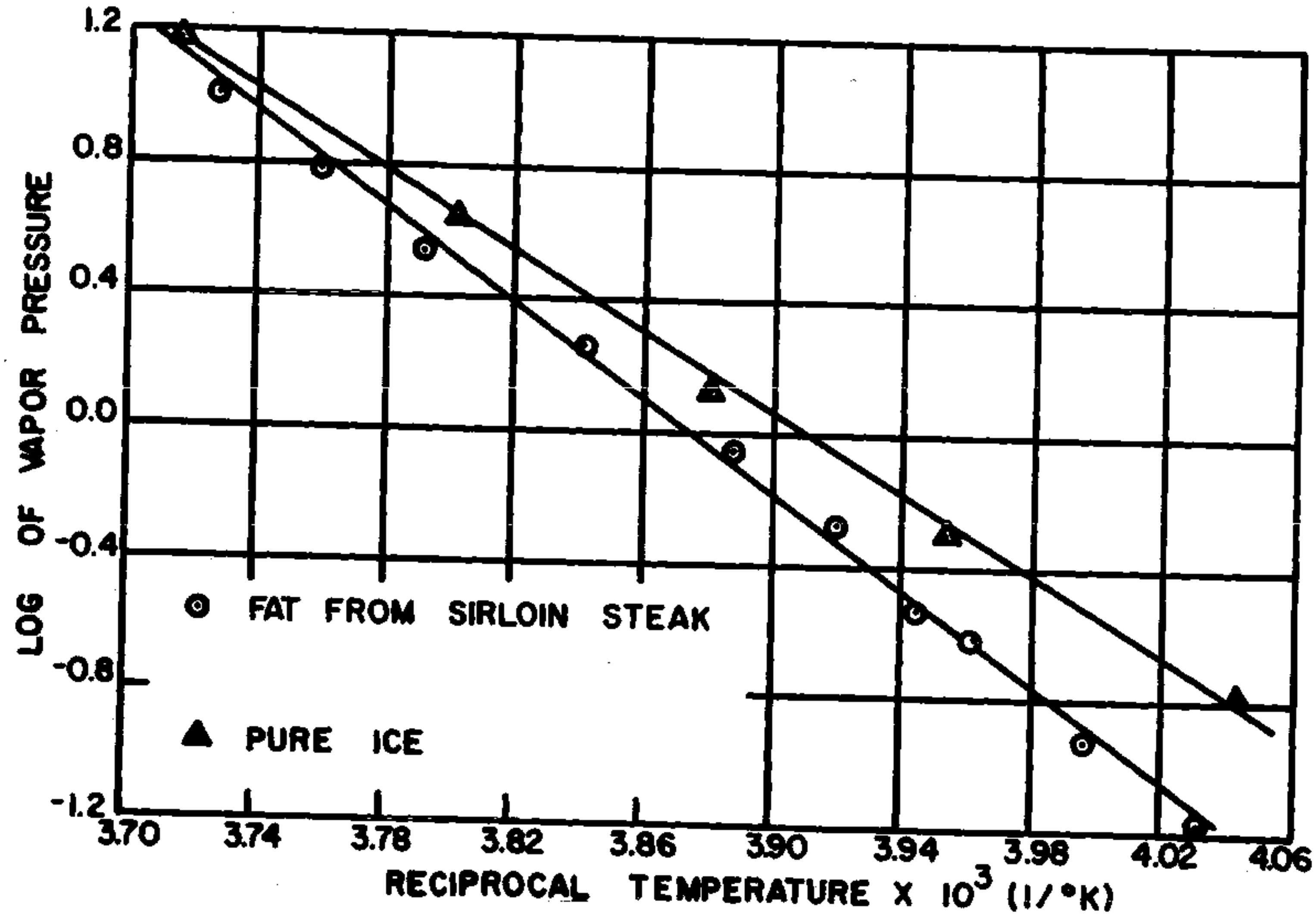

Figure 16. Logarithm of Vapor Pressure vs. Reciprocal of Temperature for Beef Fat.

Table 2. Heats of Sublimation for Various Frozen Meats and Water

Type of Meat	Heat of Sublimation--cal/g mole
Chicken, dark meat	13,310
Chicken, white meat	13,670
Pork, center cut of loin	13,990
Veal, leg	13,460
Lamb, leg	13,410
Fat, from sirloin steak	14,400
Beef, bovine muscle	14,880
Frozen beef juice	13,230
Pure water	12,200

Using Figures 11 through 16, empirical equations can be obtained for the equilibrium vapor pressure as a function of temperature for the meats tested. Using the equation for a straight line gives for the dark meat of chicken,

$$\bar{P}_w = \exp[26.1 - 12100/T] \tag{102}$$

for the white meat of chicken,

$$\bar{P}_w = \exp[26.8 - 12400/T] \tag{103}$$

for pork,

$$\bar{P}_w = \exp[27.3 - 12700/T] \tag{104}$$

for veal,

$$\bar{P}_w = \exp[26.3 - 12200/T] \tag{105}$$

for lamb,

$$\bar{P}_w = \exp[26.2 - 12180/T] \tag{106}$$

and for fat from sirloin steak

$$\bar{P}_w = \exp[28.1 - 13060/T] \tag{107}$$

where T is in °R and $\bar{P}_w$ in torr.

CHAPTER V

DISCUSSION OF THEORETICAL RESULTS

General

As was seen in the development of the theoretical analyses, the heat and mass transfer mechanisms are uniquely related in the freeze-drying process. As drying proceeds, the ice phase recedes inward leaving a porous dried region of the product. The heat of sublimation must then be conducted through this insulating layer and also through the frozen region (in the case of "unidirectional" drying), and the vapor must flow out through the dried layer.

The interface assumes a temperature during drying such that the heat transferred through the frozen and dried regions is just sufficient to provide the heat of sublimation of the vapor flowing outward. If a change is made in the temperature at the dried surface, in the temperature at the back face, in the water vapor partial pressure at the dried surface, or in the chamber pressure, the temperature at the interface will change until a new equilibrium condition is reached. Any restriction placed on the flow of water vapor through the dried shell, will result in a higher interface pressure, and thus a higher interface temperature. On the other hand, if heat transfer is lowered, the ice temperature will be lowered. Measurements during freeze-drying commonly show that the interface temperature is well below the melting point (approximately 28°F) throughout the majority of the drying circle. Therefore, it is usually felt that drying is limited by the rate at which heat can be transferred to the interface. Harper, et al. (24), state that if this heat transfer limitation could be removed, the drying times would only be about 10 per cent of their present values.

The heat transfer rate is restricted by the physical limitations of the process. The rate of heat flow through both the frozen and dried regions is proportional to the product of the thermal conductivity of that region and the temperature difference across the region. Inasmuch as the thermal conductivities cannot be controlled, it is important to maintain the surface temperatures of the food as high as possible without causing product damage. It should be noted that the thermal conductivity of the dried region is extremely low, ranking among the best thermal insulators. This is the main reason for the heat transfer limitation on the process. Although the thermal conductivity of the frozen region is approximately 20 times greater, the advantage of back face heating is largely offset by the fact that the temperature of the surface must be kept below the melting point of the frozen material. The dried region surface temperature can be raised to approximately 100°F. Any higher temperature would cause scorching of the surface and thus deterioration of the final product.

An additional means of increasing the heat transfer rate is by controlling the total and partial pressures in the chamber, so that the interface temperature is a minimum possible value, once the surface temperatures have been set at their maximum values. This is slightly deceiving since the thermal conductivity of the dried region is also pressure dependent. A change in chamber pressure to reduce the interface temperature, might be offset by the reduction of thermal conductivity of the dried layer.

Numerical calculations have been carried out for the freeze-drying of beef using the theoretical analyses of Chapter 2. Beef was chosen since the property data available was numerous (see Appendix E), and also experimental drying times were available for comparison with the theoretical drying times.

Theoretical Interface Temperatures

The interface temperature as a function of the dimensionless interface position, X/L, for "unidirectional" drying is plotted in Figure 17 for several different pressures. The boundary temperatures and the chamber concentration are fixed. Since the rate of heat transfer is the limiting mode of transfer for drying of beef, Figure 17 in conjunction with a knowledge of the thermal conductivities, should provide an insight as to the best pressure at which to dry beef. The thermal conductivity of the frozen region is independent of pressure and is relatively constant regardless of the average temperature of the region. In contrast, the thermal conductivity of the dried layer decreases sharply and directly with pressure below 1.0 torr. On the basis of this intuitive analysis, it would appear best to dry beef at approximately 1.0 torr.

As was pointed out in the development of the theoretical analyses, it is necessary to approximate the interface temperature by a polynomial function of X in order to solve for the drying times.

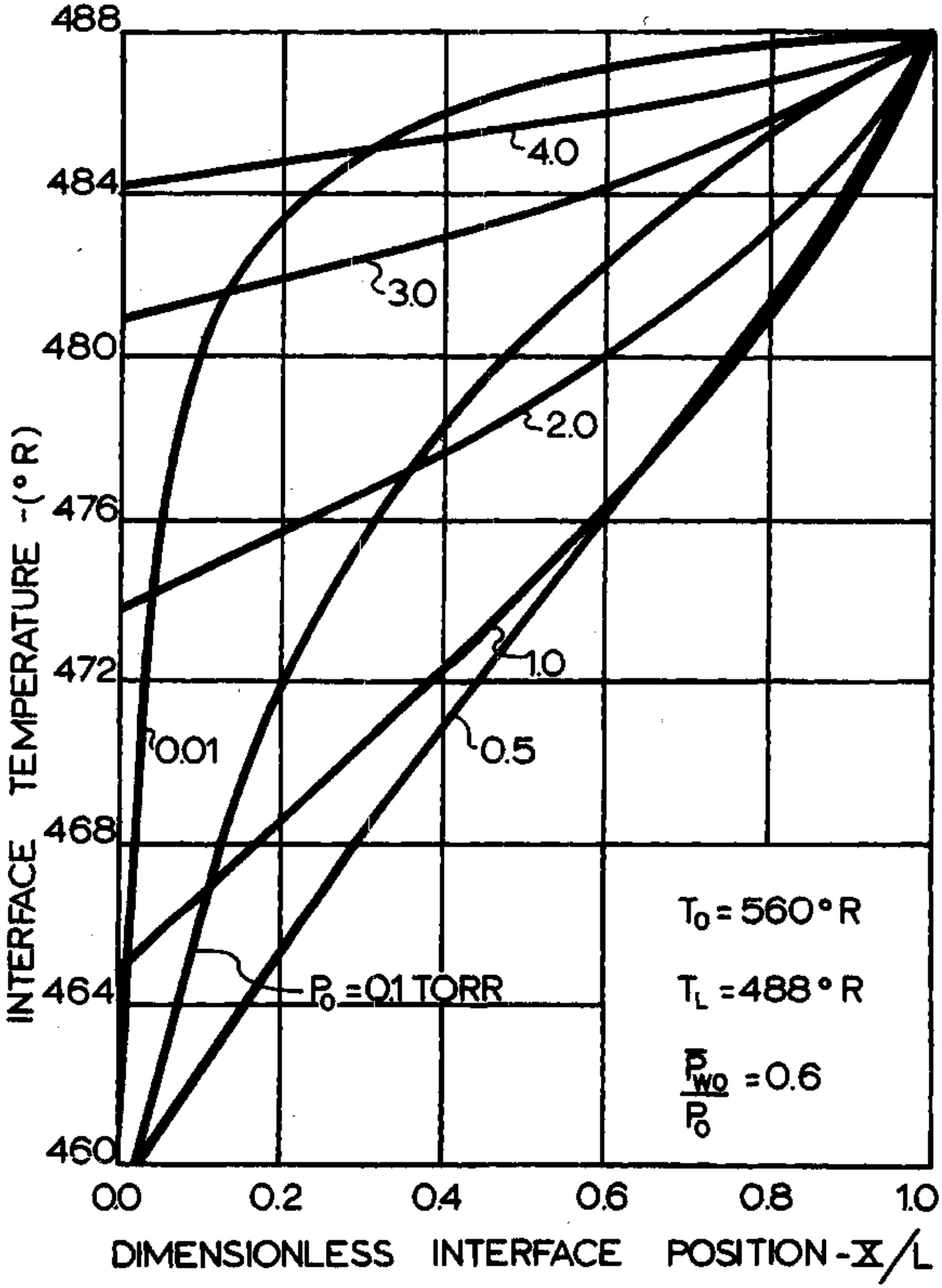

Figure 17. Interface Temperature vs. Dimensionless Interface Position for Unidirectional Drying of Beef.

The closed form Equation (76) can be used if the polynomial is of first order. It appears that for all pressures between 0.5 torr and 4.0 torr, a straight line would be sufficiently accurate. This is verified by comparing the drying times in Appendix F using a first order and third order polynomial for T_X. Figure 18 shows the inaccuracy of the linear approximation at 0.01 torr and relative accuracy of it at 1.0 torr.

Figure 19 is a plot of the constant interface temperature as a function of chamber pressure for the special case of drying from both sides. The other externally controlled conditions are held fixed. As can be seen, the interface temperature decreases with decreasing chamber pressure to a temperature equal to -44°F at a chamber pressure of 0.01 torr. Again since the thermal conductivity of the dried region (only path of heat transfer for this case) decreases rapidly below 1.0 torr, optimum drying would occur in the vicinity of this pressure.

In Figure 20, a plot is made of the interface temperature at two pressures in the continuum regime, one at 35 torr and the other at atmospheric pressure. As can be seen, for the case of no back face heating, the interface temperature is constant as was predicted by Equation (68). Very slow drying rates should be expected, not only because the interface temperatures are relatively high, but because the dried food surface temperature cannot be raised above 28°F. The reason for this is that the pressure is above the triple point of water, and the product would melt if any higher temperature were used. In addition, the chamber concentration must be kept at or close to 0.0 since the vapor pressure at the interface (values given in Chapter 4)

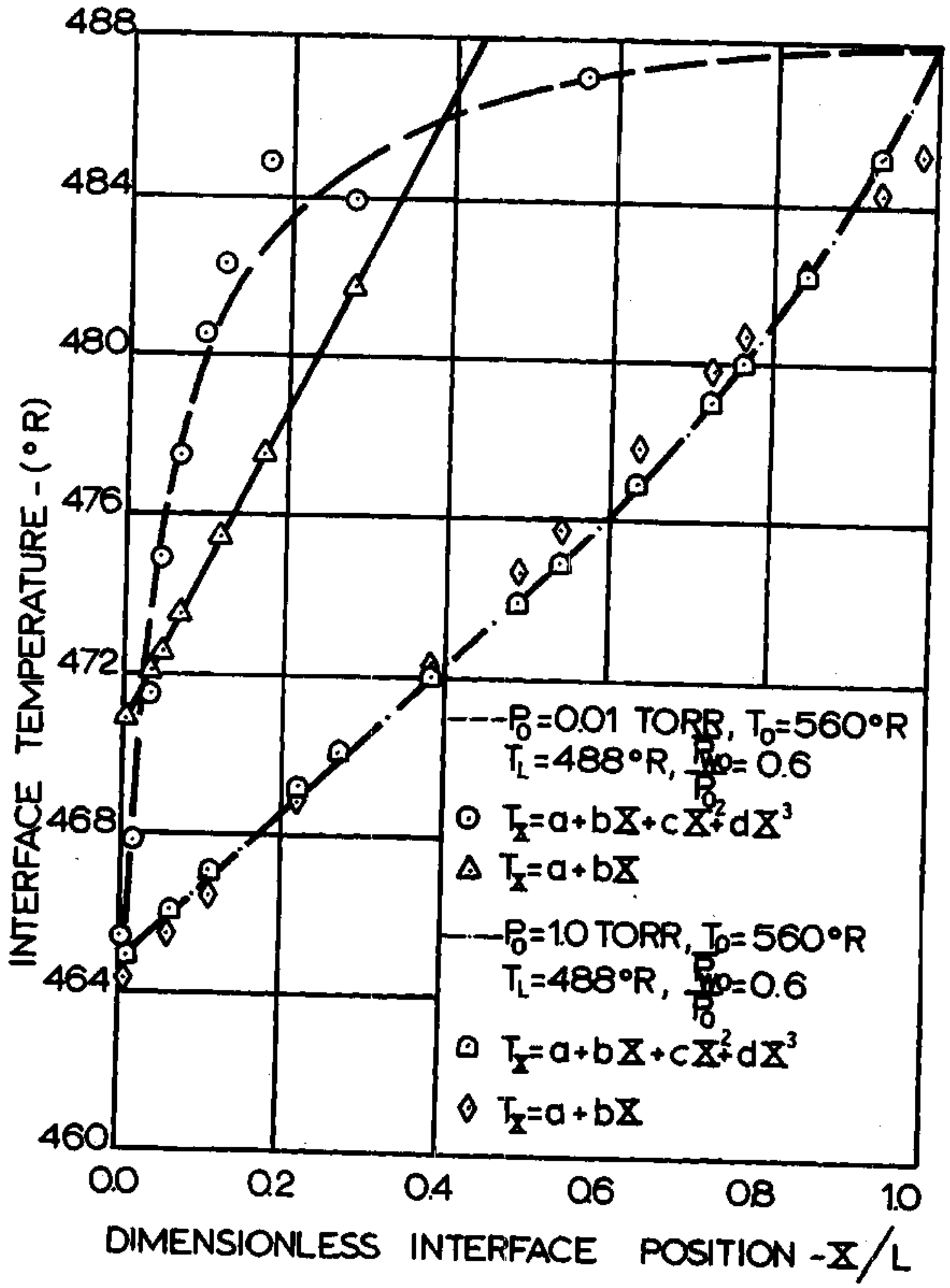

Figure 18. Accuracy of Interface Temperature Approximations.

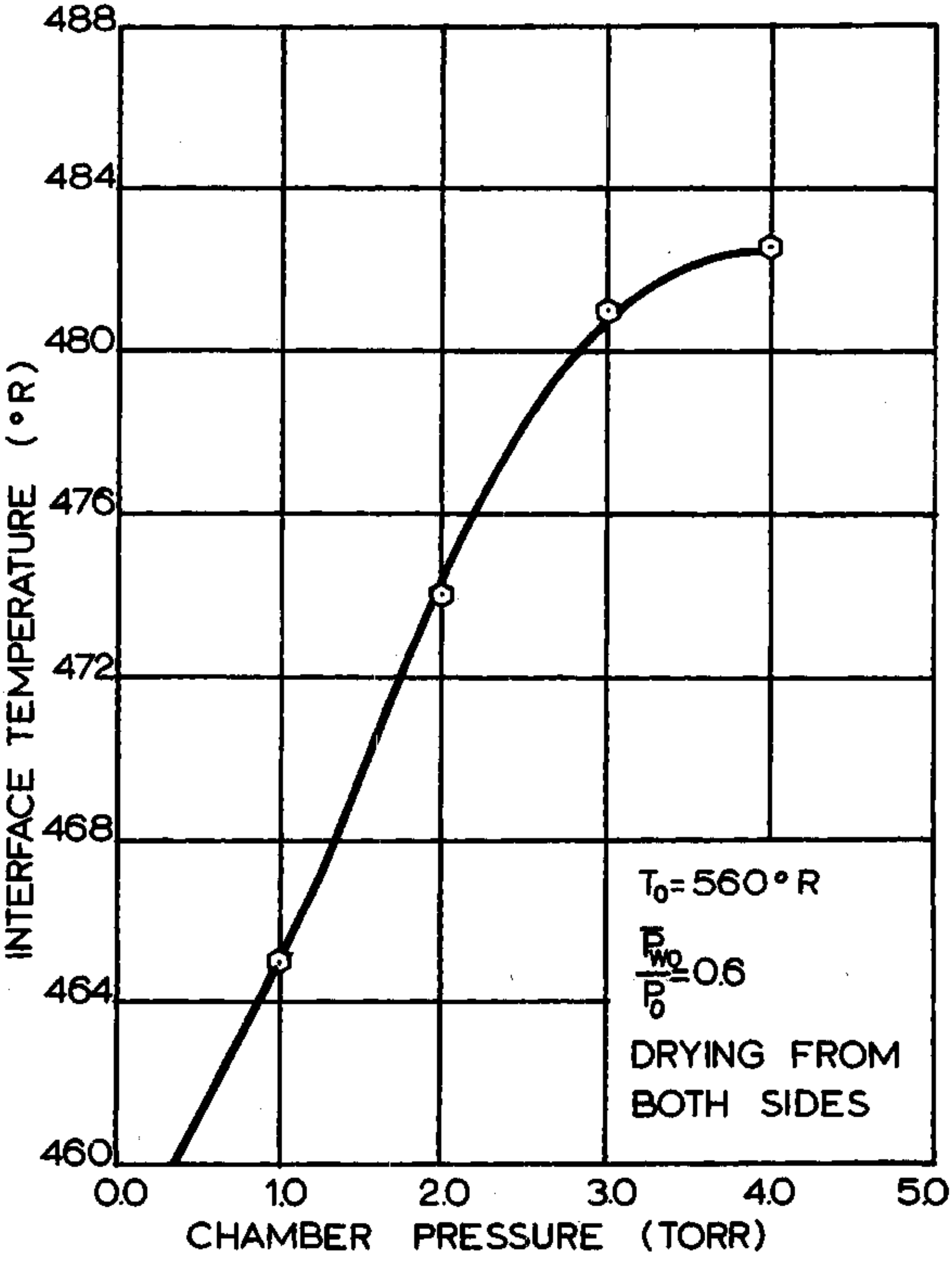

Figure 19. Interface Temperature vs. Chamber Pressure for Freeze-Drying of Beef from Both Sides.

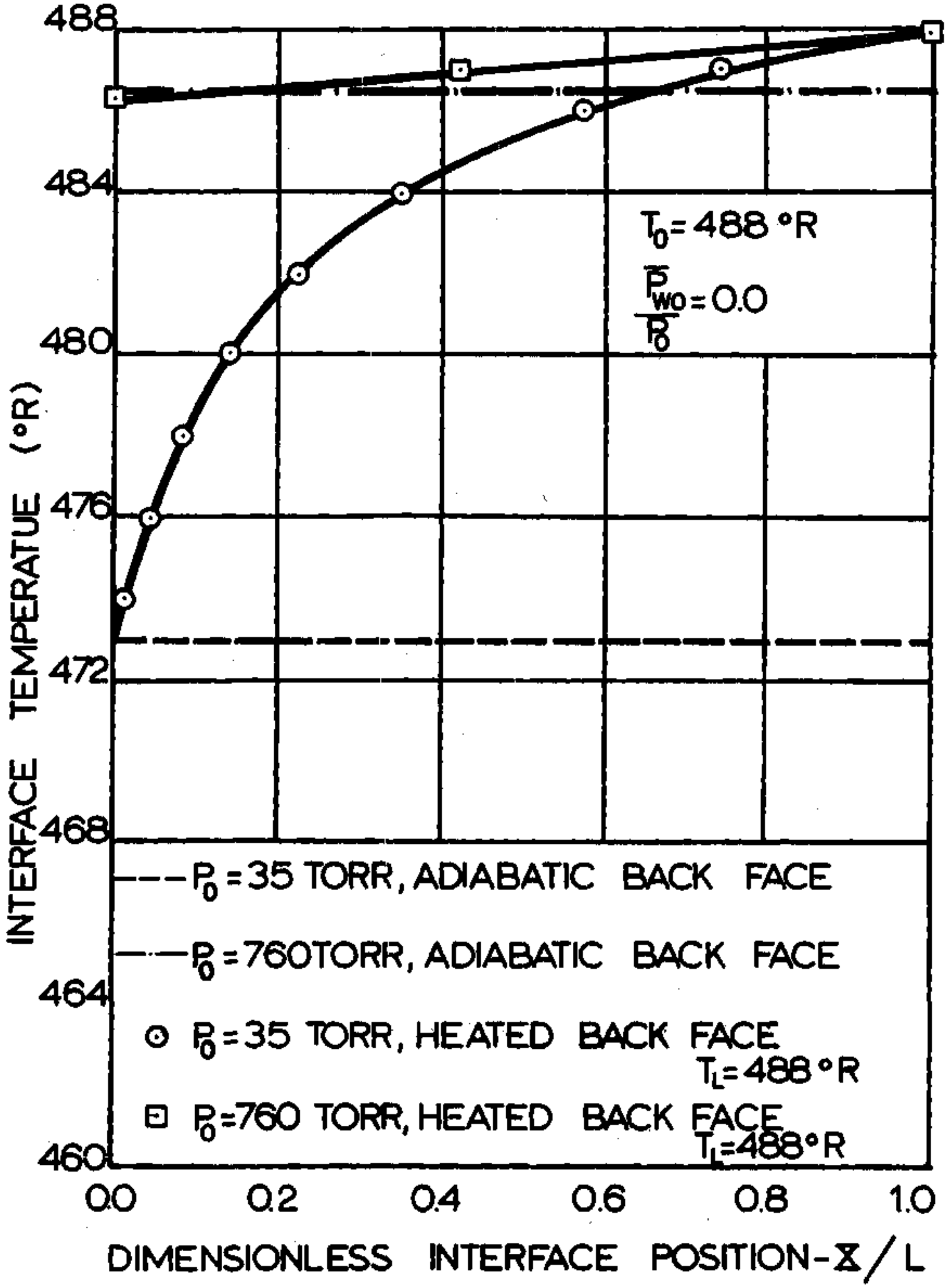

Figure 20. Interface Temperature vs. Dimensionless Interface Position for Drying of Beef in the Continuum Regime.

must be higher than the partial pressure of the water vapor in the chamber to affect the vapor flow in the proper direction. This can be seen from Equation (34). The theoretical analysis of this thesis applied to drying at atmospheric pressure is unique in that all previous analyses have considered atmospheric freeze-drying and ordinary evaporation drying as governed by the same equations. Burke and Decareau (7) point out that no valid theories incorporating foodstuff parameters, such as pore size have been attempted. This has been done in the present work.

Figure 21 shows the dependence of interface temperature on the chamber concentration. As can be seen, a lower chamber concentration will cause a decrease in the interface temperature. This can be explained from an analysis of the vapor flow. If the exit partial pressure is decreased, the vapor flow rate will increase as can be seen from Equation (48). This in turn will result in a decrease in the partial pressure of the water vapor at the interface and consequently a decrease in the interface temperature.

Theoretical Drying Rates

In Figure 22, the drying rate is shown plotted versus the dimensionless interface position, for the general case of back face heating. The drying rate was calculated using Equation (55) and the interface temperature relations. As can be seen, drying will occur the fastest in the pressure range 0.5 to 1.0 torr. Figure 23 shows that, in addition, drying will occur faster if the water vapor is quickly removed from the vacuum chamber so that the exit partial

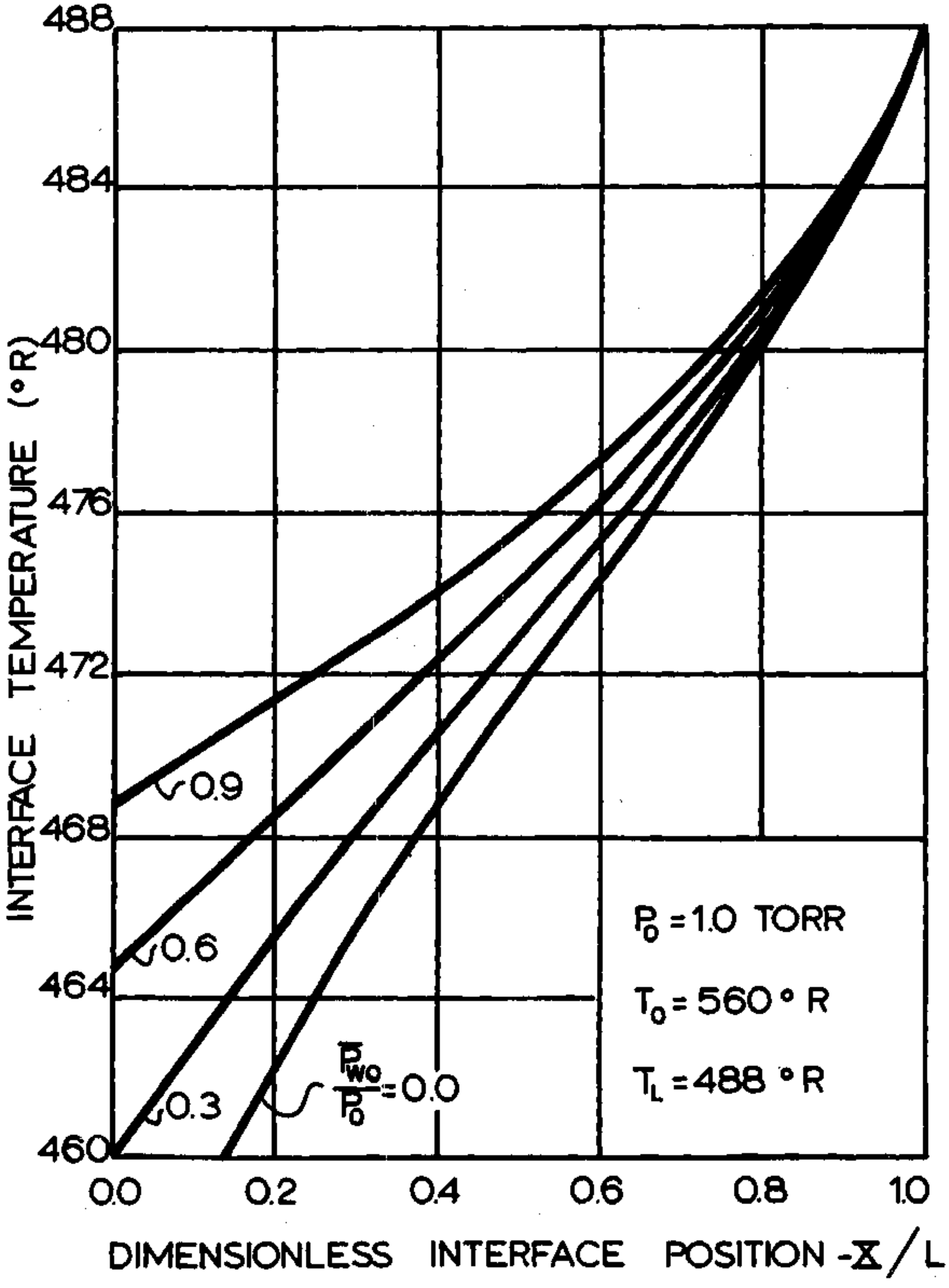

Figure 21. Interface Temperature vs. Dimensionless Interface Position for Unidirectional Drying of Beef at 1 torr and Several Chamber Concentrations.

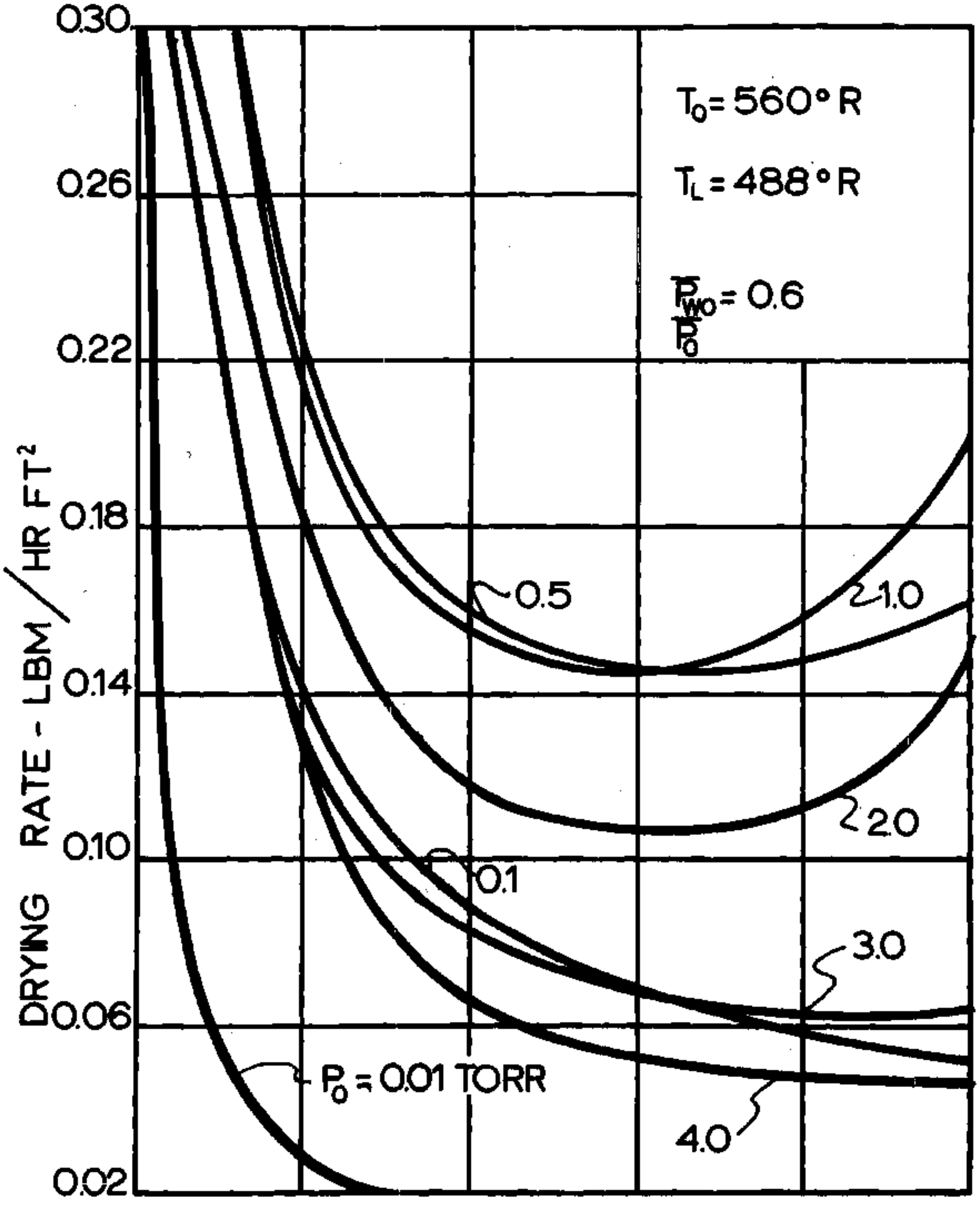

Figure 22. Drying Rate vs. Dimensionless Interface Position for Unidirectional Drying of Beef.

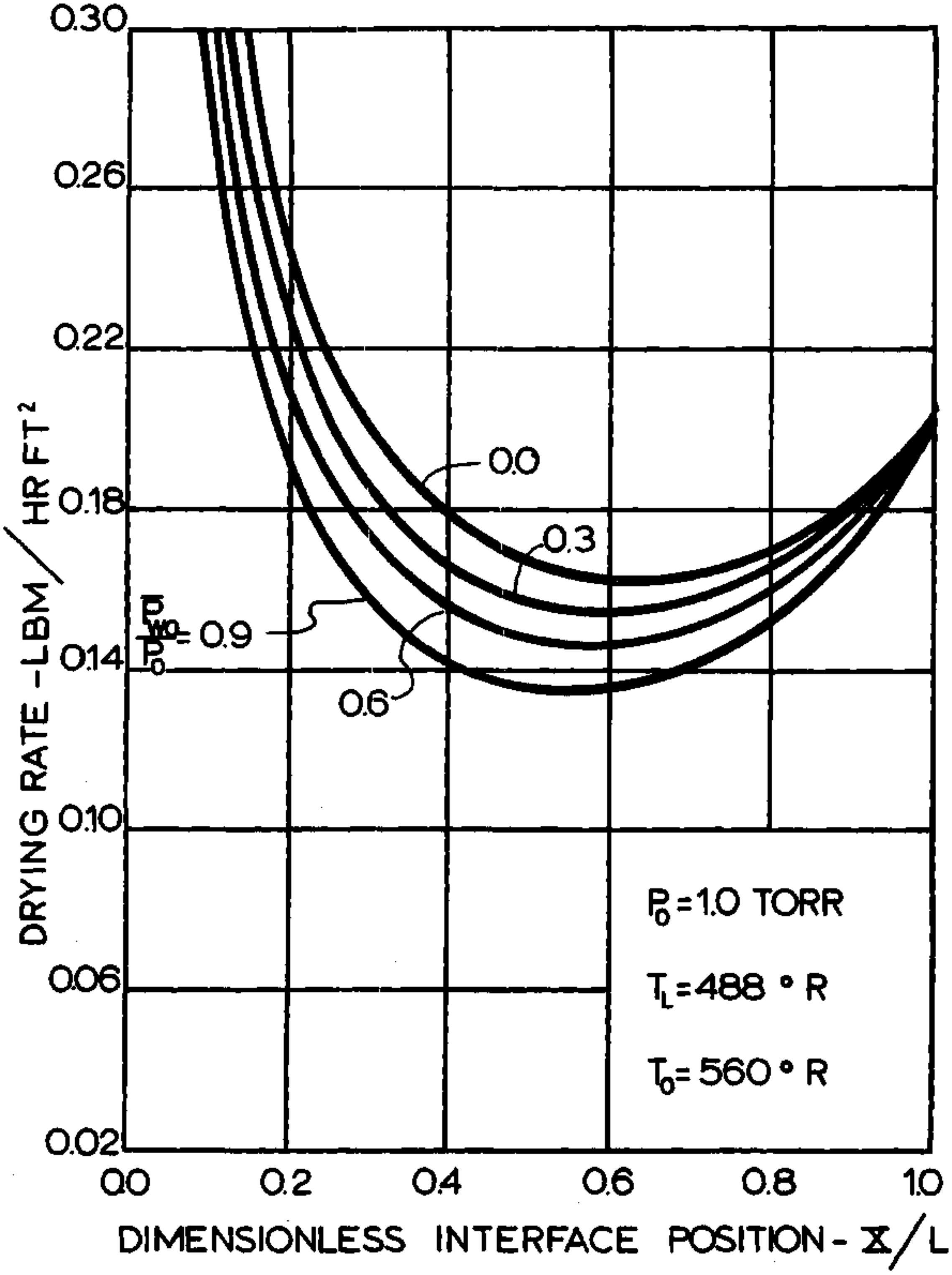

Figure 23. Drying Rate vs. Dimensionless Interface Position for Unidirectional Drying of Beef at 1 torr and Several Chamber Concentrations.

pressure of water vapor is at a minimum. Similar curves could be drawn for the case of an adiabatic back face. As shown in Figure 22, the flow rate is initially high and decreases as the thickness of the dried region increases. For "unidirectional" drying the drying rate increases again toward the end of the drying cycle but does not for the case of drying from both sides. This can be seen from Figures 38, 39, and 40 and explained by Equation (55).

$$\frac{\dfrac{k_{II}[T_X - T_L]}{X - L} + \dfrac{k_I[T_0 - T_X]}{X}}{\Delta H + [C_p/2][T_0 - T_X]} = -N_w \qquad (55)$$

For "unidirectional" drying, the term in the numerator containing the thermal conductivity of the frozen region predominates, particularly toward the end of the cycle and continually gets larger since the quantity (X - L) approaches zero. For an adiabatic back face or drying from both sides, this term does not appear in the energy balance and the flow rate steadily decreases with increasing time, since the interface position in the denominator of the energy balance steadily increases with increasing time.

Theoretical Drying Times

In Figure 24, the interface position is plotted as a function of time for the general case where heat in conducted through both regions of a beef slab 1-1/2 inches thick. As was expected, drying at 1.0 torr is the fastest, taking approximately 30 hours. In Figure 25,

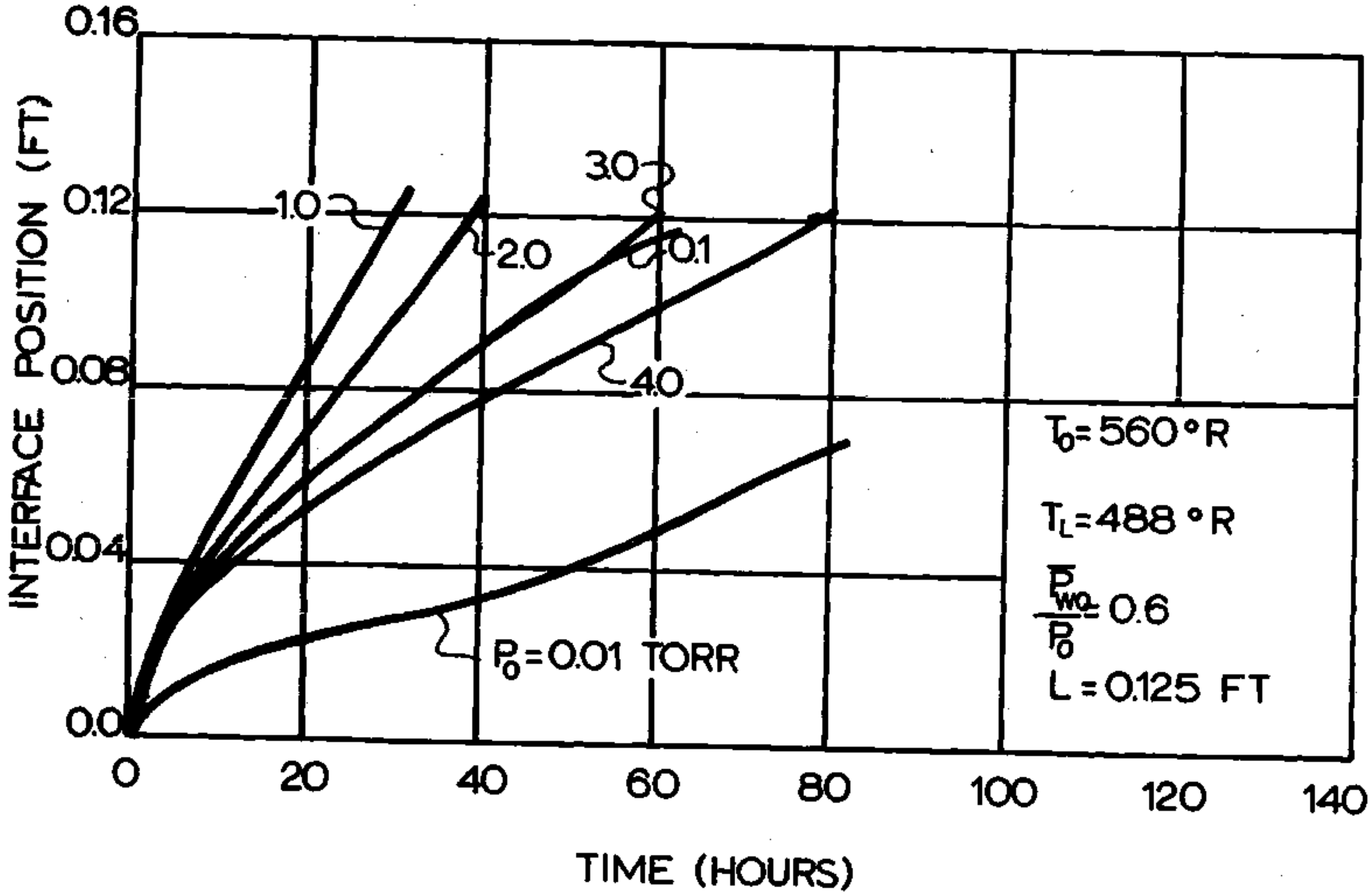

Figure 24. Interface Position vs. Time for Unidirectional Drying of Beef.

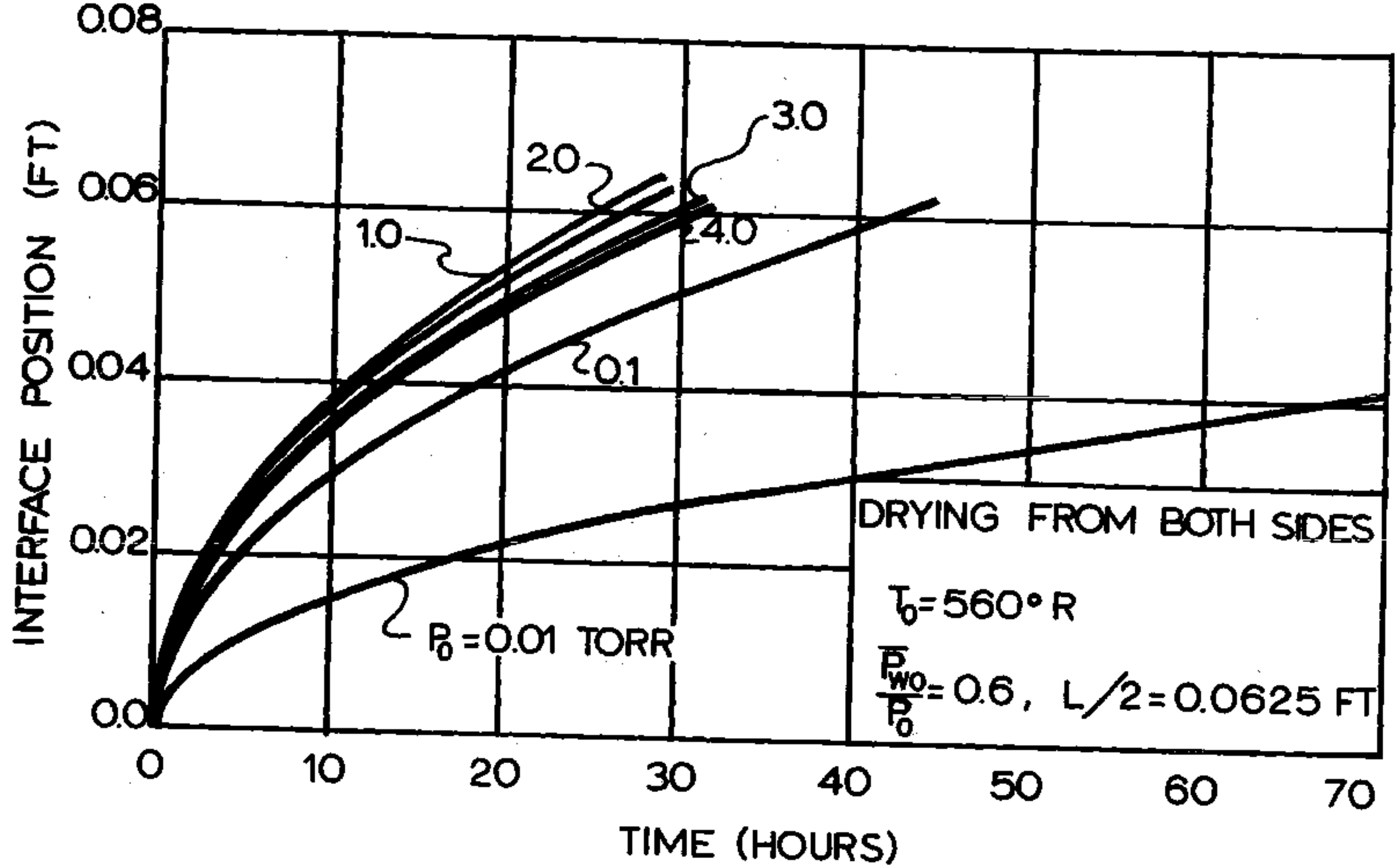

Figure 25. Interface Position vs. Time for Drying of Beef from Both Sides.

the same result is shown for the case where beef is dried equally from both sides. However, the increase in drying time at 2.0, 3.0, and 4.0 torr is not nearly as large for drying from both sides as it is for "unidirectional" drying.

Figure 26 shows the interface movement for drying in the continuum regime. As would be expected, drying occurs faster at 35 torr than at atmospheric pressure, and at both pressures occurs faster with the back face heated. It might be noted that under the condition of "unidirectional" drying, it takes approximately 700 hours to dry a 1-1/2 inch slab of atmospheric pressure as compared to 144 hours at 35 torr. This seems extremely uneconomical, however, atmospheric freeze-drying could be used for thinner slabs of food. For instance, a piece of beef 1/8 inch thick could be dried in approximately 15 hours when allowed to dry from both sides.

Figure 27 shows the influence of back face temperature on drying time. As would be expected, the higher the back face temperature, the shorter is the drying time. It is interesting to note that for the back face temperature of 0°F, the interface temperature remains above 0°F throughout the whole process. Therefore, some of the energy conducted through the dried layer to the interface is lost by conduction out through the frozen region.

In Figure 28 and 29, it is shown that the drying times are smaller if the chamber concentration is reduced, regardless of the drying arrangement.

In Figure 30, the interface movement is plotted for 1.0, 2.0, and 3.0 torr for the cases where the back face is heated and where it

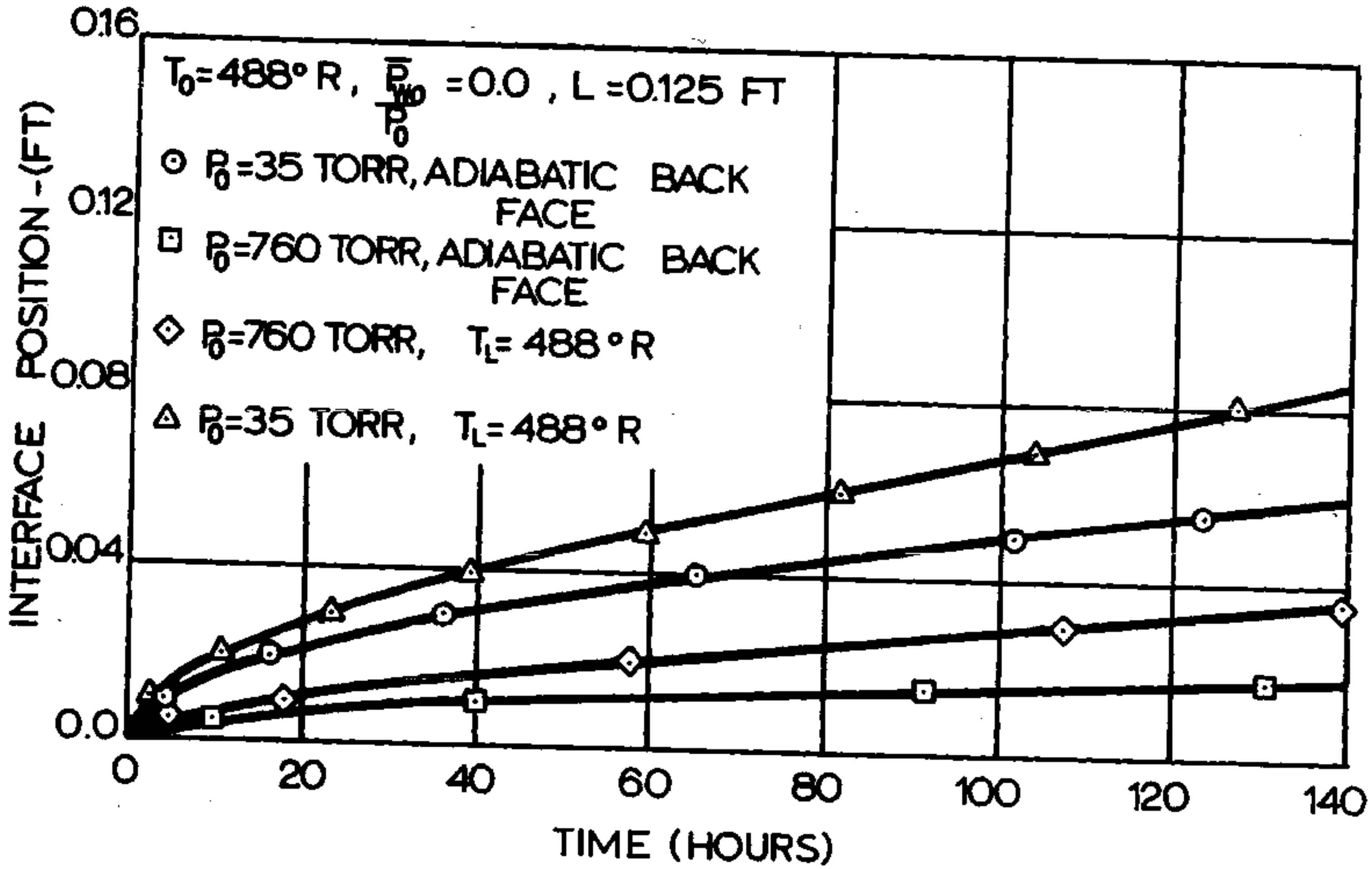

Figure 26. Interface Position vs. Time for Drying of Beef in the Continuum Regime.

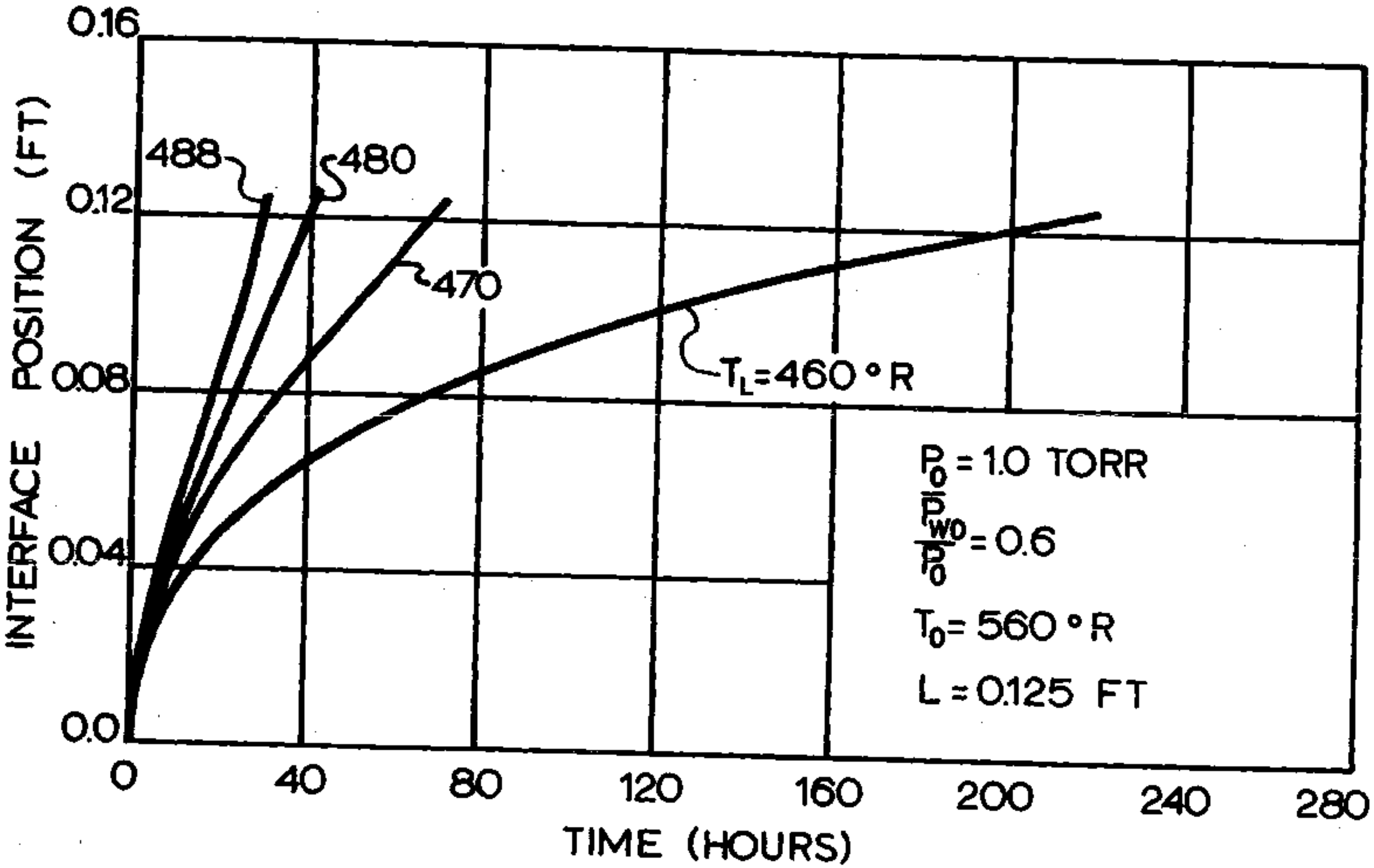

Figure 27. Interface Position vs. Time for Unidirectional Drying of Beef at 1 torr and Several Back Face Temperatures.

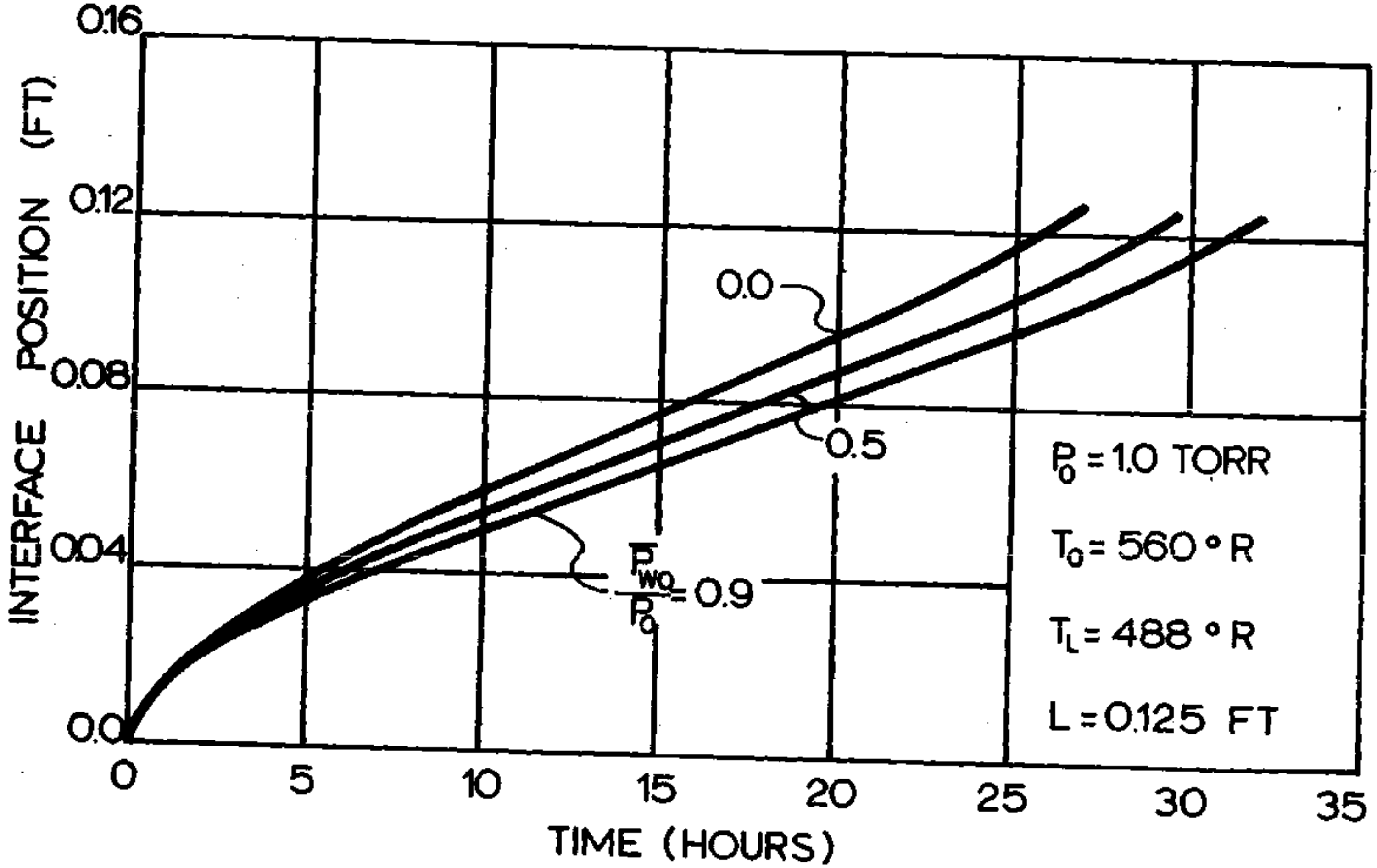

Figure 28. Interface Position vs. Time for Unidirectional Drying of Beef at 1 torr and Several Chamber Concentrations.

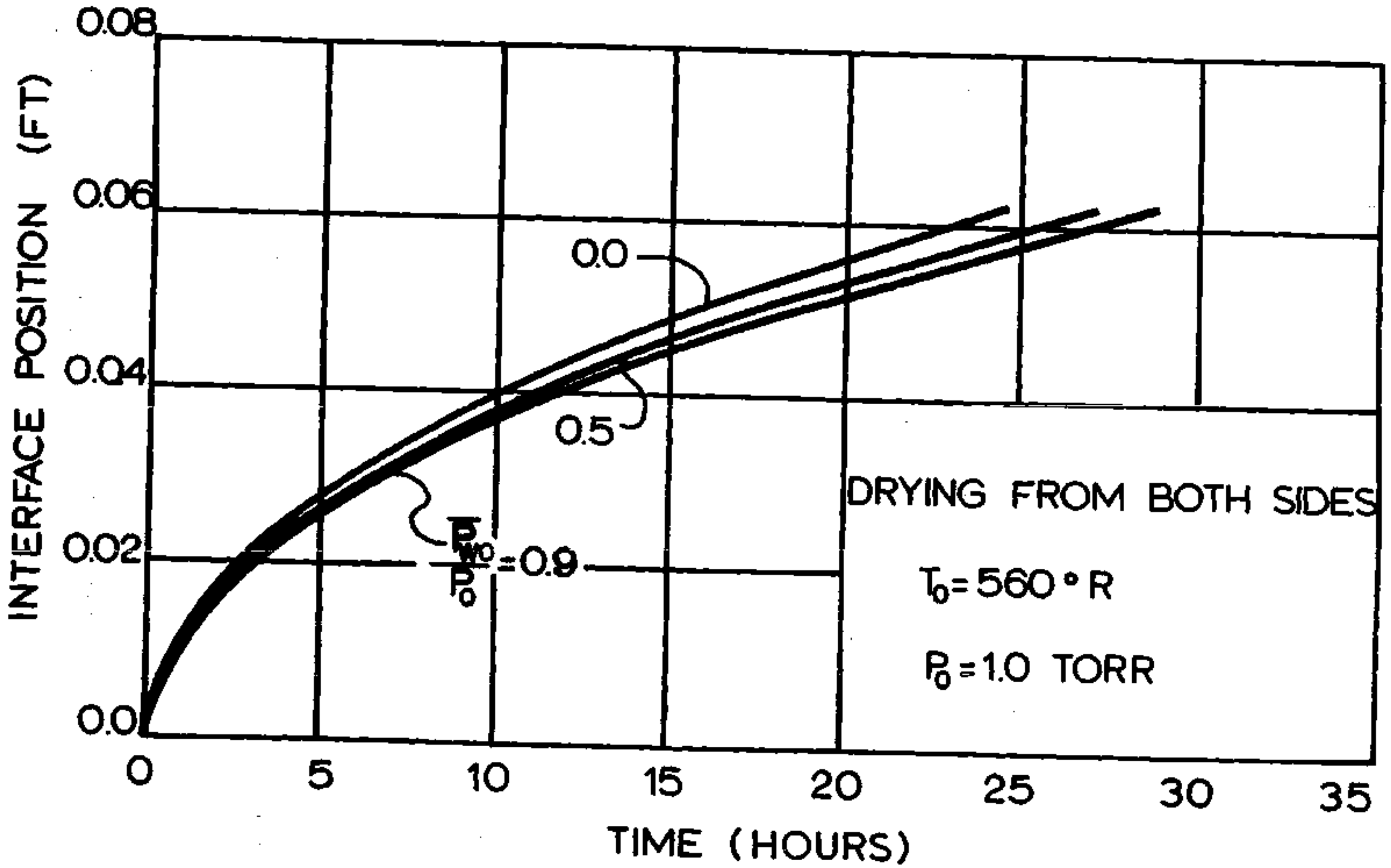

Figure 29. Interface Position vs. Time for Drying of Beef from Both Sides at 1 torr and Several Chamber Concentrations.

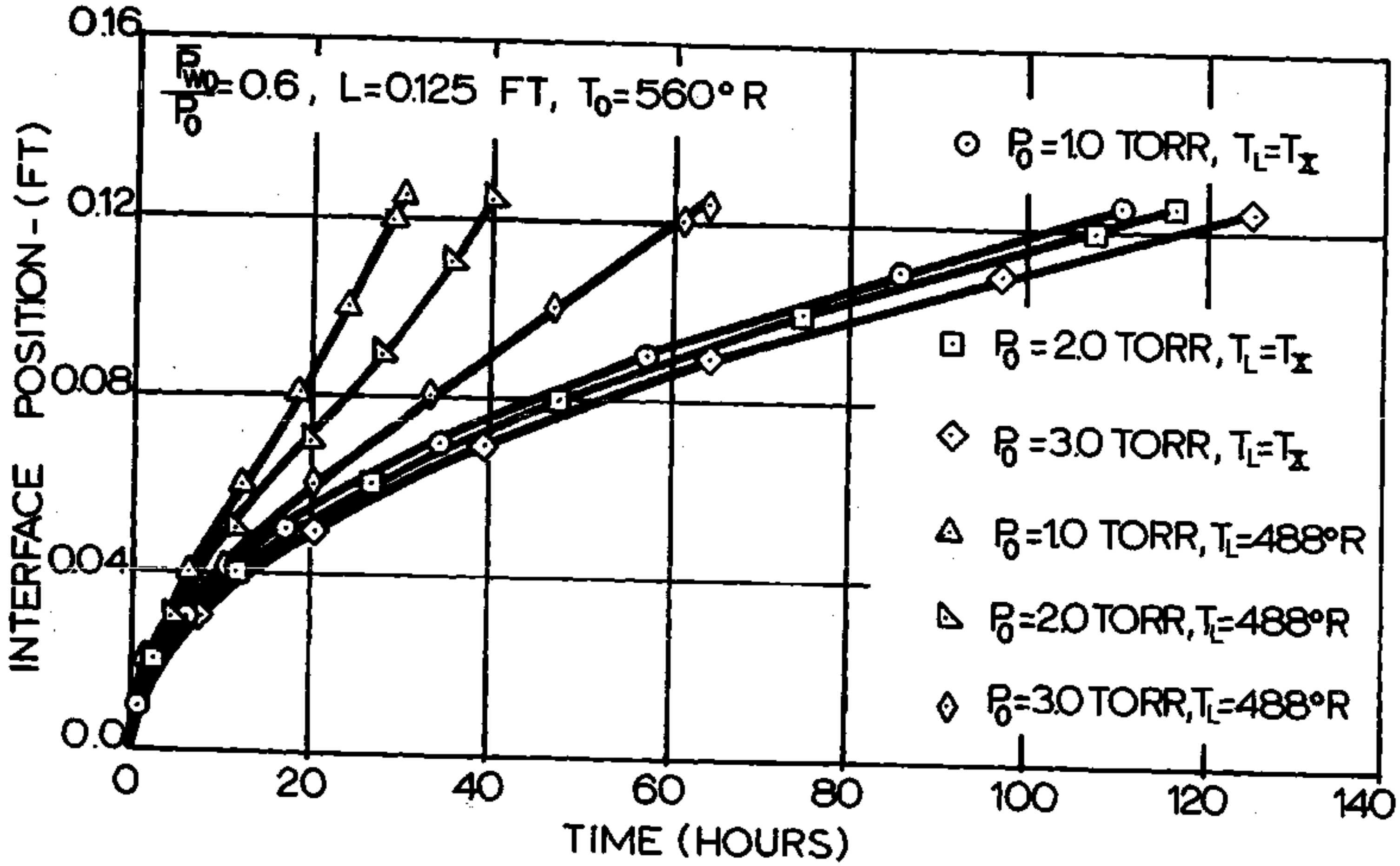

Figure 30. Interface Position vs. Time for Unidirectional Drying of Beef at 1, 2, and 3 torr.

is insulated. The drying time at 1.0 torr is about 400 per cent longer when the back face is insulated. The immediate conclusion seems to be that back face heating has tremendous potential for reducing the drying time and thus the cost of the freeze-drying operation. However, if the back face is going to be insulated, the product might as well be allowed to dry from both sides. The total interface movement for drying from both sides is plotted and compared with unidirectional" drying in Figure 31. Even though the total time for drying a slab 1-1/2 inches thick is approximately the same at 1.0 torr, in all cases the sample dries faster when allowed to dry from both sides. It has been pointed out by Dyer, et al. (42), that a slab 2 inches thick, drying at 1.0 torr, will dry 40 per cent faster when heated from the back than when allowed to dry from both sides. This can be seen if the curves of Figure 31 are extrapolated to 2 inches. However, for all beef samples of 1-1/2 inches or less, there appears to be no advantage to "unidirectional" drying.

Comparison Between Theoretical and Experimental Drying Times

Hatcher (26) measured the movement of the interface as a function of time during the freeze-drying of beef. His data was taken by using a gamma radiation beam and is shown in Figures 32, 33, and 34. He attempted to dry 2-inch thick samples of beef unidirectionally by thermally insulating the sides and back of cylindrical-shaped samples with 2-inch thick fiberglass insulation. If perfect insulation had existed, the experimental data would be expected to follow the theoretical results for an adiabatic back face. It can be seen that,

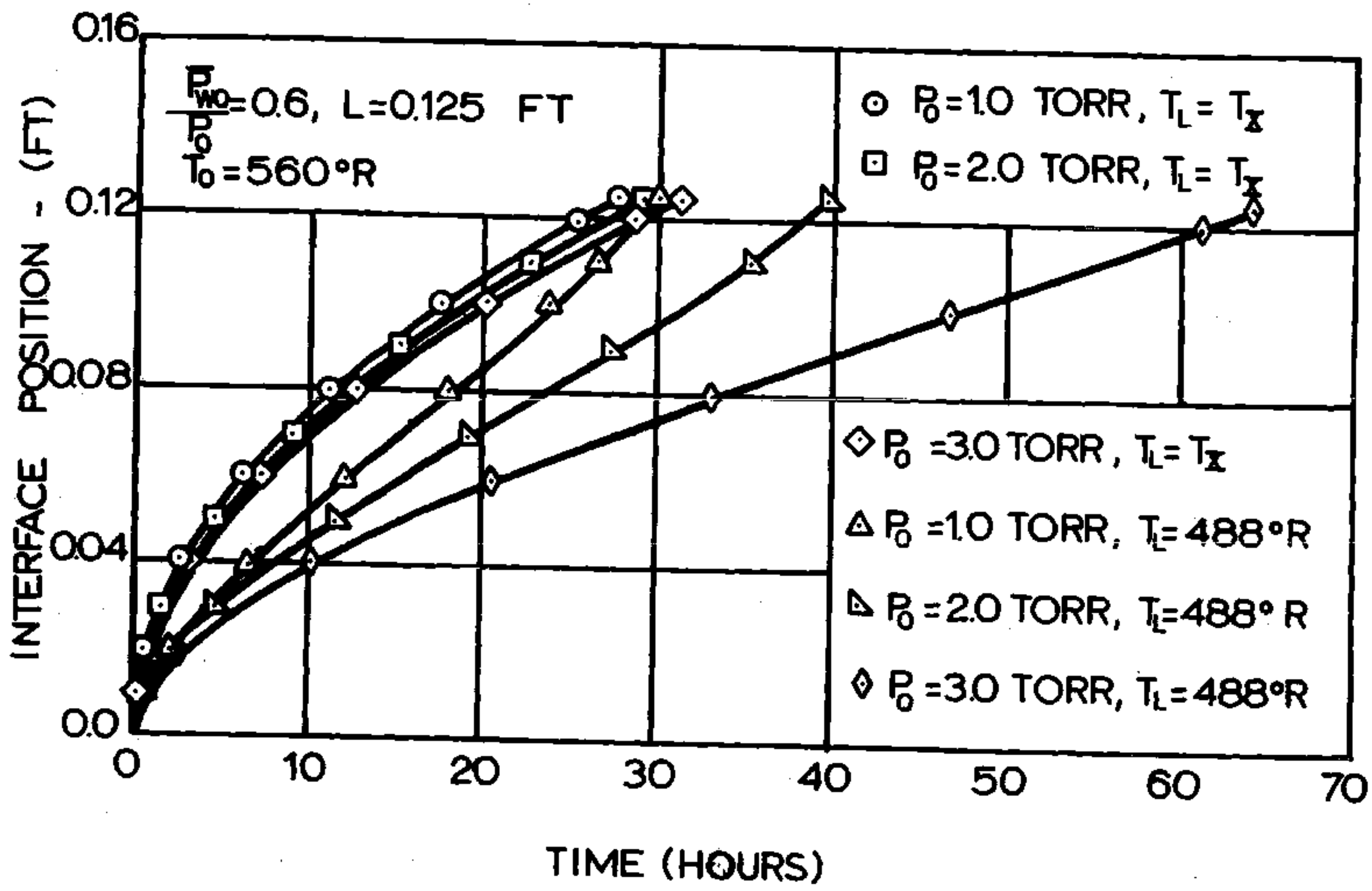

Figure 31. Interface Position vs. Time for Drying of Beef at 1, 2, and 3 torr.

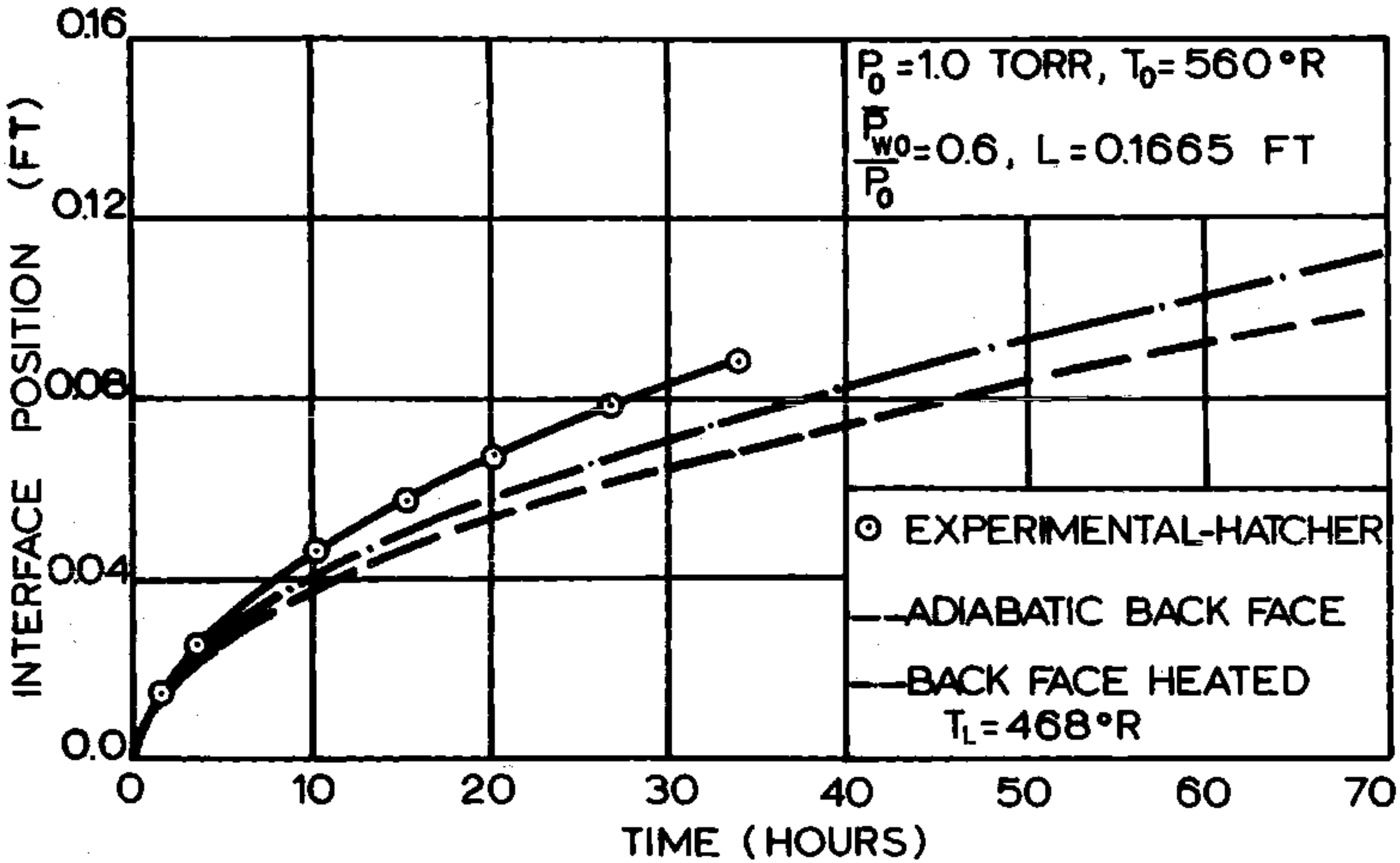

Figure 32. Comparison of Theoretical and Experimental Drying Time Curves at 1 torr.

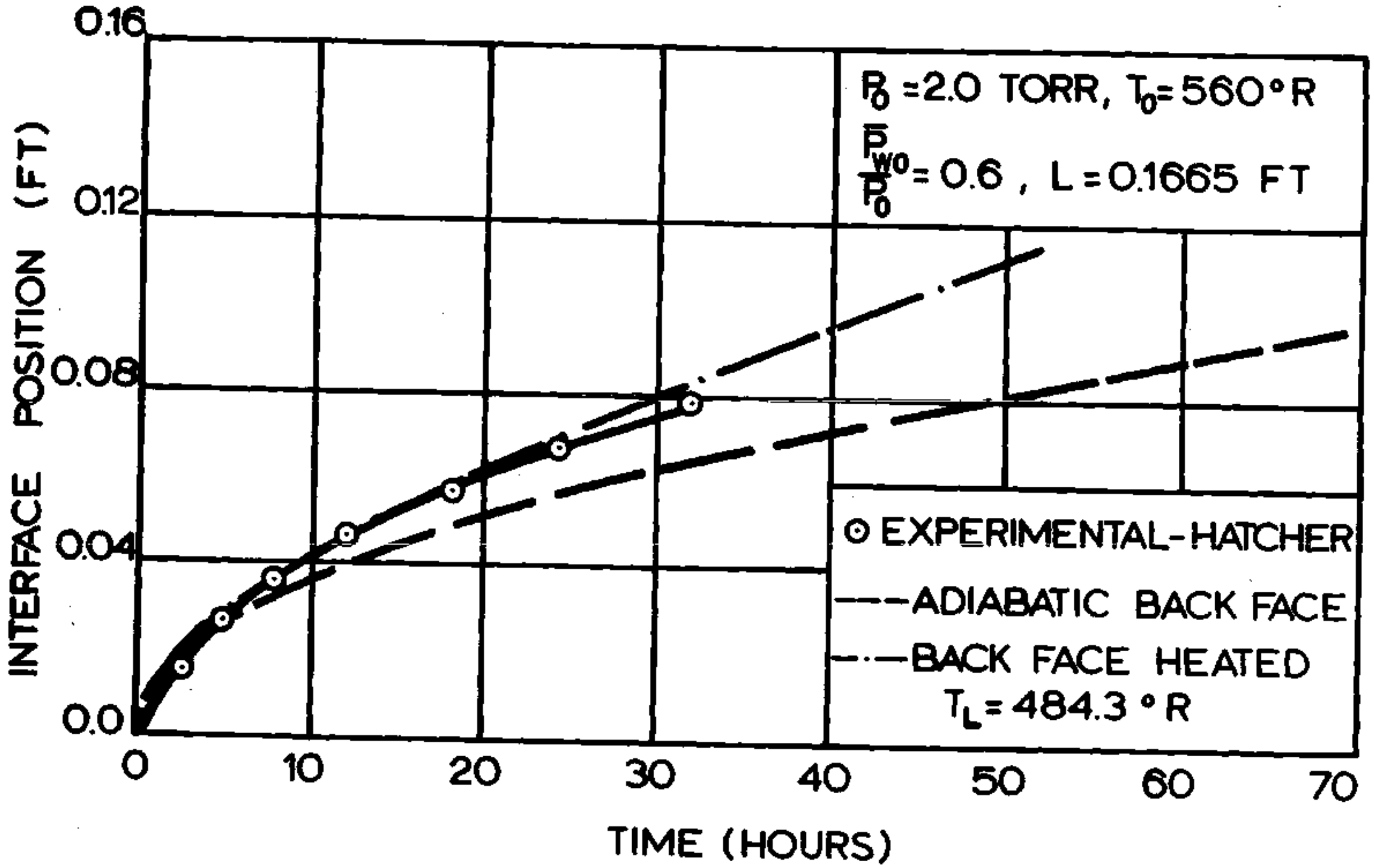

Figure 33. Comparison of Theoretical and Experimental Drying Time Curves at 2 torr.

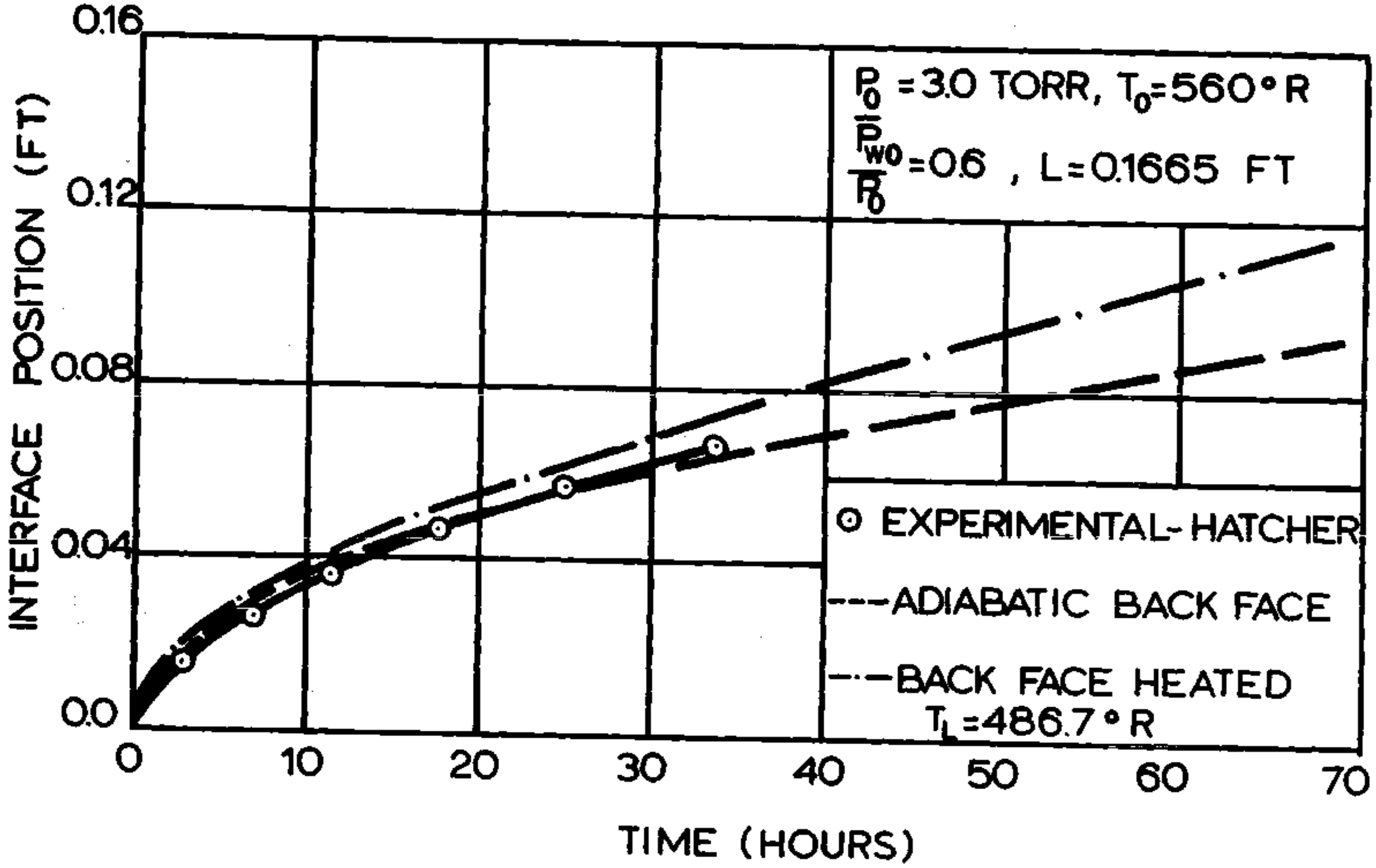

Figure 34. Comparison of Theoretical and Experimental Drying Time Curves at 3 torr.

during the initial stages of drying, the experimental and theoretical curves compare closely, while at later stages of drying, a progressively faster experimental drying rate is achieved. A careful analysis of Hatcher's experiment shows that initially there was a negligible temperature gradient in the frozen layer but at later stages a temperature difference of 2 to 3°F existed. It was felt that an upper limit for the interface movement should be if the back face is heated at the temperature experimentally measured there. The results of these calculations are also shown in Figures 32, 33, and 34. As can be seen, for a pressure of 2.0 and 3.0 torr, the experimental curve lies between the two theoretical curves. However, for a chamber pressure of 1.0 torr, the experimental drying time is faster than the theoretical time if the back face is heated at 468°R. The explanation of this discrepancy might be that the "unidirectional" drying results for such a low back face temperature as this, might not account for all the heat transferred through the sides and back of the sample. It was pointed out in the last section, that for a back face temperature of 460°R, the "unidirectional" results showed that the heat transfer in the frozen region was actually away from the interface.

Hardin (8) presents data for the drying of beef at 0.5, 2.0, and 3.0 torr. His results are shown in Figures 35 through 40. Hardin also used cylindrical samples which he tried to dry unidirectionally and insulate the back face. He used an aluminum foil vapor seal and fiberglass insulation around the sides and bottom. However, the thickness of the insulation was only 1/2 inch on the bottom and 3/4 inch on the side. Therefore, more heat transfer should have taken place

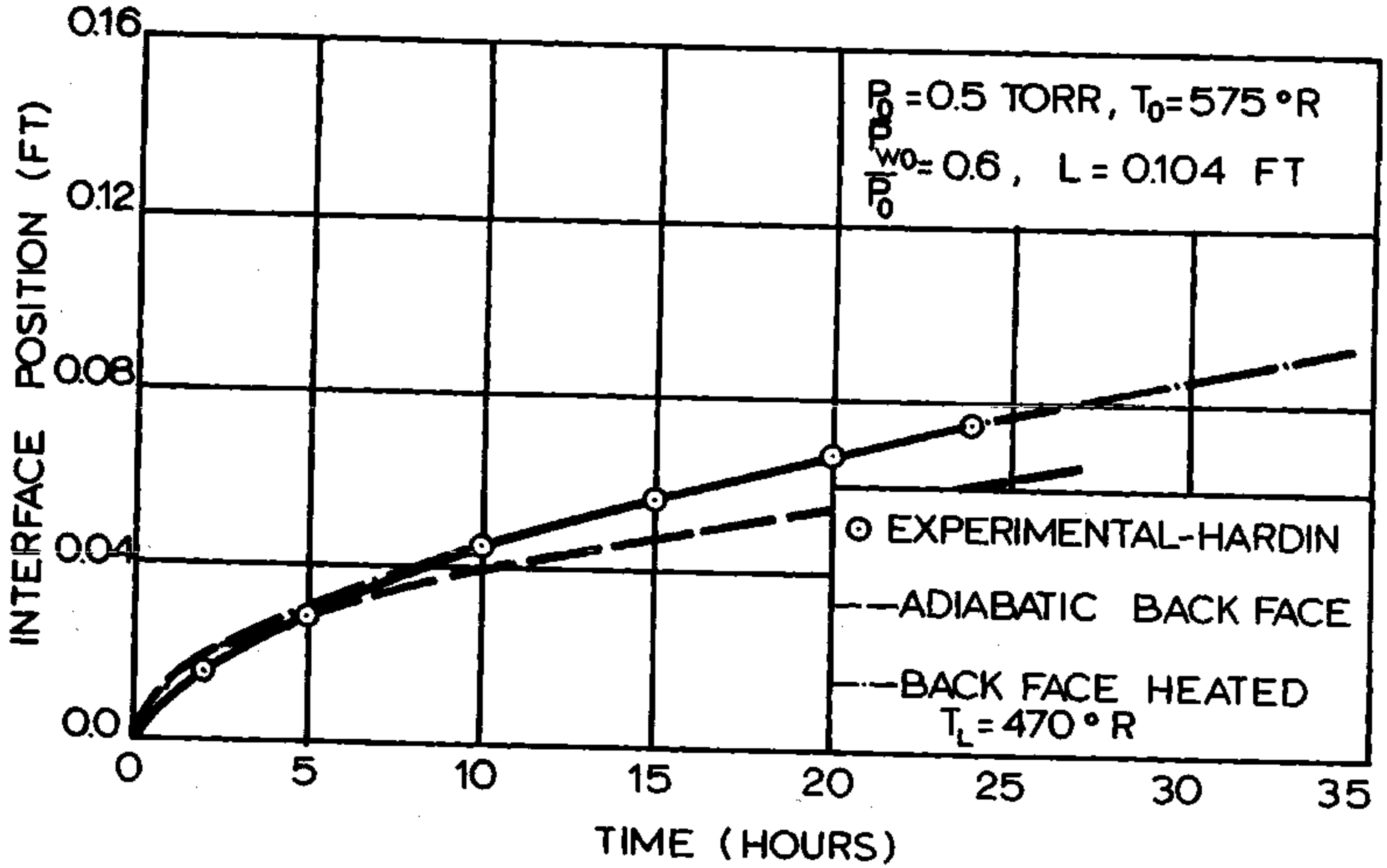

Figure 35. Comparison of Theoretical and Experimental Drying Time Curves at 0.5 torr.

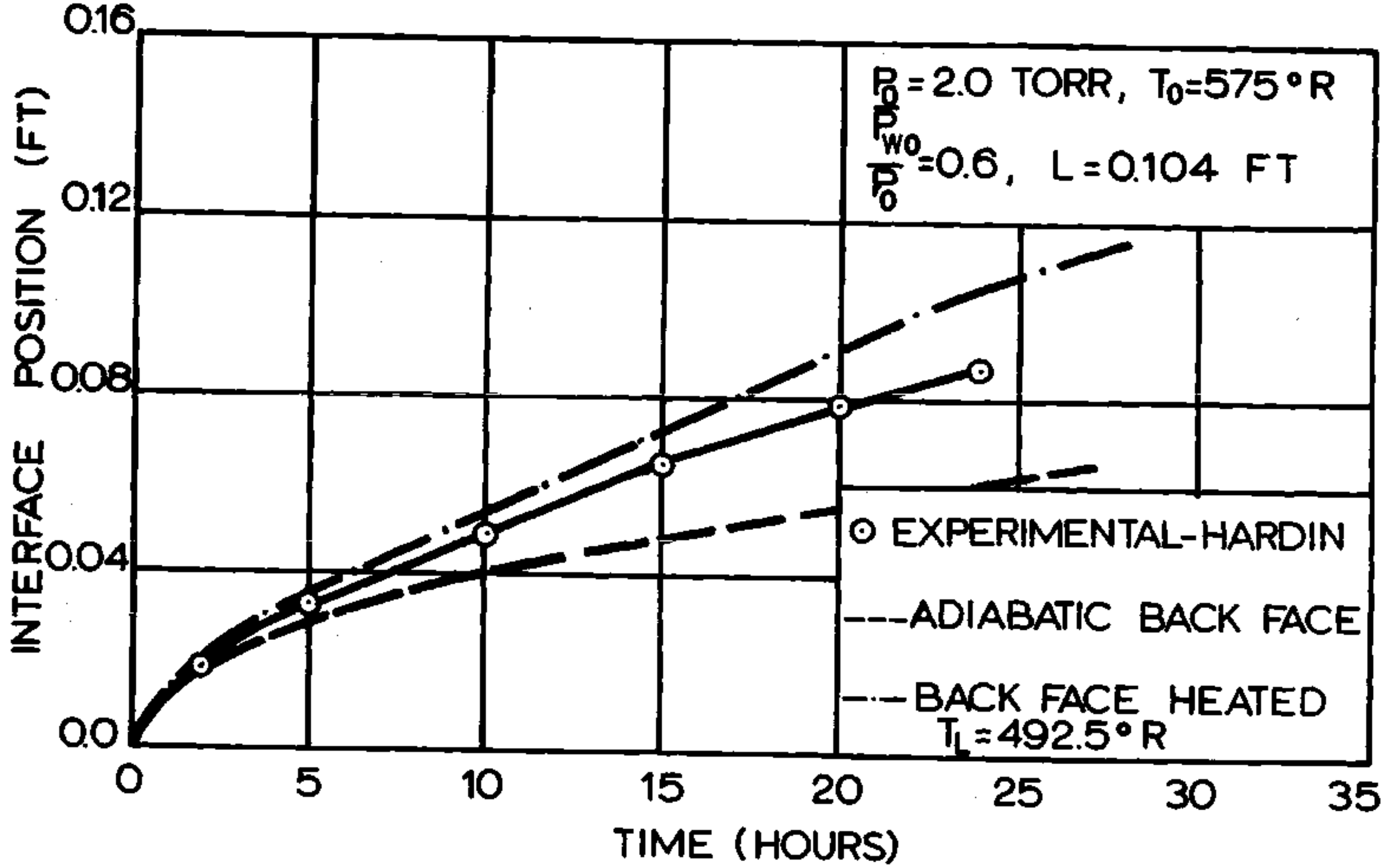

Figure 36. Comparison of Theoretical and Experimental Drying Time Curves at 2 torr.

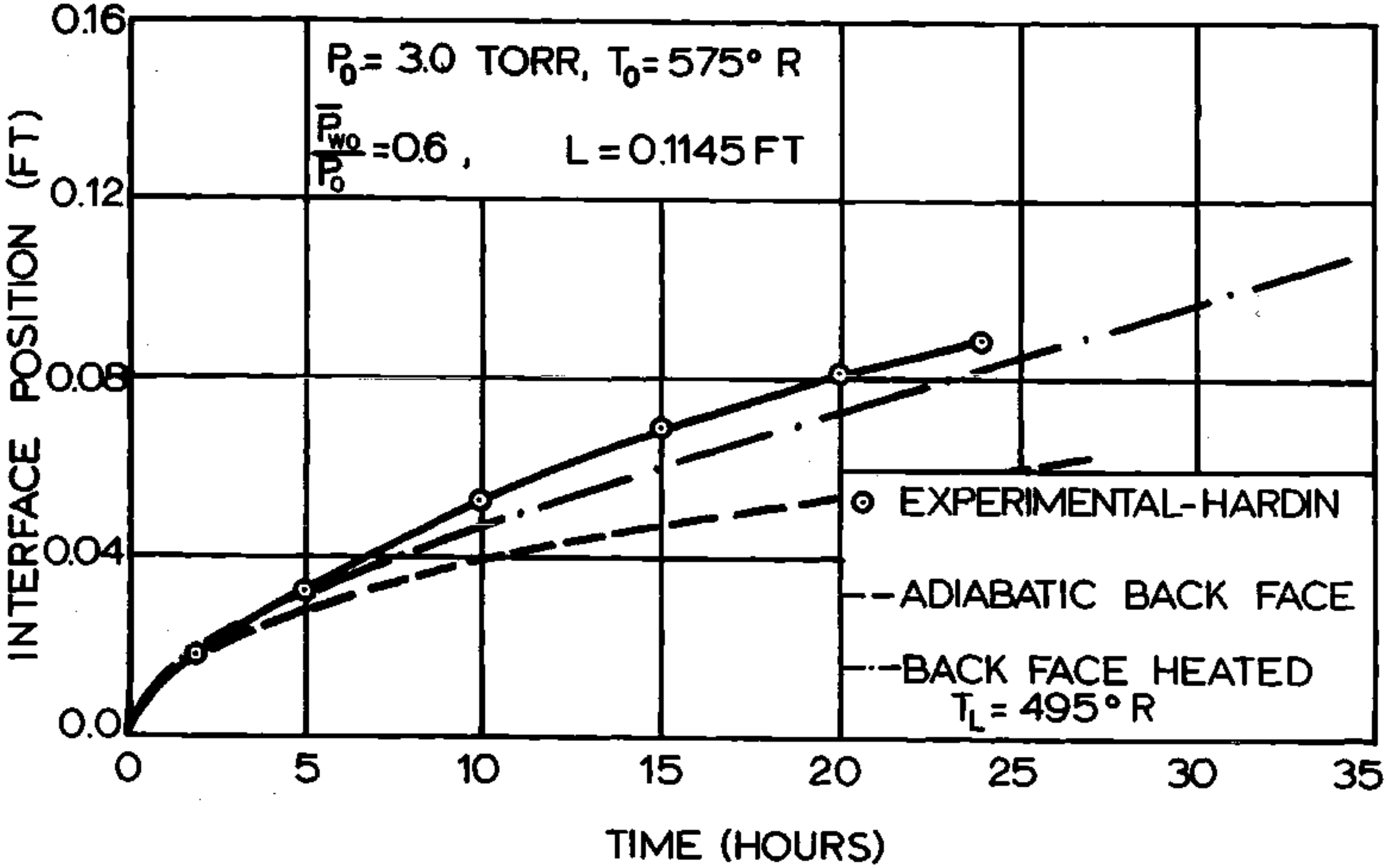

Figure 37. Comparison of Theoretical and Experimental Drying Time Curves at 3 torr.

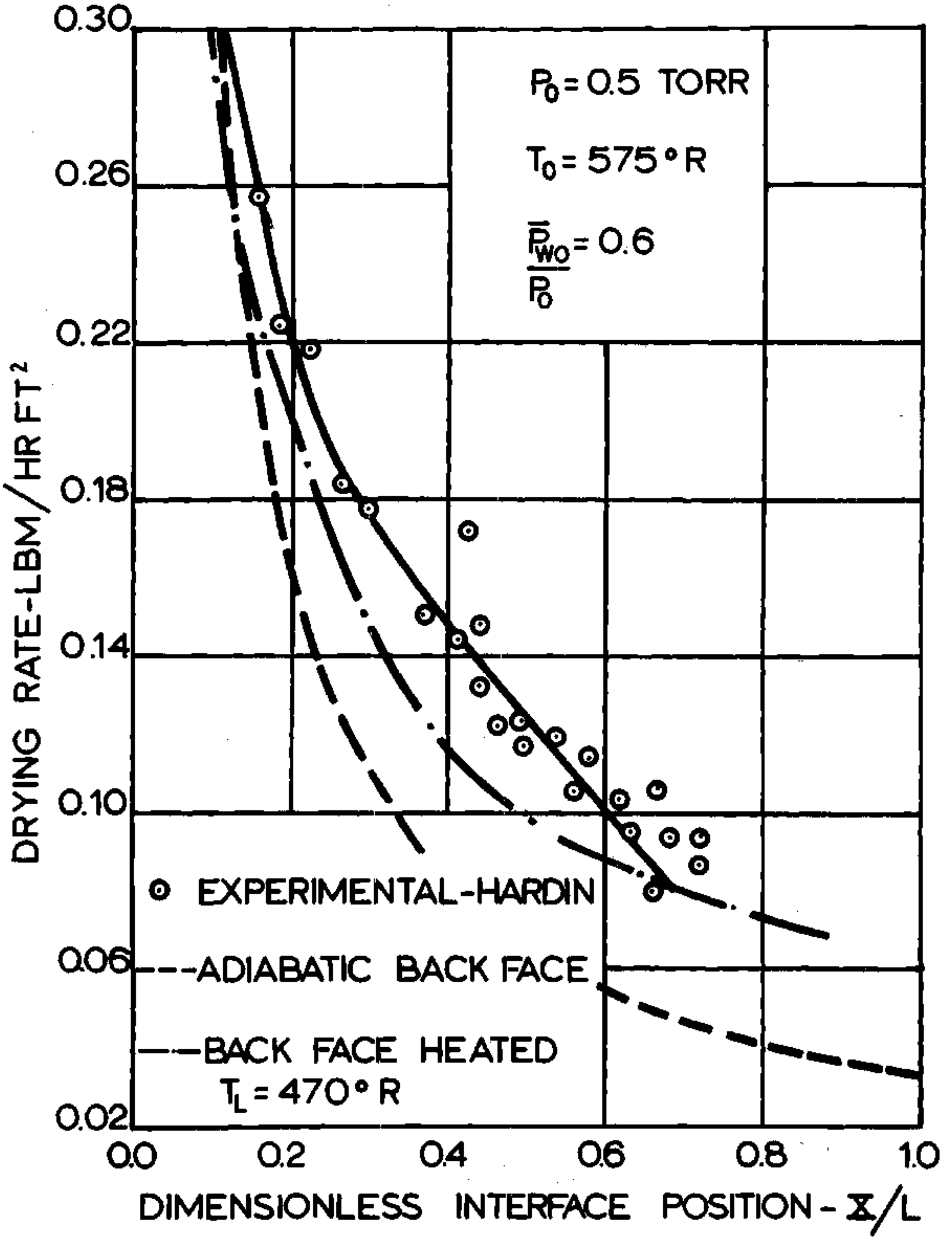

Figure 38. Comparison of Theoretical and Experimental Drying Rate Curves at 0.5 torr.

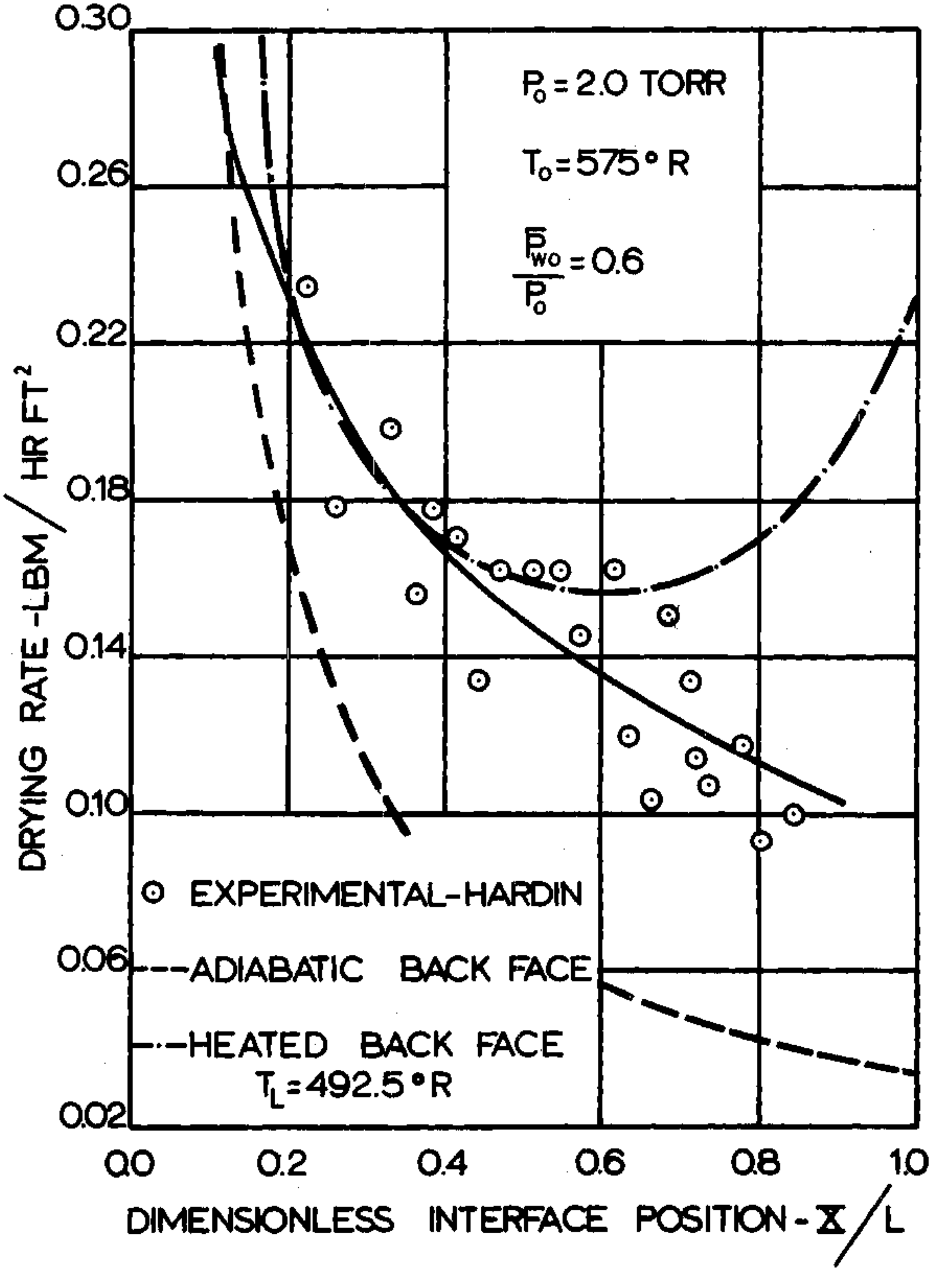

Figure 39. Comparison of Theoretical and Experimental Drying Rate Curves at 2 torr.

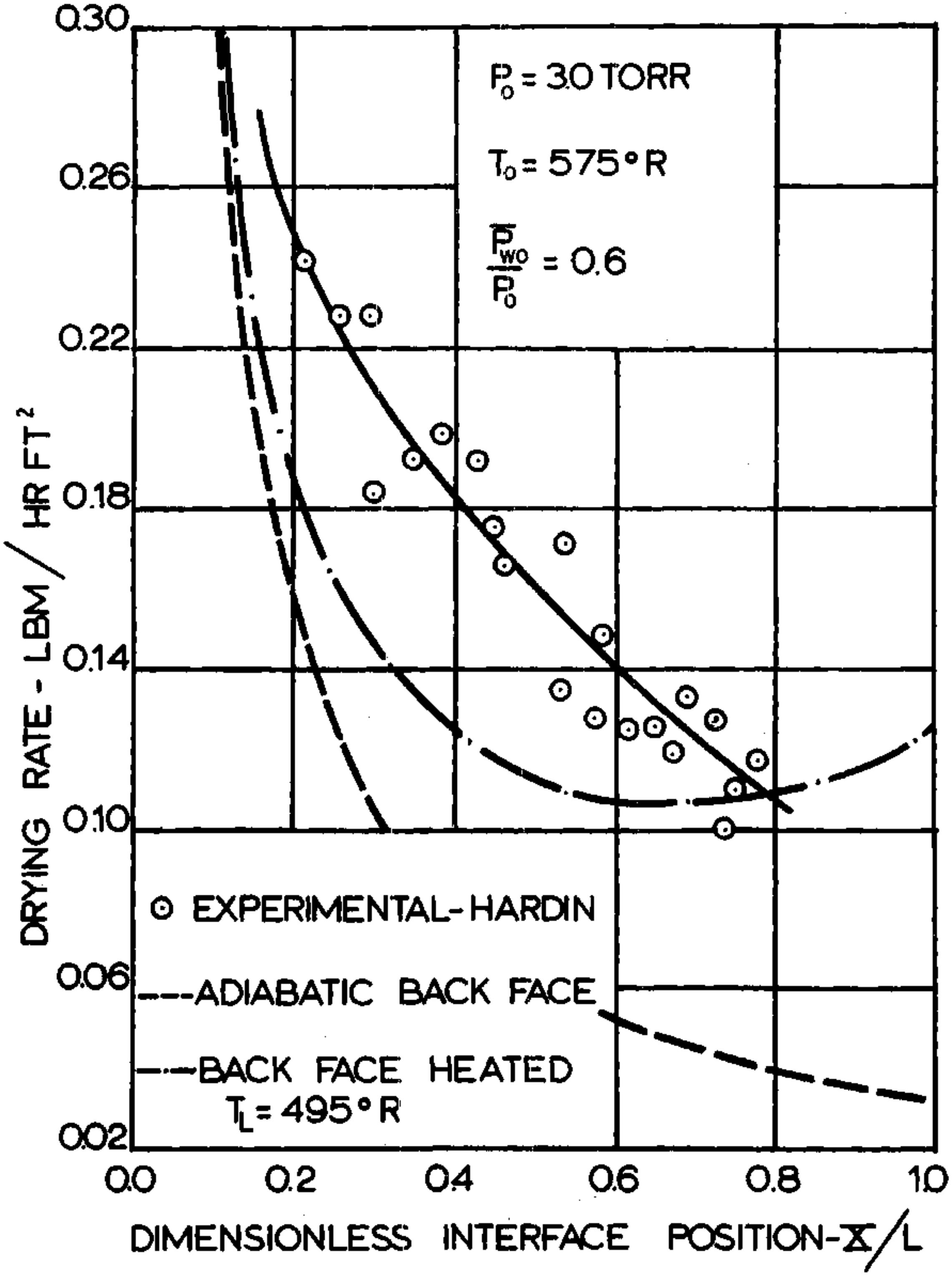

Figure 40. Comparison of Theoretical and Experimental Drying Rate Curves at 3 torr.

through the sides and bottom and thus the experimental data should lie closer to the theoretical case of back face heating than did in Hatcher's case. As can be seen, for a pressure of 0.5 and 2.0 torr the interface movement does lie closer to the theoretical results of back face heating. For a pressure of 3.0 torr, the interface movement was actually faster. Hardin attributed this to the fact that the radial heat flux was larger at 3.0 torr than at 0.5 and 2.0 torr, since fiberglass insulation decreases in effectiveness as the pressure increases.

Figures 38, 39, and 40 contain experimental drying rate data points that were measured by Hardin. Again, the data of 0.5 torr and 2.0 torr agree more closely with the theoretical results than does the data of 3.0 torr.

CHAPTER VI

CONCLUSIONS

The principal conclusions drawn from both the theoretical and experimental analyses of this investigation are:

1. The equilibrium vapor pressure of frozen beef fat, lamb, veal, pork, and chicken is depressed between 13 and 20 per cent below that of pure ice. In addition, pockets of juices that might exist within frozen meats have no effect on the equilibrium vapor pressure.

2. The latent heat of sublimation of frozen beef fat, lamb, veal, pork, and chicken is between 9 and 22 per cent higher than that of pure ice.

3. The effective average diffusion coefficient for an air-water vapor diffusion process in a porous solid in the transition regime, can be calculated with sufficient accuracy from Equation (51).

4. When a product is dried from one side and the back face is heated and sealed against vapor flow, the interface temperature varies with interface position and the relationship is given by Equation (56).

5. When a product is dried from one side and the back face is insulated, or when it is dried from both sides, the interface temperature is constant throughout the drying process and is given by Equations (67), (68), and (70) for the free-molecule, continuum, and transition flow regimes, respectively.

6. When beef is dried from one face and heated and sealed

against vapor flow on the back face in the pressure range 0.5 to 4.0 torr, the interface temperature can be approximated by a linear function of interface position. In addition, Equation (76) can be used to calculate the interface position as a function of time.

7. The optimum pressure at which to freeze-dry beef is 1.0 torr, regardless of the arrangement.

8. Atmospheric freeze-drying appears to be economical and practical for products that have a small thickness.

9. Drying times for the freeze-drying process can be reduced by increasing the dried region surface temperature and frozen region surface temperature, and decreasing the partial pressure of the water vapor in the chamber.

10. Drying times for the freeze-drying process cannot necessarily be reduced by decreasing the total pressure at which drying takes place.

11. Beef samples which are equal to or less than 1-1/2 inches in thickness, can be freeze-dried faster by drying from both sides than drying from one side and conducting heat through the frozen region on the other side.

APPENDIX A

DERIVATION OF DRIED REGION ENERGY EQUATION

Consider the control volume taken from the dried region and shown in Figure 41.

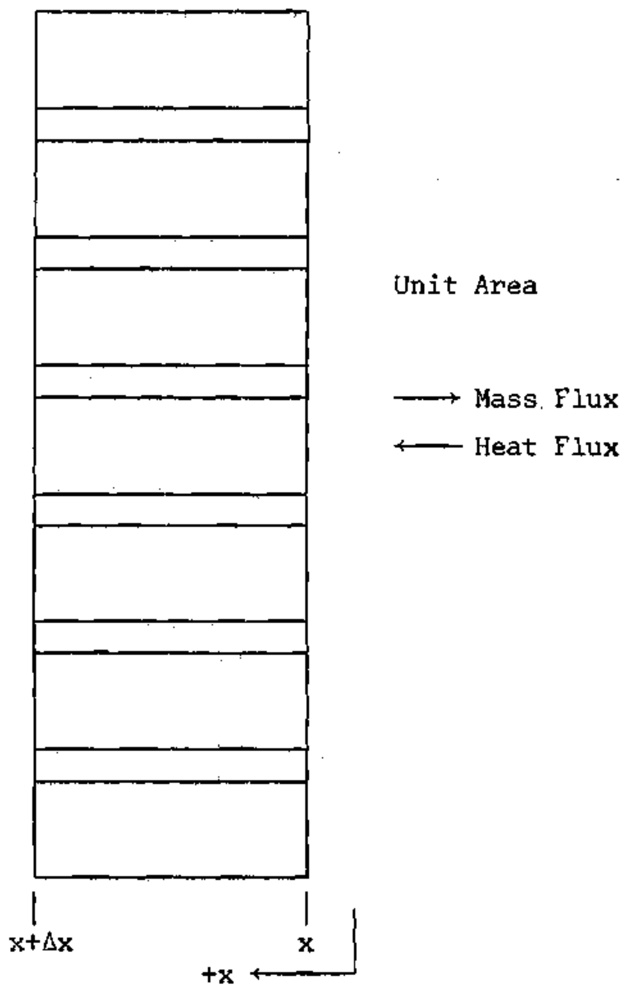

Figure 41. Energy Control Volume for Dried Region

The conservation of energy for the control volume is

$$\left[-k_I \left.\frac{dT_I}{dx}\right|_{x+\Delta x} + N_w \, C_p \, T_I \Big|_{x+\Delta x} \right] \tag{108}$$

$$- \left[-k_I \left.\frac{dT_I}{dx}\right|_{x} + N_w \, C_p \, T_I \Big|_{x} \right] = 0$$

Equation (108) equates the rate of energy flowing out of the control volume to the rate flowing in for "quasi-steady" drying. The first two terms represent the energy conducted and convected out of the control volume, and the remaining two terms represent the energy conducted and convected into the control volume. If Equation (108) is divided by $-k_I \Delta x$ and the limit taken as $\Delta x \to 0$, it reduces to

$$\frac{d^2 T_I}{dx^2} - \frac{N_w \, C_p}{k_I} \, \frac{dT_I}{dx} = 0 \tag{109}$$

Since the mass flow rate can be expressed by

$$-\rho_i \, \sigma \, \frac{dX}{dt}$$

Equation (109) becomes

$$\frac{d^2 T_I}{dx^2} + \frac{\rho_i \, \sigma \, C_p}{k_I} \frac{dX}{dt} \frac{dT_I}{dx} = 0 \tag{110}$$

APPENDIX B

THERMAL TRANSPIRATION EFFECT

Kennard (28) shows that for flow of a gas in a capillary tube, a positive temperature gradient along the axis of the tube will produce an increased flow rate over that of the isothermal flow. The equations for the case of non-uniform temperature are for the free-molecule regime,

$$N_w = - \frac{4\ r_c [16T]^{1/2}}{3\ \bar{v}_w\ \pi} \left[\frac{1}{T^{1/2}} \frac{dP}{dx} - \frac{1}{2} \frac{P}{T^{3/2}} \frac{dT}{dx} \right] g_c \tag{111}$$

for the transition regime,

$$N_w = - \frac{r_c^{\ 2}\ P}{8\ \eta\ R\ T} \left[1 + \frac{4\ \xi}{r_c} \right] \frac{dP}{dx} + \frac{3\ \eta}{4\ T} \frac{dT}{dx} g_c \tag{112}$$

where

$$\xi = 2\ C_9 \frac{2 - S}{S} \lambda$$

and

$$.491 < C_9 < .499$$

and for the continuum regime,

$$N_w = - \frac{r_c^{\,2}\,P}{8\,\eta\,R\,T}\frac{dP}{dx} + \frac{3\,\eta}{4\,T}\,\frac{dT}{dx}\,g_c \qquad (113)$$

The terms on the right side of all three equations represent respectively the contributions to the mass flow of a total pressure and temperature gradient.

Since the temperature gradients in freeze-drying work are relatively steep, it is desirable to ascertain whether the flow due to the temperature gradient can be neglected. Dyer (9) showed that the ratio of the flow due to thermal transpiration to that due to a total pressure gradient was less than 0.03 for freeze-drying in the transition regime. His calculations were based on Equation (112). The author used Equations (111) and (113) to calculate similar ratios for freeze-drying in the free-molecule and continuum regimes. For typical freeze-drying conditions, the ratio was found to be approximately 0.05 and 0.03, respectively. It, therefore, appears that the thermal transpiration effect can be neglected in the freeze-drying analyses.

APPENDIX C

ANALYSIS OF THE GASEOUS MIXTURE FLOW IN THE TRANSITION REGIME

The analysis of the flow of the gaseous mixture in the transition regime is given here basically as presented by Dyer (9).

The porous material will be idealized as a bundle of capillaries of circular cross section. It will be sufficient to analyze the flow in a single capillary and modify the results for the porous material. It is assumed that incompressible, steady, one-dimensional flow exists in a constant area capillary. Slip effects at the wall will be considered.

For flow in a circular tube, the velocity distribution obtained from the Navier Stokes equation is

$$u = \frac{1}{4}\,\frac{P_2 - P_1}{\eta\,\ell}\,r^2 + C_{10} \tag{113}$$

The constant C_{10} will be determined by choosing an appropriate boundary condition at the wall. In the continuum regime, the velocity at the wall is taken to be zero. For the case under consideration, the mean free path is approximately equal to the diameter of the tube. This condition results in the so-called "slip-flow" in which a velocity exists at the wall. The following definition is made for a force coefficient at the wall

$$C_F = \frac{F_{wall}}{u_c \pi 2 r_c \ell} \tag{114}$$

where F_{wall} is the viscous force on the wall. By applying a force balance on the wall of the tube, it can be shown that (29)

$$u_c = - \frac{\eta}{C_F} \left.\frac{du}{dr}\right|_{r=r_c} \tag{115}$$

The value of C_{10} can be determined from Equations (113) and (115). Substituting the resulting value of C_{10} into Equation (113) gives

$$u = - \frac{P_2 - P_1}{4 \eta \ell} \left[\frac{\eta}{C_F} 2 r_c + r_c^2 - r^2\right] \tag{116}$$

To obtain the mass flow rate, it is necessary to multiply Equation (116) by the gas density and integrate over the cross sectional area of the capillary to give

$$N' = - \frac{\pi \rho [P_2 - P_1]}{8 \eta \ell} r_c^4 \left[1 + \frac{\eta}{C_F} \frac{4}{r_c}\right] \tag{117}$$

The ratio η/C_F is called the coefficient of slip. For a Maxwellian gas, the coefficient can be determined analytically to be (29)

$$\frac{\eta}{C_F} = \frac{\eta}{P_m} \frac{2 - S}{S} \frac{\pi}{4} \bar{v} \tag{118}$$

Substituting this expression into Equation (117) and assuming completely diffuse reflections gives

$$N' = -\frac{\pi\ \rho[P_2 - P_1]}{8\ \eta\ \ell} r_c^4 \left[1 + \frac{\eta}{P_m} \frac{\pi}{4} \bar{v} \frac{4}{r_c}\right] \tag{119}$$

Equation (119) is valid for flow through a single capillary. Several corrections enumerated below will make the equation valid for use with porous media.

1. The flow rate will be converted to per unit area of the food sample by multiplication of the equation by the porosity σ, which is defined as the ratio of the pore volume to the total food volume.

2. The vapor actually travels a longer, tortuous path through the food sample so that Equation (119) must be corrected by multiplying the length by the tortuosity factor τ.

3. In addition, a first order correction for the nonroundness and other irregularities of the capillaries can be made by multiplying Equation (119) by a constant Γ.

Applying the above corrections to Equation (119) gives the following equation for flow through porous media.

$$N' = -\frac{\pi\ \rho[P_2 - P_1]\Gamma\ \sigma\ r_c^4}{8\ \eta\ \tau\ \ell} \left[1 + \frac{\eta}{P_m} \frac{\pi}{4} \bar{v} \frac{4}{r_c}\right] \tag{120}$$

Define

$$\Delta P = P_2 - P_1 \tag{121}$$

$$B_4 = \frac{\Gamma \pi r_c^4 \sigma}{8 \tau} \tag{122}$$

and

$$B_5 = \eta \frac{\pi}{4} \bar{v} \frac{4}{r_c} \tag{123}$$

Equation (120) now takes the form

$$N' = - \frac{\Delta P}{\ell} \frac{\rho}{\eta} B_4 \left[1 + \frac{B_5}{P_m}\right] \tag{124}$$

Note that B_4 and B_5 are only functions of the porous material, average temperature, and gas flowing and should be constant for a given gas, temperature, and porous material. Scott and Dullien (34) point out that Equation (124) fails to correlate experimental data for flow through porous media. The reason for this failure is attributed to the fact that in the derivation of the slip flow term, all of the molecules were assumed to have undergone intermolecular collisions between two successive wall collisions. At r_c/λ approximately equal to 1/2, it seems logical that a fraction of the molecules do not undergo these intermolecular collisions. A modification of Equation (124) is required to take this into account. We assume a certain fraction of the molecules $F(r_c/\lambda)$ do not undergo intermolecular collisions. This fraction to a first approximation is considered to flow as described by Knudsen's equation for molecular streaming. Equation (124) is assumed to describe properly the remaining fraction of the molecules. With this background, Equation (124) can be modified as follows

$$N' = \left[1 - F(r_c/\lambda)\right] \left[- \frac{B_4 \, \Delta P \, \rho}{\eta \, \ell} \left[1 + \frac{B_5}{P_m}\right]\right] \tag{125}$$

$$- B_3 \frac{\Delta P}{\ell} F(r_c/\lambda)$$

where B_3 is a constant given by kinetic theory (34)

$$B_3 = \frac{2 \, \pi \, r_c^{\,3}}{3} \frac{\bar{v}}{RT} \frac{\Gamma\sigma}{\tau} \tag{126}$$

and Equation (126) has been corrected in order that it applies to flow in porous media. Scott and Dullien show that by assuming diffuse reflections and a long capillary tube, the fraction $F(r_c/\lambda)$ is given approximately by

$$F(r_c/\lambda) = e^{-\sinh^{-1}\left[\frac{2 \, r_c}{\lambda}\right]} \tag{127}$$

Substituting Equation (127) into (126) yields

$$N' = \left[1 - e^{-\sinh^{-1}\left[\frac{2r_c}{\lambda}\right]}\right]\left[-\frac{B_4\ \Delta P\ \ \rho}{\eta\ \ell}\left[1 + \frac{B_5}{P_m}\right]\right] \tag{128}$$

$$- B_3\ \frac{\Delta P}{\ell}\ e^{-\sinh^{-1}\left[\frac{2r_c}{\lambda}\right]}$$

By analogy with Darcy's law for the present case of transition flow, the permeability will be defined by

$$\varepsilon = -\frac{\eta\ N\ \ell}{\rho\ \Delta P} \tag{129}$$

By comparing Equations (128) and (129) it is seen that

$$\varepsilon = \left[1 - e^{-\sinh^{-1}\left[\frac{2r_c}{\lambda}\right]}\right]\left[B_6\left[1 + \frac{B_5}{P_m}\right]\right] \tag{130}$$

$$+ \frac{\eta}{\rho}\ B_7\ e^{-\sinh^{-1}\left[\frac{2r_c}{\lambda}\right]}$$

where

$$B_6 = \frac{\Gamma\ r_c^{\ 2}\ \sigma}{8\ \tau} \tag{131}$$

and

$$B_7 = \frac{2\ r_c}{3} \frac{\bar{v}}{RT} \frac{\Gamma\sigma}{\tau} \qquad (132)$$

Note that in the absence of external forces, the above derivation is valid for gas mixture transport as well as for a pure gas.

APPENDIX D

VAPOR FLOW APPROXIMATIONS

As was pointed out in Chapter 2, Equation (45) for flow of the water vapor in the transition regime was approximated by Equation (48), in which the term $\frac{P_m}{\Delta P} \ln\left[1 + \frac{\Delta P}{P_O}\right]$ was assumed to be 1 for the pressures encountered in freeze-drying. In addition, to enable a closed form relation for the interface temperature to be developed in the continuum regime, the following approximation was made to Equation (33)

$$\ln\left[\frac{1 - y_{wX}}{1 - y_{wO}}\right] = 2\left[\frac{y_{wO} - y_{wX}}{2 - y_{wO} - y_{wX}}\right] + \frac{2}{3}\left[\frac{y_{wO} - y_{wX}}{2 - y_{wO} - y_{wX}}\right]^3 + \cdots \qquad (133)$$

The higher ordered terms were neglected to give the following modified form of Equation (33)

$$N_w \approx \frac{P\ D_{aw}}{R\ T\ X}\, 2\left[\frac{y_{wO} - y_{wX}}{2 - y_{wO} - y_{wX}}\right] \qquad (134)$$

The accuracy of the above approximations were checked in the following manner:

1. The interface temperature was calculated using Equation (56) and the value of Q for the specific flow regimes. Note that these relations were developed using the above approximations.

2. The flow rate of vapor was then calculated using Equation (55).

3. Appropriate equations for the two flow regimes were then used to calculate the total pressure at the interface (Equation (18) for the continuum regime and Equation (35) for the transition regime).

4. These values of interface total pressure, along with values of chamber total and partial pressure and interface partial pressure (from the equilibrium vapor pressure experimental measurements), were used in the original flow equations (before approximations were made) to calculate water vapor flow rates.

5. The flow rates calculated in steps (2) and (4) above were compared and the accuracy of the approximations were considered by comparing the closeness of the two flow rates.

Tables 3 and 4 show the results of the above calculations for typical freeze-drying conditions in the transition and continuum flow regimes, respectively. As can be seen, the difference in the flow rates is negligible. It is therefore concluded that the above approximations cause no appreciable error in the freeze-drying analysis.

Table 3. Flow Rate of Water Vapor for Freeze-Drying of Beef in the Transition Regime

T_0 = 560°R P_0 = 1.0 torr

T_L = 488°R $\bar{P}_{w0}$ = 0.6 torr

Dimensionless Interface Position X/L	Flow Rate (lbm/ft^2sec) x 10^5 Equation (55)	Flow Rate (lbm/ft^2sec) x 10^5 Equation (45)
0.010	69.57	69.50
0.113	8.37	8.36
0.221	5.49	5.47
0.330	4.56	4.54
0.437	4.18	4.16
0.540	4.05	4.01
0.637	4.06	4.01
0.725	4.18	4.11
0.803	4.37	4.28
0.871	4.65	4.51
0.930	5.00	4.81

Table 4. Flow Rate of Water Vapor for Freeze-Drying of Beef in the Continuum Regime

T_0 = 488°R P_0 = 35 torr

T_L = 488°R $\bar{P}_{w0}$ = 0.0 torr

Dimensionless Interface Position X/L	Flow Rate (lbm/ft^2sec) x 10^5 Equation (55)	Flow Rate (lbm/ft^2sec) x 10^5 Equation (33)
0.001	91.881	91.896
0.027	4.981	4.981
0.062	2.457	2.457
0.111	1.555	1.556
0.179	1.076	1.076
0.283	0.766	0.767
0.448	0.542	0.542
0.746	0.365	0.365

APPENDIX E

TRANSPORT PROPERTY DATA USED IN THE THEORETICAL CALCULATIONS

The following equations and data were used for carrying out numerical calculations for the freeze-drying of beef:

Reference Number

1. Constant pressure specific heat of water vapor

$$C_p = 0.445 \frac{\text{Btu}}{\text{lbm °R}} \qquad (45)$$

2. Mean radius of capillary channels in freeze-dried beef

$$r_c = 0.000164 \text{ ft} \qquad (23)$$

3. Thermal conductivity of freeze-dried beef

$$k_I = 0.535 \left[\frac{1}{1 + \frac{0.0902}{P_0}}\right] \frac{\text{Btu}}{\text{hr ft °R}} \qquad (20)$$

where P_0 is in torr.

4. Thermal conductivity of frozen beef

$$k_{II} = 2.60 - \frac{2.04}{[490]^2} T_{IIm}^2 \frac{\text{Btu}}{\text{hr ft °R}} \tag{17}$$

where T_{IIm} is in °R.

5. Latent heat of sublimation of frozen beef

$$\Delta H = 1488 \quad \text{Btu/lbm} \tag{21}$$

6. Absolute viscosity of water vapor

$$\mu = \frac{0.659\, T_{Im}^{3/2} \times 10^{-6}}{623.0 + T_{Im}} \frac{\text{lbm}}{\text{ft sec}} \tag{48}$$

where T_{Im} is in °R.

7. Density of the water vapor

$$\rho = \frac{P_0}{R\, T_{Im}} \tag{47}$$

where P_0 is in $\frac{\text{lbf}}{\text{ft}^2}$ and T_{Im} is in °R.

8. Equilibrium vapor pressure of frozen beef

$$\bar{P} = \exp\,[27.7 - 12900/T] \text{ torr} \tag{21}$$

where T is in °R.

9. Porosity of freeze-dried beef

$$\sigma = 0.70 \tag{6}$$

10. Gas constant for water vapor

$$R = 85.8 \frac{\text{ft lbf}}{\text{lbm } ^\circ\text{R}} \tag{47}$$

11. Diffusion coefficient for air and water vapor

$$D_{aw} = [1.09]\ 0.0018583 \frac{\left[T_{Im}^3 \left[\frac{1}{M_a} + \frac{1}{M_w}\right]\right]^{1/2}}{P_0\ \sigma_{aw}^2\ \Omega_{D,aw}} \ \frac{\text{cm}^2}{\text{sec}} \tag{33}$$

where P_0 is in atm and T_{IM} is in °K. The procedure for evaluating σ_{aw}^2 and $\Omega_{D,aw}$ is given in reference (33). In addition, the quantity 1.09 in the above equation is suggested by reference (48).

12. Average velocity of the water vapor molecules

$$\bar{v}_w = \left[\frac{2.55\ KT_{Im}}{m}\right]^{1/2} \ \frac{\text{m}}{\text{sec}} \tag{30}$$

where m is the mass of the water vapor molecule is kgm, T_{Im} is in °K, and K is Boltzmann's constant in joule/°K.

13. Permeability of freeze-dried beef to the flow of water vapor in the transition regime

$$\varepsilon = \frac{L}{2} \times 10^{-8} \left[13.5 - 10.8 \ln \frac{P_0}{2.781} \right] ft^2 \tag{9}$$

where P_0 is in lbf/ft^2.

14. Permeability of freeze-dried beef to flow of water vapor in the continuum regime

$$\varepsilon_D = \frac{\sigma[2\ r_c]^2}{16\ \tau\ [2.5]}\ ft^2 \tag{31}$$

15. First order correction factor for nonroundness of the capillary tubes in the freeze-dried region

$$\Gamma = 0.8 \tag{31}$$

16. Tortuosity factor for freeze-dried beef

$$\tau = 4.4 \tag{23}$$

17. Density of frozen beef, approximated by the density of ice

$$\rho_i = 62.4\ \frac{lbm}{ft^3} \tag{45}$$

APPENDIX F

DRYING TIMES FOR FREEZE-DRIED BEEF

Table 5. Drying Times for Drying of Beef from Both Sides

T_0 °R	P_0 torr	$\bar{P}_{w0}/P_0$	L ft	Drying Time Hours
560	0.01	0.6	0.1250	168.8
560	0.10	0.6	0.1250	44.9
560	0.50	0.6	0.1250	28.0
575	0.50	0.6	0.1040	17.7
560	1.00	0.0	0.1250	24.6
560	1.00	0.1	0.1250	25.1
560	1.00	0.2	0.1250	25.7
560	1.00	0.3	0.1250	26.3
560	1.00	0.4	0.1250	26.7
560	1.00	0.5	0.1250	27.1
560	1.00	0.6	0.1250	27.6
560	1.00	0.7	0.1250	27.9
560	1.00	0.8	0.1250	28.4
560	1.00	0.9	0.1250	28.8
560	2.00	0.6	0.1250	29.2
575	2.00	0.6	0.1040	17.4
560	2.00	0.7	0.1250	29.8
560	3.00	0.6	0.1250	31.3
560	3.00	0.7	0.1250	32.0
560	3.00	0.8	0.1250	32.7
575	3.00	0.6	0.1145	22.3
560	4.00	0.6	0.1250	31.7
488	35.00	0.0	0.1250	159.0
488	760.00	0.0	0.1250	1582.4

Table 6. Drying Times for Unidirectional Drying of Beef with the Back Face Insulated

T_0 °R	P_0 torr	$\bar{P}_{w0}/P_0$	L ft	Drying Time hours
560	0.01	0.6	0.1250	675.0
560	0.10	0.6	0.1250	179.7
575	0.50	0.6	0.1040	70.7
560	0.50	0.6	0.1250	112.2
560	1.00	0.0	0.1250	98.3
560	1.00	0.1	0.1250	100.6
560	1.00	0.2	0.1250	103.0
560	1.00	0.3	0.1250	105.0
560	1.00	0.4	0.1250	106.6
560	1.00	0.5	0.1250	108.2
560	1.00	0.6	0.1250	110.5
560	1.00	0.7	0.1250	111.6
560	1.00	0.8	0.1250	113.4
560	1.00	0.9	0.1250	115.3
575	2.00	0.6	0.1040	69.4
560	2.00	0.7	0.1250	119.0
560	2.00	0.6	0.1250	116.8
575	3.00	0.6	0.1145	89.1
560	3.00	0.7	0.1250	127.9
560	3.00	0.8	0.1250	130.8
560	3.00	0.6	0.1250	125.2
560	4.00	0.6	0.1250	126.7
488	35.00	0.0	0.1250	635.8
488	760.00	0.0	0.1250	6329.6

Table 7. Drying Times for Unidirectional Drying of Beef with the Back Face Heated

T_0	T_L	P_0	$\bar{P}_{w0}/P_0$	L	Drying Time (Hours)	
					$T_X=r_o+r_1X$	$T_X=r_o+r_1X$ $+r_2X^2+r_3X^3$
°R	°R	torr		ft		
560	488.0	0.5	0.6	0.1250	30.9	30.9
560	488.0	1.0	0.6	0.1250	30.2	30.1
560	480.0	1.0	0.6	0.1250	40.0	40.7
560	470.0	1.0	0.6	0.1250	68.1	70.1
560	460.0	1.0	0.6	0.1250	217.0	220.0
560	488.0	1.0	0.0	0.1250	27.1	27.0
560	488.0	1.0	0.1	0.1250	27.3	27.4
560	488.0	1.0	0.2	0.1250	27.6	27.9
560	488.0	1.0	0.3	0.1250	28.5	28.5
560	488.0	1.0	0.4	0.1250	29.0	29.0
560	488.0	1.0	0.5	0.1250	29.5	29.5
560	488.0	1.0	0.7	0.1250	31.1	30.7
560	488.0	1.0	0.8	0.1250	31.4	31.3
560	488.0	1.0	0.9	0.1250	32.5	32.0
560	468.0	1.0	0.5	0.1665	120.3	123.4
560	468.0	1.0	0.6	0.1665	132.9	136.1
560	488.0	2.0	0.6	0.1250	40.8	40.1
575	492.5	2.0	0.5	0.1040	22.3	22.1
575	492.5	2.0	0.6	0.1040	23.1	22.7
560	484.3	2.0	0.5	0.1665	77.5	77.5
560	484.3	2.0	0.6	0.1665	82.2	82.2
560	488.0	3.0	0.6	0.1250	63.3	64.2
575	495.0	3.0	0.5	0.1145	33.8	34.2
575	495.0	3.0	0.6	0.1145	36.4	36.2
560	486.7	3.0	0.5	0.1665	104.1	105.5
560	486.7	3.0	0.6	0.1665	117.0	117.3
560	488.0	4.0	0.6	0.1250	79.5	81.7
488	488.0	760.0	0.0	0.1250	702.5	

APPENDIX G

FLOW RATES FOR CHANNEL FLOW CALCULATED BY THE DISCRETE ORDINATE METHOD

The flow rate equation for rarefied gas flow between parallel plates based on the discrete ordinate method (Equation (87)) was not coupled with the energy equation in the theoretical development to give an interface temperature relationship. However, water vapor flow rates were calculated using the pressure drops that were obtained from Equation (35). The results for drying of beef at 1.0 and 3.0 torr are shown in Figure 42. Although the per cent difference between the values obtained from Equation (87) and those obtained from Equation (53) is relatively high, the values are certainly of the same order of magnitude. The difference would seem to be the fact that on one hand it is assumed that the porous medium can be approximated by a bundle of capillary tubes, and on the other by a bundle of rectangular channels. It is doubtful whether the difference would cause any appreciable change in the interface temperature and pressure calculations. It appears that the results of the discrete ordinate method would certainly be applicable to drying when experimental permeabilities are not available.

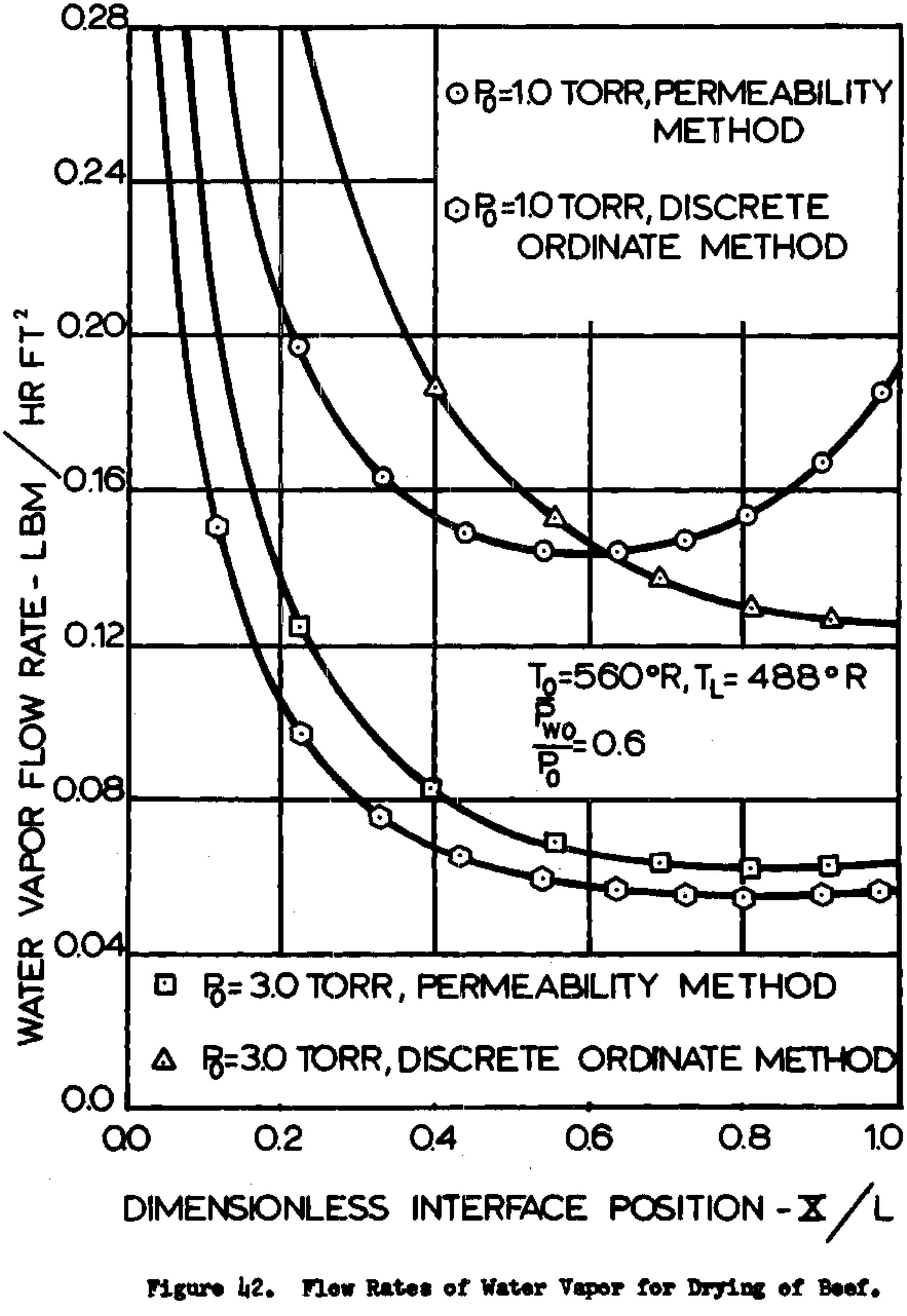

Figure 42. Flow Rates of Water Vapor for Drying of Beef.

LITERATURE CITED

1. Flosdorf, E. W., *Freeze-Drying,* Reinhold, New York, 1949.

2. Harris, R. J. C., *Biological Applications of Freezing and Drying,* Academic Press, New York, 1954.

3. Van Arsdel, W. B., *Food Dehydration,* The AVI Publishing Company, Inc., Westport, Connecticut, 1963.

4. Desrosier, N. W., *The Technology of Food Preservation,* The AVI Publishing Company, Inc., Westport, Connecticut, 1963.

5. Charm, S. E., *The Fundamentals of Food Engineering,* The AVI Publishing Company, Inc., Westport, Connecticut, 1963.

6. Harper, J. C. and A. L. Tappel, *Advances in Food Research,* Vol. VII, Academic Press, New York, 1957, pp. 171-234.

7. Burke, R. F. and R. V. Decareau, *Advances in Food Research,* Vol. XIII, Academic Press, New York, 1964, pp. 1-88.

8. Hardin, T. C., *Heat and Mass Transfer Mechanisms in Freeze-Drying,* Ph.D. Thesis, Georgia Institute of Technology, Atlanta, Georgia, 1965.

9. Dyer, D. F., *Transport Phenomena in Sublimation Dehydration,* Ph.D. Thesis, Georgia Institute of Technology, Atlanta, Georgia, 1965.

10. Bannister, J. D., *Heat and Mass Transfer Mechanisms in Sublimation Drying,* M. S. Thesis, Northwestern University, 1961.

11. Koumoutsos, N. G. and J. E. Sunderland, "Freeze Dehydration," *Technika Chronika,* Athens, Greece, 1963.

12. Dyer, D. F. and J. E. Sunderland, "The Transient Temperature Distribution During Sublimation Dehydration," *ASME Journal of Heat Transfer,* p. 109, 1967.

13. Dyer, D. F. and J. E. Sunderland, "Bulk and Diffusional Transport in the Region Between the Molecular and Viscous Flow," *International Journal of Heat and Mass Transfer,* Vol. 9, 1966, pp. 519-526.

14. Dyer, D. F. and J. E. Sunderland, "Heat and Mass Transfer Mechanisms in Sublimation Dehydration," (to be published).

15. Lambert, J. B., *Heat and Mass Transfer in Freeze-Drying*, Ph.D. Dissertation, University of Wisconsin, 1956.

16. Kan, B. and F. de Winter, "The Acceleration of the Freeze-Drying Process Through Improved Heat Transfer," (to be published).

17. Hill, J. E., J. D. Leitman and J. E. Sunderland, "Thermal Conductivity of Various Meats," *Food Technology*, (to appear August, 1967).

18. Harper, J. C. and A. F. El Sahrigi, "Thermal Conductivities of Gas Filled Porous Solids," *I. and E. C. Fundamentals*, Vol. 3, 1964, pp. 318.

19. Lusk, G. M., M. Karel and S. A. Goldblith, "Thermal Conductivity of Some Freeze-Dried Fish," *Food Technology*, Vol. 18, 1964, pp. 121.

20. Massey, W. M., Jr. and J. E. Sunderland, "Measurement of Thermal Conductivity During Freeze-Drying of Beef," *Food Technology*, Vol. 21, 1967, pp. 90A.

21. Dyer, D. F., D. K. Carpenter and J. E. Sunderland, "Equilibrium Vapor Pressure of Frozen Bovine Muscle," *Journal of Food Science*, Vol. 31, No. 2, 1966, pp. 196-201.

22. Sevcik, V. J. and J. E. Sunderland, "Emissivity of Beef," *Food Technology*, Vol. 16, No. 9, 1962, pp. 124-126.

23. Harper, J. C., "Transport Properties of Gases in Porous Media at Reduced Pressures with Reference to Freeze-Drying," *American Institute of Chemical Engineers Journal*, Vol. 8, No. 3, 1962, pp. 298-302.

24. Harper, J. C., C. O. Chichester and T. E. Roberts, "Freeze-Drying of Foods," *Agricultural Engineering*, Vol. 43, 1962, pp. 78.

25. Harper, J. C. and C. O. Chichester, "Improvements in Rates of Freeze-Drying," *Vacuum Symposium Transactions*, 1963, pp. 47-53.

26. Hatcher, J. D., *The Use of Gamma Radiation to Measure Moisture Distribution During Drying Processes*, Master's Thesis, Georgia Institute of Technology, Atlanta, Georgia, 1964.

27. Massey, W. M., Jr., *Measurement of Thermal Conductivity During Freeze-Drying of Beef*, Master's Thesis, Georgia Institute of Technology, Atlanta, Georgia, 1966.

28. Kennard, E. H., *Kinetic Theory of Gases*, McGraw-Hill, New York, 1939.

29. Loeb, L. B., *The Kinetic Theory of Gases,* McGraw-Hill, New York, 1934.

30. Present, R. D., *Kinetic Theory of Gases,* McGraw-Hill, New York, 1958.

31. Carman, P. C., *Flow of Gases Through Porous Media,* Academic Press, New York, 1956.

32. Schneider, P. V., *Conduction Heat Transfer,* Addison Wesley, New York, 1956, pp. 218-221.

33. Bird, B. R., W. E. Stewart and E. N. Lightfoot, "Diffusivity and the Mechanisms of Mass Transport," *Transport Phenomena,* John Wiley and Sons, New York, 1960, pp. 495-515.

34. Scott, D. S. and F. A. Dullien, "The Flow of Rarefied Gases," *American Institute of Chemical Engineers Journal,* Vol. 8, No. 3, 1962, pp. 293-297.

35. Scott, D. S. and F. A. Dullien, "Diffusion of Ideal Gases in Capillaries and Porous Solids," *American Institute of Chemical Engineers Journal,* Vol. 8, No. 1, 1962.

36. Dyer, D. F., "Bulk and Diffusional Transport of Non-Uniform Pressure Gases," *Transactions of the Faraday Society,* Vol. 63, No. 531, 1967, pp. 573-578.

37. Goodman, T. R., "Application of Integral Methods to Transient Nonlinear Heat Transfer," *Advances in Heat Transfer,* Vol. 1, 1964, pp. 51-122.

38. Goodman, T. R., "The Heat-Balance Integral and Its Application to Problems Involving a Change of Phase," *Transactions of A.S.M.E.,* 1958, pp. 335.

39. Chapman, S. and T. G. Cowling, *The Mathematical Theory of Non-Uniform Gases,* Cambridge University Press, Cambridge, 1961, pp. 415.

40. Pollard, W. G., and R. D. Present, "On Gaseous Self-Diffusion in Long Capillary Tubes," *Physical Review,* Vol. 73, 1948, pp. 762-774.

41. Huang, A. B., D. P. Giddens and C. W. Bagnal, "Rarefied Gas Flow Between Parallel Plates Based on the Discrete Ordinate Method," *The Physics of Fluids,* Vol. 10, No. 3, 1967, pp. 498-502.

42. Dyer, D. F., T. C. Hardin and J. E. Sunderland, "A Quasi-Steady Solution for Unidirectional Freeze-Drying," (unpublished).

43. Mayne, R. W., *Humidity Measurements Under Low Vacuum Conditions*, M. S. Thesis, Georgia Institute of Technology, Atlanta, Georgia, 1965.

44. Dyer, D. F. and J. E. Sunderland, "A Standard for Vapor Pressure Measurement," *Vacuum*, Vol. 14, 1964, pp. 396.

45. Keenan, J. H. and F. G. Keyes, Thermodynamic Properties of Steam, John Wiley and Sons, New York, 1936.

46. Saravacos, G. D. and R. M. Stinchfield, "Effect of Temperature and Pressure on the Sorption of Water Vapor by Freeze-Dried Food Materials," *Journal of Food Science*, Vol. 30, No. 5, 1965, pp. 779.

47. Lay, J. E., *Thermodynamics*, Charles E. Merrill, 1963.

48. Reid, R. C. and T. K. Sherwood, *The Properties of Gases and Liquids*, McGraw-Hill, New York, 1958.

VITA

James E. Hill was born in Bluefield, West Virginia on January 19, 1942. He spent his pre-college years in Bluefield and was graduated from Bluefield High School in May, 1959.

He began his college work in September, 1959, at Virginia Polytechnic Institute. He received a B.S. degree in Mechanical Engineering there in June, 1963, and was commissioned a 2nd Lt. in the United States Air Force. Since September, 1963, he has been doing graduate work at the Georgia Institute of Technology where he received a M.S. degree in Mechanical Engineering in June, 1966.

Mr. Hill was married in 1963 to the former Carol Zane Thompson and they have one child, Kathryn Courtney.